UNIVERSITY OF CALIFORNIA
RIVERSIDE

Respiratory System and Head Segmentation Revealed From Trilobite Appendages

A Dissertation submitted in partial satisfaction
of the requirements for the degree of

Doctor of Philosophy

in

Geological Sciences

by

Jin-bo Hou

March 2021

Dissertation Committee:
Dr. Nigel C. Hughes, Chairperson
Dr. Mary L. Droser
Dr. Paul De Ley

The Dissertation of Jin-bo Hou is approved:

Committee Chairperson

University of California, Riverside

ACKNOWLEDGEMENTS

This study was funded by US National Science Foundation EAR-1124303 and EAR-1849963 and the Smithsonian Institution Fellowship Program. I thank D. H. Erwin and C. C. Labandeira for providing me an opportunity to study at NMNH; D. H. Erwin, M. Florence, K. Hollis, F. Marsh, C. C. Labandeira, J. Strotman, S. Whittaker of NMNH for accessing the specimens and providing research techniques; D. E. G. Briggs and S. Butts for providing me an opportunity to study at YPM; D. E. G. Briggs, S. Butts, E. Martin, J. Utrup, and Z.-T. Zhang of YPM for accessing the specimens and research techniques; N. D. L. Clark of GLAHM for access to specimens; J. D. Cundiff for assessing MCZ specimens; M. Coyne for assessing GSC specimens; M. H. Chase and A. Smith of the AMNH MIF lab for technical support, P. Funkhouser for assistance with segmentation; D. Shu, J. Han, and M. Chen of ELI for providing the figures of *Yunnanozoan*; J. Bruthansová for the figure permission of the *Ectilaenus (katzeri) katzeri*; M. L. Droser, L. and C. Casey for logistic support and discussing this project.

Thanks to my committee members, M. L. Droser and P. De Ley for continually discussing and improving my study with critical comments and technical help; to P. Sadler and R. A. Minnich for giving me helpful comments that improved my project.

Also, thanks to M. J. Hopkins of the American Museum of Natural History for providing huge help to make this project possible by analyzing data, discussing and editing content.

Extreme thanks to my advisor, Nigel C. Hughes, for creating opportunities to make this study practical, paying exceedingly large effort on improving this project in many different ways, e.g. carefully editing and discussing content, correcting English grammar, helping to sharpen the project, and providing tremendous help in my daily life.

Also, thanks to S. J. Wernette for discussing and improving my research and providing a lot of help in my daily life; and those who have improved my teaching skills and helped my UCR life: P. Boan, N. Barth, A. Bekker, K. Chaudhuri, S, Evans, H. Ford, A. Ghost, C. Hall, M. Heather, J. Herring, J. Humphreys, B. Kelly, A. Kovalick, B. Lee, B. Li, G. Love, N. Marshall, A. Martinez, M. Mendoza, D. Oglesby, P. Vervoort, K. Pehr, A. Rizzo, R. Surprenant, S. Srivastava, E. Vargas-Parra, C. Tu, B. Wu, X. Zhao, M. Zill.

Chapter one of this dissertation is mainly reprinted from the published work from "Hou, J. B., Hughes, N. C., Hopkins, M. J. (2021). The trilobite upper limb branch is a well-developed gill. *Science Advances*, 7, eabe7377."

To my parents, sisters, wife, and son

ABSTRACT OF THE DISSERTATION

Respiratory System and Head Segmentation Revealed From Trilobite Appendages

by

Jin-bo Hou

Doctor of Philosophy, Graduate Program in Geological Sciences
University of California, Riverside, March 2021
Dr. Nigel C. Hughes, Chairperson

Arthropod evolution represents one of the main foci of the evolutionary study of early life. The well-preserved Paleozoic fossil Lagerstätten provide soft-bodied arthropods available for exploring this issue. Here I present work on the appendages of two exquisitely preserved trilobites, the olenid *Triarthrus eatoni* from the Ordovician Beecher's Bed and the corynexochid *Olenoides serratus* from the Cambrian Burgess Shale, to reveal new evidence that sheds light on the early evolution of arthropods. Firstly, three pieces of evidence work together to support the respiratory function of the upper branch of the "biramous" appendage. The cross-section of the filament is closely comparable to the gill system of modern crustaceans, that circulate the bulk flow of hemolymph. The articulation between the limb and the body shows that the upper branch is connected ventrally to the limb base of the lower branch and dorsally to the body wall by extended arthrodial membrane, and this articulation is similar to the way in which the book gills of *Limulus* connect with the body wall. The anterior imbrication of upper branches limits their location between the ventral dorsal exoskeleton and limb lower

branch, restricting the efficient the use of the upper branch in swimming but protecting the fragile gill filaments. Secondly, the mechanical rotation of upper branch creates a down backward going water current, which forms a convection system with upward flowing hemolymph. Such convection initiated the countercurrent exchange mechanism that efficiently enabled the oxygen uptake task. An efficient gas exchange mechanism is indicated to be, at a minimum, already established in the early Cambrian. Finally, one more pair of appendages has been discovered in front of the traditionally recognized "1st" pair of cephalic biramous appendages. This pair of appendages revises our understanding of the trilobite head, revealing five pairs of cephalic appendages; one pair of antennae followed by four pairs of "biramous" appendages. The mismatched ventral appendages and dorsal furrows resulted from the merged muscle attachment sites of the 2nd and 3rd pairs of cephalic appendages indicated by the bifurcation of the S1 glabellar furrow. This may represent the general mismatch pattern among arthropods.

TABLE OF CONTENTS

INTRODUCTION 1

CHAPTER 1. THE TRILOBITE UPPER LIMB BRANCH IS A WELL-DEVELOPED GILL 5

Abstract 5

Introduction 5

Materials and methods 7

Results 9

Discussion 17

Dumbbell-shaped filament 17

Articulation of the upper branch 21

Structural limitations of the upper branches 27

Implications for the comparative biology of arthropod appendages 28

Supplementary figures 32

CHAPTER 2. EFFICIENT COUNTERCURRENT GAS EXCHANGE ESTABLISHED AMONG EARLY METAZOANS 47

Abstract 47

Introduction 48

Materials and methods 50

Results and discussion 51

Stroke of the upper branch 51

Hemolymph flow 54

Interaction of the oxygen gradient and the water current 55
Withstanding oxygen stress 58
Deuterostome 59
CHAPTER 3. MISMATCH OF EARLY EUARTHROPOD CEPHALIC STRUCTURES IS SOLVED WITH HIDDEN APPENDAGES 63
Abstract 63
Introduction 64
Materials and methods 65
Description 67
Triarthrus eatoni 67
Olenoides serratus 70
Discussion 72
Head segments of trilobites 72
Head segmental mismatch 74
Supplementary information 82
Taphonomy of trilobite appendages 82
Figure legends and abbreviations 82
Comments on *Triarthrus eatoni* 83
Comments on *Olenoides serratus* 84
Comments on relationship of dorsoventral structures 86
Supplementary figures 88

LIST OF FIGURES

Figure 1 10

Figure 2 13

Figure 3 15

Figure 4 19

Figure 5 21

Figure 6 23

Figure 7 24

Figure 8 52

Figure 9 56

Figure 10 60

Figure 11 68

Figure 12 69

Figure 13 71

Figure 14 75

LIST OF SUPPLEMENTARY FIGURES

Figure S1. 32

Figure S2 34

Figure S3 36

Figure S4. 38

Figure S5. 40

Figure S6. 41

Figure S7 43

Figure S8. 44

Figure S9. 46

Figure S10 88

Figure S11. 89

Figure S12 90

Figure S13. 91

Figure S14 93

Figure S15 95

Figure S16 96

Figure S17 98

Figure S18 99

Figure S19 101

Figure S20 102

Figure S21. 103

Figure S22 104

INTRODUCTION

The particularly well-preserved early fossil Lagerstätten (Briggs *et al*. 1994; Yang *et al*. 2013; Walossek and Müller 1990; Siveter *et al*. 2003; Van Roy *et al*. 2010; Droser *et al*. 2017; Xiao *et al*. 1998; Shu *et al*. 1999) have attracted large attention in the study of the early evolution of organisms. The evolution of arthropods is a big focus among evolutionary studies as arthropods have most successfully occupied the world in which we live. Those Paleozoic deposits (Gaines *et al*. 2008; Gaines 2014) contain a large number of exquisitely preserved arthropods, which are the basis for our view of early history of arthropod evolution. Trilobites are the most easily recognizable early arthropod group.

Before any trilobite body fossils appeared in the lower Cambrian fossil record, the bilateral trace fossils, *Cruziana* and *Rusophycus*, are represented and are generally considered to be the product of trilobites or trilobite-like arthropods (Seilacher 1985). After their body fossils appeared, the quick diversification of trilobites in the Cambrian (Webster 2007) was a large component of the rise of the Cambrian fauna. However, such a successful development reached its peak at the early Ordovician and then declined to extinction at the end of Permian (Foote 1993a, b; Adrain *et al*. 1998; Hughes 2005). Revealing the evolutionary history of trilobites will help us to understand the evolutionary history of arthropods as a whole.

Out of about 20,000 trilobite species, there are only about thirty trilobites recorded with soft parts (Hughes 2003). Since the appendages were reported in *Triarthrus eatoni* (Beecher 1893) and *Olenoides serratus* (Walcott 1918), many detailed

works had accumulated in the last century (Cisne 1981, 1975; Whittington 1975, 1980; Whittington and Almond 1987b), which together with the lately reported *Eoredlichia intermedia* (Shu *et al*. 1995; Ramsköld and Edgecombe 1996) had served as a good model for understanding the early evolution of arthropods (Briggs and Fortey 1989; Ortega-Hernández *et al*. 2013; Legg *et al*. 2013; Stein *et al*. 2013; Aria and Caron 2017b). Revealing more information about trilobites will deeply improve our understanding of arthropod evolution as a whole, especially as trilobites can yield unusually large numbers of soft bodied specimens available for further study.

Here, I present in three chapters new evidence revealed from soft-bodied trilobites and discuss its implications for our understanding of the early evolution of arthropods and possibly even triploblasts as a whole.

The upper branch of the Paleozoic "biramous" limb remains a subject of debate as to whether it was respiratory or not in function (Whittington 1975; Williams *et al*. 2011; Bergström 1969; Suzuki and Bergström 2008; Haug and Haug 2016; Walcott 1881; Størmer 1939). In early studies, the gill function was systematically questioned based on its presumed rigidity and lacking respiratory organ (Bergström 1969; Suzuki and Bergström 2008; Haug and Haug 2016). This challenge was accompanied by the studies of limb development, e.g. basis, coxa, protopodite in the agnostoid *Agnostus pisiformis* (Walossek 1993; Walossek and Müller 1990). These studies together argued that the trilobite upper branch was exopodal function, rather than a gill. The function inferred from the exopodal morphology favored a ventilation role for the upper branch but not its function as a respiratory organ itself. However, without detailed analysis of the structure

itself, it is hard to make a conclusion about its adaptations. To reveal the fine detail of this structure, diverse imaging techniques are applied to investigate the precise anatomy of the upper branch and show the evidence for a respiratory design that is comparable in multiple respects to the gills of both modern crustaceans and chelicerates. Together with other evidence, including attachment type of limb and protection of the fragile structures, this issue is the subject of Chapter 1.

By following the study in Chapter 1, questions are considered of how exactly the hemolymph is charged with oxygen and how efficient the respiration discussed in chapter 1. These questions include how early metazoans took advantage of rising oxygen ambient level in the ocean to build their complex body plans. Through analyzing the mechanical function of the upper branch and its complementary effect on water current, the most efficient respiratory mechanism is revealed to be already designed in not only trilobites but also in Cambrian deuterostome gills, which is the central focus of Chapter 2.

Although matching the same features typical of the "biramous" limb, cephalic and trunk limbs functioned differently. Cephalic limbs and their structures are relevant to broad issues of relationships among all arthropods. The number of cephalic limbs is used to define high level taxa in classification of the panarthropods (Damen *et al*. 1998; Telford and Thomas 1998; Budd 2002; Scholtz and Edgecombe 2006; Mayer *et al*. 2013; Richter *et al*. 2013). Understanding the transition from early panarthropods to crown group of arthropods is a challenge. Trilobite cephalic limbs have debated for a long time, recently some consensus has been reached (Scholtz and Edgecombe 2005; Park and Kihm 2017; Bruton and Haas 2003). However, these studies are based on the limb tips,

which may have been rotated forward or backward, and often do not provide firm evidence on the exact number of cephalic appendages. By tracing the limb base close to the body wall, a more reliable count of the numbers of cephalic limbs is presented in Chapter 3, based on new observations. However, the updated number of cephalic limbs challenges the previous evidence of a distinct match between the numbers of cephalic limbs and that of dorsal furrows. The mismatch problem is discussed in the same chapter with an explanation for how it arose in trilobites, which may represent a general growth model applicable more widely in arthropod history.

CHAPTER 1. THE TRILOBITE UPPER LIMB BRANCH IS A WELL-DEVELOPED GILL

Abstract

Whether or not the upper limb branch of Paleozoic "biramous" arthropods, including trilobites, served a respiratory function has been much debated. Here, new imaging of the trilobite *Triarthrus eatoni* shows that dumbbell-shaped filaments in the upper limb branch are morphologically comparable with gill structures in crustaceans that aerate the hemolymph. In *Olenoides serratus* the upper limb's partial articulation to the body via an extended arthrodial membrane is morphologically comparable to the junction of the respiratory book gill of *Limulus* and differentiates it from the typically robust exopod junction in Chelicerata or Crustacea. Apparently limited mechanical rotation of the upper branch may have protected the respiratory structures. Partial attachment of the upper branch to the body wall may represent an intermediate state in the evolution of limb branch fusion between dorsal attachment to the body wall, as in Radiodonta, and ventral fusion to the limb base, as in extant Euarthropoda.

Introduction

Early metazoan diversification was coincident with important ecological and environmental changes, such as increased trophic complexity and metazoan mobility, and rising ambient oxygen availability (Lyons *et al*. 2014; Droser*, et al*. 2017; Sperling *et al*. 2015). How increasing energetic demands were accommodated anatomically among early

metazoans remains unclear. Our understanding of non-skeletal form in fossil organisms is limited to sites of exceptional preservation (Lagerstätten) (Briggs, *et al*. 1994; Yang, *et al*. 2013; Walossek and Müller 1990; Siveter, *et al*. 2003), from which Paleozoic arthropod soft tissue preservation provides an opportunity to assess structural innovation among soft tissues. However, debate remains about the interpretation of such soft tissues, such as whether the upper branch of the earliest "biramous" limbs was respiratory or not (Whittington 1975; Williams, *et al*. 2011; Bergström 1969; Suzuki and Bergström 2008; Haug and Haug 2016; Walcott 1881; Størmer 1939). Here we present new imaging that confirms its function as a gill.

The Paleozoic "biramous" appendage consists of an upper branch and a lower branch, similar to the modern arthropod biramous appendage that is composed of a non-respiratory outer exopod and an inner endopod. The apparent similarity between the Paleozoic "biramous" appendages and modern biramous limbs (e.g. Anaspidacea) suggests the possible homology of these two sets of structures (Suzuki and Bergström 2008; Haug and Haug 2016; Boxshall 2004; Walossek and Müller 1998). At least one cell lineage study, however, suggests that the modern biramous limb of crustaceans such as *Orchestia* formed via a subdivision of the main proximal-distal limb axis (Wolff and Scholtz 2008), and this might not have been the case in the Paleozoic "biramous" appendage (Boxshalll and Jaume 2009). Thus it may be that the two branches seen in many Paleozoic arthropods are not homologous with the modern limb but are rather a uniramous walking leg with an associated exite that evolved into the upper branch but was originally an additional axis (Wolff and Scholtz 2008) as in stem lineage arthropods,

such as Radiodonta (Van Roy *et al*. 2015; Daley *et al*. 2009). Resolving this issue requires better understanding of the detailed anatomy of the upper branch.

Trilobites are a well-defined clade (Fortey 2001), but only two species, the corynexochid *Olenoides serratus* (Rominger 1887) from the Cambrian Burgess Shale and the olenid *Triarthrus eatoni* (Hall 1838) from the Ordovician Beecher's Beds, are sufficiently well preserved to provide information relevant to this analysis, and both are routinely used in phylogenetic analyses of early arthropods (Briggs and Fortey 1989; Stein, *et al*. 2013). Critically, the Burgess Shale and Beecher's Beds Lagerstätten are characterized by different modes of preservation, and while each preserves anatomical features not normally captured in the fossil record, neither preserves organisms with complete fidelity. Thus some features observable on specimens from one locality may not be observable from specimens at the other locality, even if they had been present when the organisms were alive. Nonetheless by applying diverse imaging technologies, we are able to report details of the upper limb branch of both trilobite species that indicate its respiratory function and also bear on arthropod limb evolution.

Materials and Methods

Material described in this paper is housed in the American Museum of Natural History (AMNH), New York, USA; Geological Survey of Canada (GSC), Ontario, Canada; The Hunterian Museum, University of Glasgow (GLAHM), UK; National Museum of Natural History (NMNH) of Smithsonian Institution, Washington D.C., USA; Yale Peabody Museum of Natural History (YPM), Yale University, USA.

The pyritized specimens of *Triarthrus eatoni* are from the Beecher's Trilobite Beds of the Katian (Late Ordovician) Frankfort Shale of upper New York State, USA and the Katian (Late Ordovician) Whetstone Gulf Formation ("Martin Quarry") (Briggs *et al*. 1991; Farrell *et al*. 2009). About 150 specimens of *T. eatoni* were examined and small, well-preserved ones were selected for the Environmental Scanning Electron Microscope (ESEM) and micro-CT scanning. Specimens of *Olenoides serratus* are from the Burgess Shale Biota of the middle Cambrian (Wuliuan Stage) Burgess Shale Formation (previously known as the Stephen Formation) of British Columbia, Canada (Briggs, *et al*. 1994). About 100 specimens of *O. serratus* were examined. Both species occupied relatively deep shelfal marine environments that may have experienced periodic oxygen availability stress.

The specimen of the crab *Cancer (Metacarcinus) anthonyi* from the west coast of North America was quickly killed with a pair of anatomical scissors.

Triarthrus eatoni specimens were scanned with a Phoenix | tome | x μCT scanner (General Electric Company, Fairfield, CT, USA) at the AMNH Microscopy and Imaging Facility. Post-processing and volume-rendering of the CT images was done using the Phoenix DATOS | x 2 reconstruction software (GE Sensing & Inspection Technologies, Hürth, Germany) and VGStudio MAX v. 3.2 (Volume Graphics, Heidelberg, Germany). Tiff image stacks are archived at www.morphosource.org, project P1197.

The specimens were photographed by the Olympus DSX100 Opto-Digital Microscopy, Canon EOS 50D, Leica MZ16 with DFC420 lens, Leica M205C with DFC 700T lens, and PHILIPS XL-30 Environmental Scanning Electron Microscope (ESEM). The

Olympus DSX100 Opto-Digital Microscopy and the Leica M205C are installed with stack or non-stack function. ESEM is applied using both the backscattered-electron (BSE) and gaseous secondary electron (GSE) techniques, which are described in the figures. As specimens are captured with different directions of light to show particular structures, the details of orientation and illumination angles are given in the image of the figures. Figures were prepared using CorelDRAW 2018.

Results

Outstandingly well-preserved material shows that the shaft of the upper branch in *Triarthrus eatoni* is segmented and comprised of annulation-like articles (figs. S1A, D, S2A–C). It tapers distally with a terminal, elongate spoon-like article similar to the filaments that are attached to the articles (Fig. 1A and figs. S1A, S2A–C). The filaments are reduced in length along the proximal-distal axis of the branch (figs. S1A, S2A–B). The longest filament is about 3.5 times the length of the distal article, and the shortest filament is almost one third of the length of the distal article (fig. S2A–B). When viewed from the rear of the animal, cross sections of the filaments show inflated bulbs at the top and bottom that are connected via a narrow central region to form a dumbbell shape (Figs. 1A–I, 2A–V and figs. S1A–F, S3A–N, S4A–C, S5A–D, S6D, S7A–D). Measured at the thickest part, the marginal bulbs are about 31-49 μm in width, and the narrow central region is about 15-26 μm in width. The interval between adjacent marginal bulbs is about 15-28 μm wide. The inflated marginal bulb grades into the narrow central region without distinct boundary, and the whole of the inflated marginal bulb is wider than the

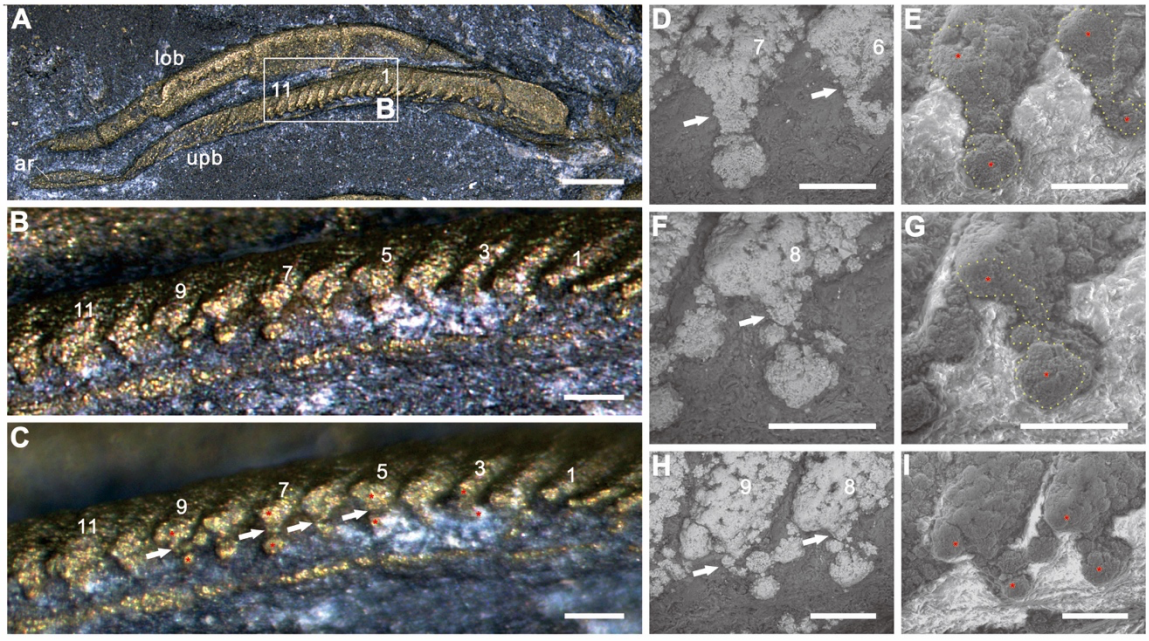

Figure 1 – Dumbbell-shaped filaments of *Triarthrus eatoni*. (A–I) YPM 204 (part). (A) Dorsal view. (B) Posterior view of the truncated filaments in stacked figure A. (C) Same area of figure B with non-stack function. (D–E) The 6th and 7th filaments showing dumbbell-shaped outline, tilted about 40º to the dorsal view. (D) High contrast backscattered-electron (BSE) image. (E) High contrast, gaseous secondary electron (GSE) image. (F–G) The 8th filament showing dumbbell-shaped outline, tilted about 40º to the dorsal view. (F) BSE image. (G) GSE image. (H–I) Top view of the 8th and 9th filaments showing dumbbell-shaped outlines. (H) BSE image. (I) GSE image. Yellow dashed lines mark the cross section of the filaments (E, G). Arabic numbers are references for locating the cross section of filaments in figure A. Asterisks locate the top and bottom inflated marginal bulbs of dumbbell-shaped filaments. Small white arrows indicate the narrow central region of dumbbell-shaped filament. BSE image distinguishes bright filament from dark surrounding matrix. GSE image distinguishes dark filament

from bright surrounding matrix. ar, article of shaft; lob and upb, lower and upper branches of the limb. Scale bars are 500 μm (A), 100 μm (B–C), 50 μm (D–I).

central region (Fig. 1A–I, 2A–V and figs. S1A–C, S3A–N, S6D, S7A–D). Inflated marginal bulbs are commonly well preserved while the central regions generally are less so (figs. S1D–F, S2C, S4A–C, S5A–D, S6C, E).

The limb base, the most proximal unit of the lower branch of *Olenoides serratus*, is a sub-rectangular structure the length of which is about 1.3 times its width (Fig. 3A, C, D–I and fig. S8A–C). Gnathobasic spines are present along its ventral and inner margins (Fig. 3C–D, F–H and fig. S8A–B). Spines on the inner margin are smaller than those on the ventral margin (Whittington 1975). The upper limb branch has two lobes, of which the proximal lobe bears long filaments on its posterior and inner margins (Fig. 3A–I and fig. S8A–C). The filaments on the inner margin extend up to the innermost edge of the proximal lobe (Fig. 3D, F–G, I–J) but not beyond. The dorsal inner region of the upper branch connects with the lateral body wall and the ventral sternite via the arthrodial membrane. This type of attachment is similar to the oblique limb articulation (Manton 1978), in which the limb joins the body in a manner where both lateral and ventral body walls connect. Arcuate, inosculating wrinkle-like structures give a rippled relief to the convex areas to which the proximal limb attached (Fig. 3A–J and fig. S8A–C) and can thus be distinguished from the blade-like gill filaments which have sharp, straight boundaries (Fig. 3C, D, G–I and S8A–C). Similar structures are also preserved in other early arthropods, including *Arthroaspis bergstroemi* (Stein, *et al*. 2013), *Misszhouia*

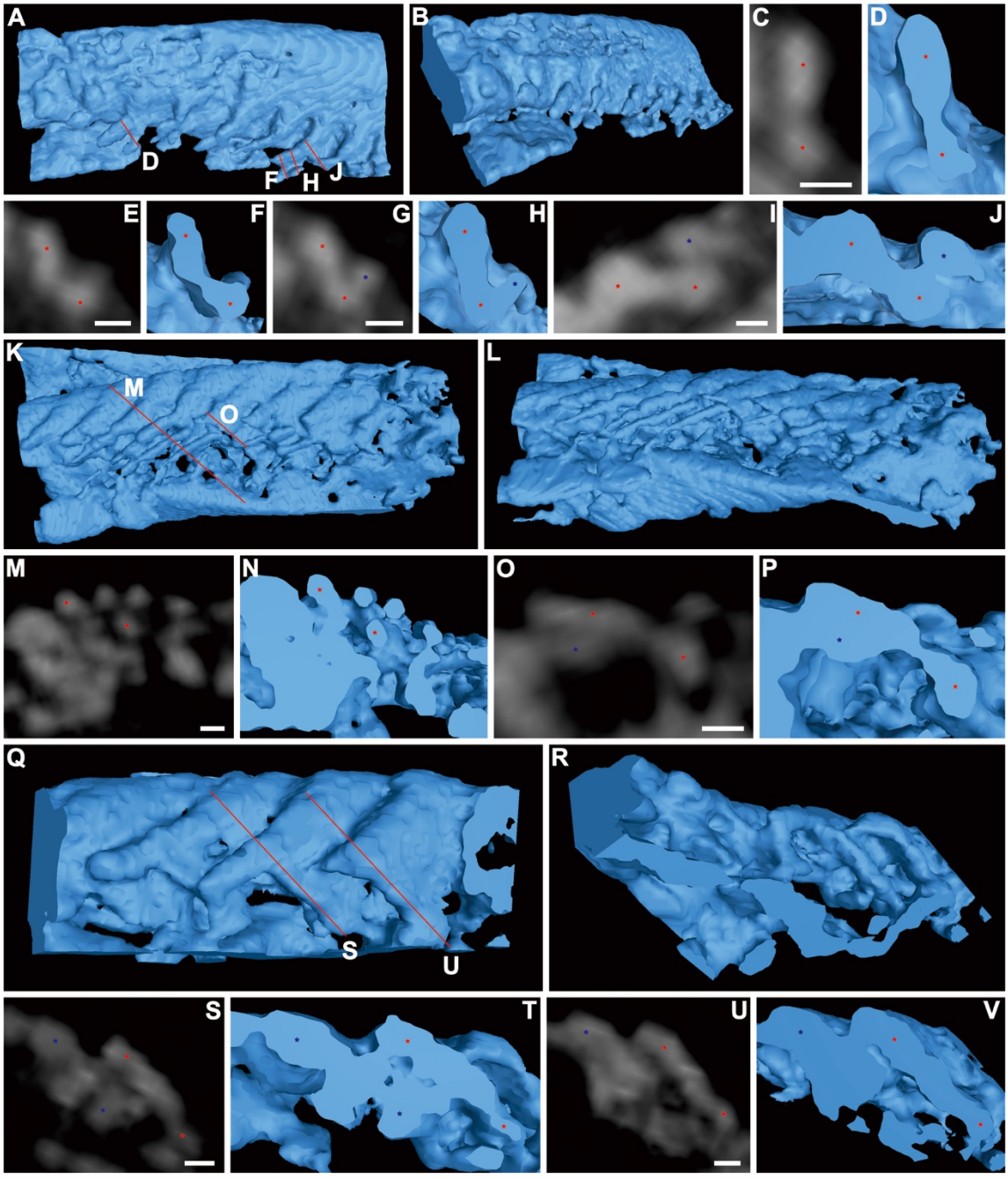
A
D
F
H
J
B
C
D
E
F
G
H
I
J
K
M
O
L
M
N
O
P
Q
S
U
R
S
T
U
V

Figure 2 – Dumbbell-shaped filaments of *Triarthrus eatoni*. (A–J) CT-reconstruction of partial limb, USNM 65527. (A) Dorsal view. (B) Posterolateral view. (C–J) Cross sections of filaments in figure 2A showing dumbbell-shaped outline with inflated marginal bulbs connected by narrow central region. (K–V) CT-reconstruction of partial limb, USNM 65523. (K) Dorsal view. (L) posterolateral view. (M–P) Cross sections of filaments in figure 2K showing separately preserved marginal bulbs. (Q) Dorsal view. (R) Posterior view. (S–V) Cross sections of filaments in figure 2Q show inflated marginal bulbs connected by narrow central region. Asterisks locate the top and bottom inflated marginal bulbs of dumbbell-shaped filaments which are connected by a narrow central region. CT-reconstructions are shown as blue color. CT-slices are displayed as grey color. Same color of asterisks represents same filament. Red lines represent the position of cross sections. Scale bars are 30 μm.

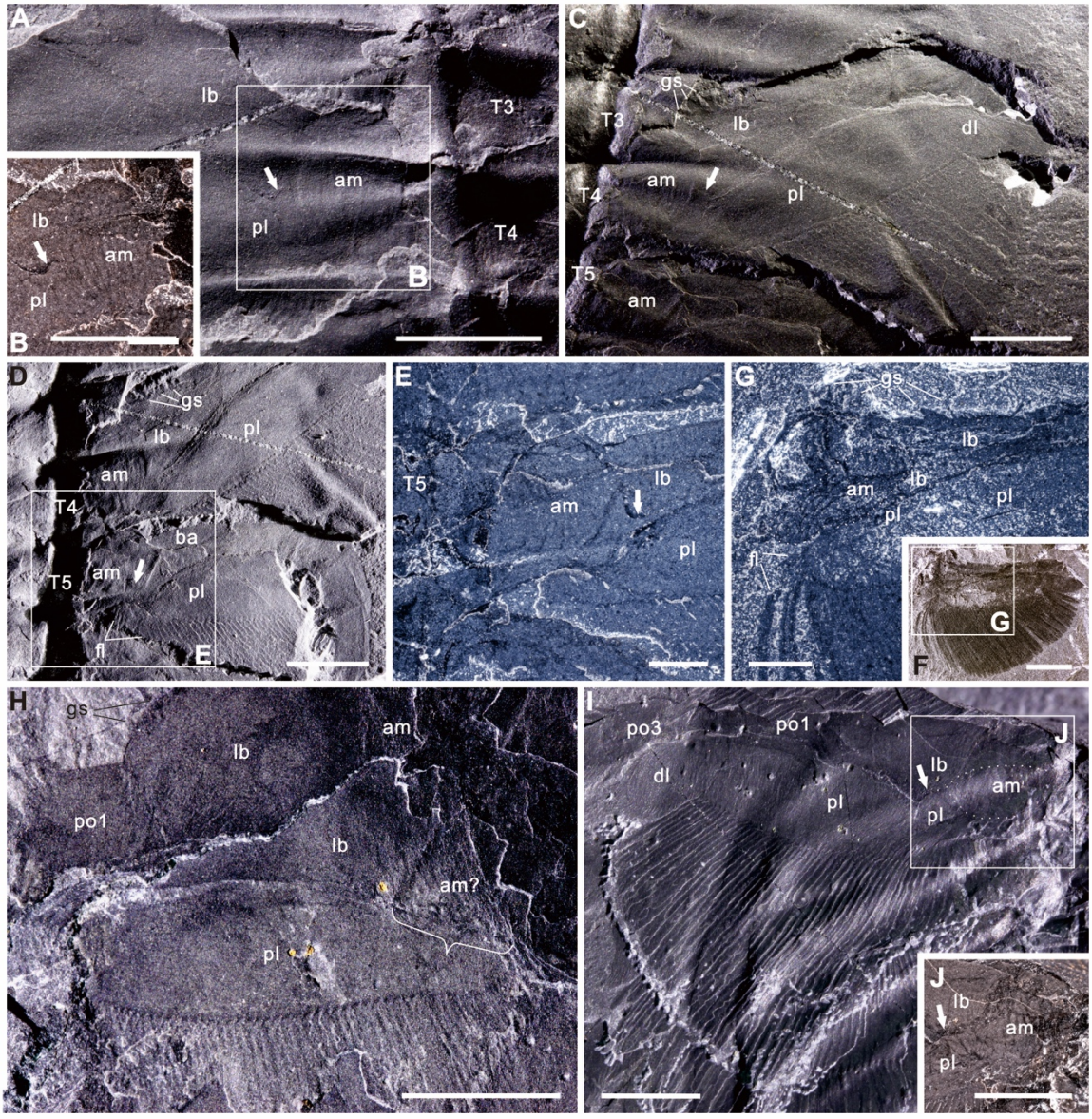
A
lb
T3
am
pl
T4
B
lb
am
pl
B
C
gs
T3
lb
dl
T4
am
pl
T5
am
D
gs
lb
pl
am
T4
ba
T5
am
pl
fl
E
E
T5
lb
am
pl
G
gs
lb
am
lb
pl
pl
fl
G
F
H
gs
lb
am
po1
lb
am?
pl
I
po3
po1
dl
pl
J
lb
am
pl
J
lb
am
pl

Figure 3 – Articulation of the upper branch of *Olenoides serratus*. (A–B) Ventral view of USNM 65519 (counterpart) showing upper branch connected directly with wrinkled arthrodial membrane and distinct from limb base. (C–E) Dorsal view of USNM 65519 (part) showing upper branch connected to wrinkled and convexly arched arthrodial membrane and separated from lower branch. (F–G) Upper branch connections with the arthrodial membrane and adjacent inner margin of the proximal lobe fringed with filaments extending posteriorly outward, USNM 188574. (H) GSC 34692b (part) showing a triangular body-limb junction, of which one side connected with the upper branch (marked by bracket). (I–J) Both branches articulated with arthrodial membrane, and upper branch clearly separated from lower branch, GSC 34695a (counterpart). (I) Lights incident from right. Arrows highlight boundary between upper branch and limb base. Dashed line marks arthrodial membrane outline. Anterior of fossil at top of all images. am, arthrodial membrane; am?, possible arthrodial membrane; gs, gnathobasic spine; dl, distal lobe of upper branch; fl, filament; lb, limb base; oc, occipital ring; pl, proximal lobe; po1-3, podomeres 1 to 3, respectively; T3-T5, thoracic segments 3 to 5, respectively. Scale bars are 5 mm (A–F, H–J), 2 mm (G).

longicaudata (Chen *et al*. 1997), *Waptia fieldensis* (Vannier *et al*. 2018), and *Leanchoilia illecebrosa* (Liu *et al*. 2007), and interpreted as extended arthrodial membrane with high flexibility. Together, the upper branch, lower branch, and inner region with wrinkle-like structures form a triangular to subcircular area (Fig 3A–J and fig. S8A–C) that marks the body-limb junction. The part of the limb joined to the body wall is about two fifths of the dorsal width of the entire limb base.

Isolated biramous limbs are commonly preserved detached from the main body (Chen, *et al*. 1997; Hou and Bergström 1997). Not only does their preservation show the strong connection between the limb basis and the proximal portion of the upper branch along a rigid hinge (Fig. 3A–J and fig. S8A–C), but some detached limbs also show the proximal part of the upper branch with arthrodial membrane still attached (Fig. 3F–G).

In dorsal view, the upper limb branches in both *T. eatoni* and *O. serratus* are distinctly overlapped above the lower limb branches (figs. S2A–E, S8A, C). Two types of imbrication can be recognized in dorsal view when an animal faces anteriorly and its dorsal side is uppermost: anterior imbrication style in which anterior structures cover posterior ones, and posterior imbrication style in which posterior structures cover anterior ones. For the lower branch, anterior imbrication characterizes the cephalic region while posterior imbrication dominates the trunk region (fig. S2B, S8A). This occurrs because, during preservation, cephalic limbs generally rotated forwards, overlapping those behind them, while the posterior ones rotated backwards (figs. S2A–B, S8A). The upper branches show anterior imbrication only, suggesting limited ability to rotate the limb in the narrow space between the lower branch and the dorsal exoskeleton (figs. S2A–E, 8A–

C). The upper branches have limited rotation compared to the lower branches, and their range of movement was thus likely impeded.

Discussion

Dumbbell-shaped filament

An inflated marginal bulb is characteristic of crustacean gills, especially in those of decapods (fig. S9A–E). It provides both mechanical support for the respiratory lamellae and guides hemolymph circulation (Luquet *et al*. 2000; Astall *et al*. 1997), and may furthermore help keep the lamellae apart during gas exchange (Maina 1990). In some modern crustaceans the cuticle of the marginal bulb is thick relative to that of the inner filament region where respiratory exchange takes place. The filament of the upper branch of *T. eatoni* with its inflated marginal bulbs and narrow central region, mimics that seen in the gills of decapods. We posit that the inflated marginal bulbs supported the filament and provided channels for hemolymph circulation, and that the narrow central region was used in gas exchange (Fig. 4A). The inflated marginal bulbs may also have provided the additional function of maintaining space between adjacent lamellae similar to the knobs or nodules seen in various crustaceans (Goodman and Cavey 1990). In these living animals, deoxygenated hemolymph flows through the afferent channel to the tip of the filament, and then re-oxygenated hemolymph flows back through the upper efferent channel of the filament (Wirkner *et al*. 2013; Le Conte 1900) into the body cavity.

The dumbbell-shaped filaments in *T. eatoni* show a strikingly similar structure, and thus we infer that they channeled hemolymph in the same way. The afferent channel

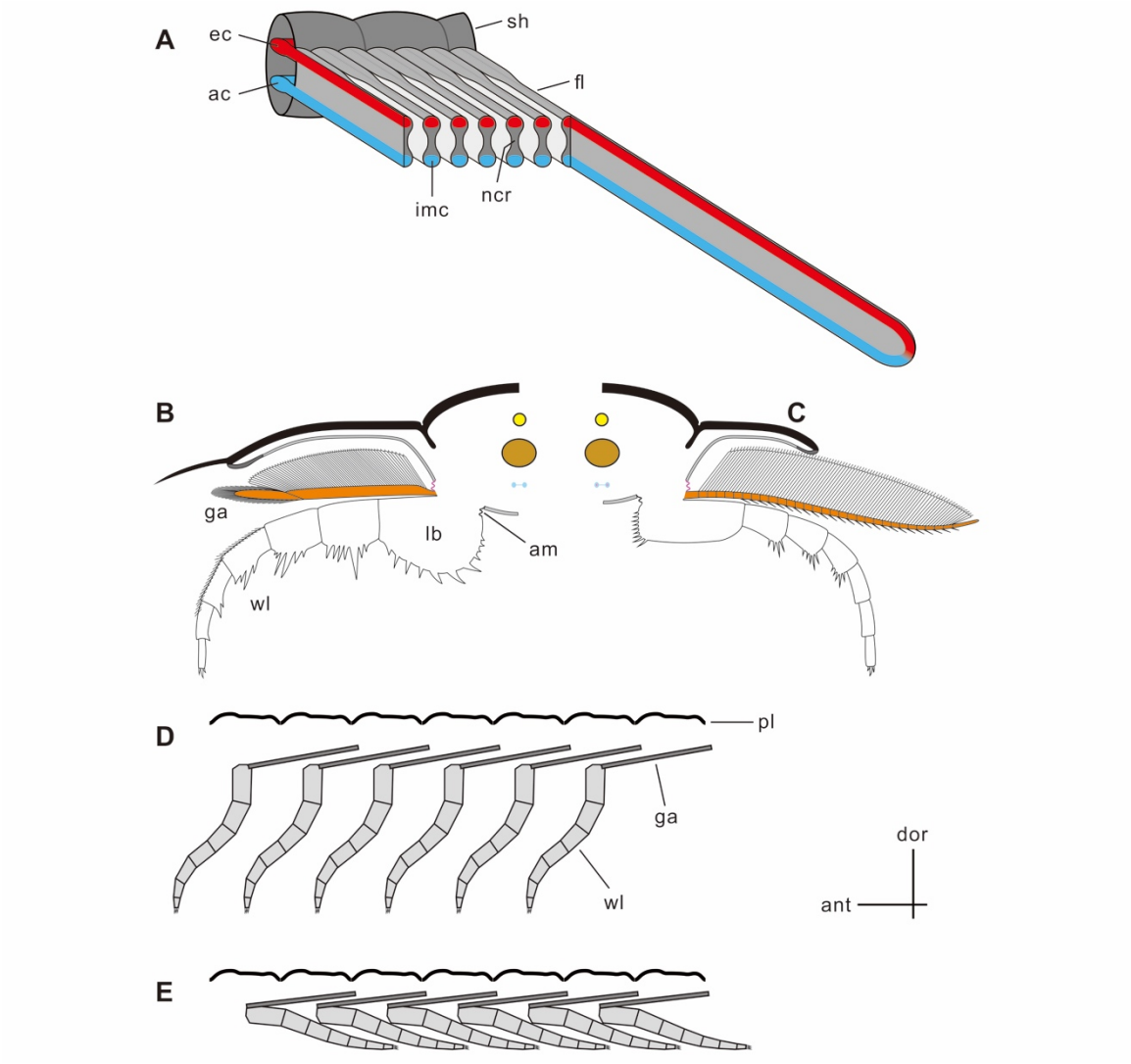
A
ec
sh
ac
fl
imc
ncr
B
C
ga
lb
am
wl
D
pl
ga
wl
dor
ant
E

Figure 4 – Reconstructions of trilobite limbs. (A) Filaments showing dumbbell-shaped cross-section with inflated marginal bulbs and narrow central region, of which the inflated marginal bulbs provide afferent and efferent channels (imc) and the narrow central region functioning for respiratory exchange. (B–C) Cross-section showing the upper branch connecting dorsally with the extended arthrodial membrane (purple color) and ventrally with the proximal limb base. The upper limb extended posterodorsally, as shown in figure 6. (B) Proposed articulation of *O. serratus* (modified from Ramsköld and Edgecombe (Ramsköld and Edgecombe 1996)); anterior view of right limb. (C) Proposed articulation of *T. eatoni* (modified from Whittington and Almond (Whittington and Almond 1987b)), anterior view of left limb. (D–E) Imbrication style of two branches limited the movement of the upper branch. (D) Upper branch showing anterior imbrication style, resulting from limited space for limb swinging. (E) Upper branches preserved in anterior imbrication style with lower branches preserved in posterior imbrication style. am, extended arthrodial membrane; ant, anterior; ac, afferent channel; dor, dorsal; ec, efferent channel; fl, filament; ga, gill appendage; imc, inflated marginal channel; lb, limb base; pl, pleura; ncr, narrow central region; sh, shaft; wl, walking leg.

is suggested to be located at the bottom of the filament and the efferent channel at the top (Fig. 4A). The loop built by both channels permits bulk flow of hemolymph. The narrow central area of the filament would have been the location for oxygen exchange. The cuticle in this region was likely thin as it is poorly preserved compared to the robust walls of the bulbs.

Comparable to the filaments in the euarthropods such as trilobites, the setal blades in the lower stem euarthropods, e.g. gilled lobopodians and radiodonts, have also attracted much attention and been widely suggested to have had respiratory function (Van Roy, *et al*. 2015; Daley, *et al*. 2009; Zhang and Briggs 2007; Briggs 2015). These blades are thin and flexible, show rounded termination and are displayed as fine lamellae (Van Roy, *et al*. 2015; Daley, *et al*. 2009). The setal blades, especially in *Opabinia regalis*, that attach either on the dorsal surface of the lateral lobe (Budd 1996; Budd and Daley 2012) and are suggested to also possess a haemocoelic channel (Budd 1996), or to the distal margin of the lateral lobe (Zhang and Briggs 2007). These structures are morphologically and functionally comparable to the filaments of the biramous arthropods, but the lateral lobe to which the blades attached apparently lacked internal muscles. The lateral, gill-bearing lobes in the lower stem euarthropods are considered to be homologous to the upper branch of biramous fossil arthropods (Budd 1996). Our results further strengthen this argument by establishing that the upper limb branch was a gill in *Triarthrus eatoni*. The limbs of basal stem Euarthropoda apparently represent an evolutionary stage before the fusion of the respiratory exite and the endopod that became the Paleozoic "biramous" limb (Van Roy, *et al*. 2015; Daley, *et al*. 2009).

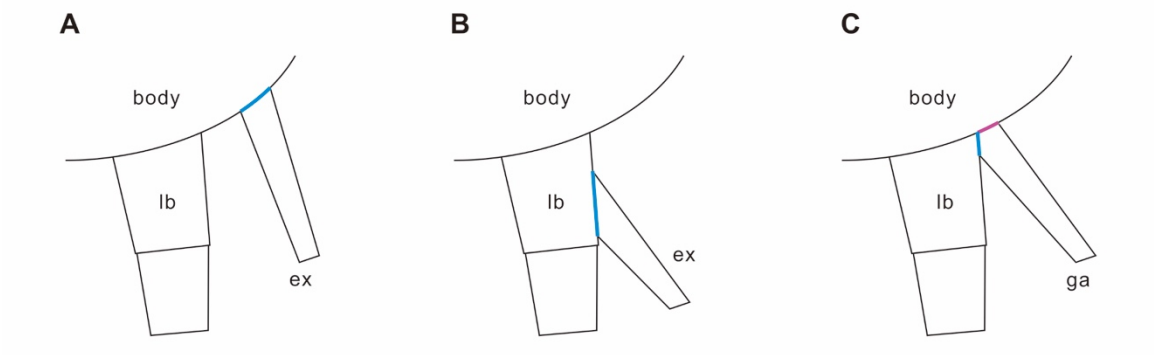

Figure 5 – Reconstructions of arthropod appendages. (A) Biramous limb of the Silurian chelicerate *Dibasterium durgae* with the exopod inserted (marked by blue color) separately and independently from the walking leg (Briggs *et al*. 2012). (B) Modern arthropodian biramous limb with exopod inserted (marked by blue color) at the limb base of the walking leg (Boxshall 2004). (C) Trilobite limb with gill appendage attached to both limb base ventrally (marked by blue color) and body wall dorsally by extended arthrodial membrane (purple color).

Articulation of the upper branch

The arrangement of the limb, determined from the posterior flattening of the upper branches in life position, results in minimum overlap between the two branches (fig. S8A–B). The limb base and upper branch are connected to the body with extended arthrodial membrane (Fig. 3A–J and fig. S8A–C). The connection between the upper branch and the arthrodial membrane shows that the upper branch was not purely an outgrowth of the limb base. The exopod originated either as an entity physically separate from the endopod (Fig. 5A) (Briggs, *et al*. 2012), or as an outgrowth of the main posterodistal limb axis (Fig. 5B) (Wolff and Scholtz 2008) - in which case it is a second

order structure. Details of the body-limb junction in fossil arthropods are poorly documented (Whittington 1975) because the margins of the two branches of the appendage tended to be superimposed during compaction. In *O. serratus*, the upper branch was attached to the inner, postero-dorsal edge of the limb base of the lower branch adjacent to the limb-body junction (Whittington 1980). The dorsal surface of the limb base is not preserved in this species, so that the nature of the limb-body junction is unknown, nor is its position on either the body or the limb base known (Whittington 1975). Two possibilities for the articulation of the lower branch and upper branch have been suggested, one is that the upper branch inserted at the distal postero-dorsal edge of the limb base (Whittington 1975, 1980) (Fig. 6A) in which case the upper branch articulated purely with the limb base, and the other is that the upper branch articulated along the entire postero-dorsal edge of the limb base (Ramsköld and Edgecombe 1996) (Fig. 6B). However, our observations show that the upper branch was clearly separate from the limb base in the area in which the upper branch connected with the arthrodial membrane (Fig. 3A–I and fig. S8A–C). This indicates that the upper branch was not connected with the distal postero-dorsal edge of the limb base, but rather connected with the proximal (or inner) dorsal edge of the limb base. The inner limb margins are usually poorly preserved because many structures, e.g. body wall, limb base, upper branch and arthrodial membrane, are superimposed when compacted. Most fossil specimens show fractured and truncated margins at this region after part and counterpart are split. Additional fossil evidence shows that truncated margins are also present in the artiopodian, naraoiid *Misszhouia*, but have not been recognized previously. In the original

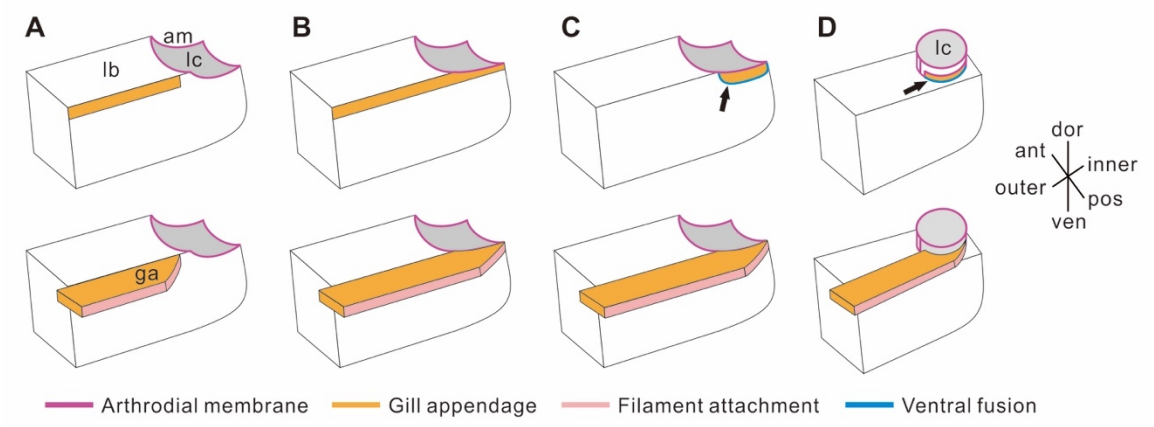

Figure 6 – Articulation of the upper branch. (A–C) Model articulation, viewed from posterior of left limb, of *Olenoides serratus*. (A) Upper branch connecting only with the posterior outer portion of the limb base. (B) Upper branch connecting with the full length of the limb base and the extended arthrodial membrane. (C) Our model showing the upper branch attached ventrally to the posterior inner portion of the limb base (marked by blue color pointed by a black arrow) and dorsally to the extended arthrodial membrane. (D) Model suggested for *Triarthrus eatoni* showing the upper branch connecting ventrally with both the inner portion of the limb base (marked by blue color pointed by a black arrow) and dorsally with the extended arthrodial membrane. Lower panel shows full reconstruction with upper branch in orange; upper panel shows limb base with only the articulation of the upper branch indicated in orange. Purple lines represent extended arthrodial membrane or limb cavity that is outlined by the extended arthrodial membrane. Blue lines indicated by black arrows show the trilobite upper branch attached to the lower branch ventrally. Pink strip indicates location of filament insertion. am, extended arthrodial membrane; ant, anterior; dor, dorsal; ga, gill appendage; lb, limb base; lc, limb cavity; pos, posterior; ven, ventral.

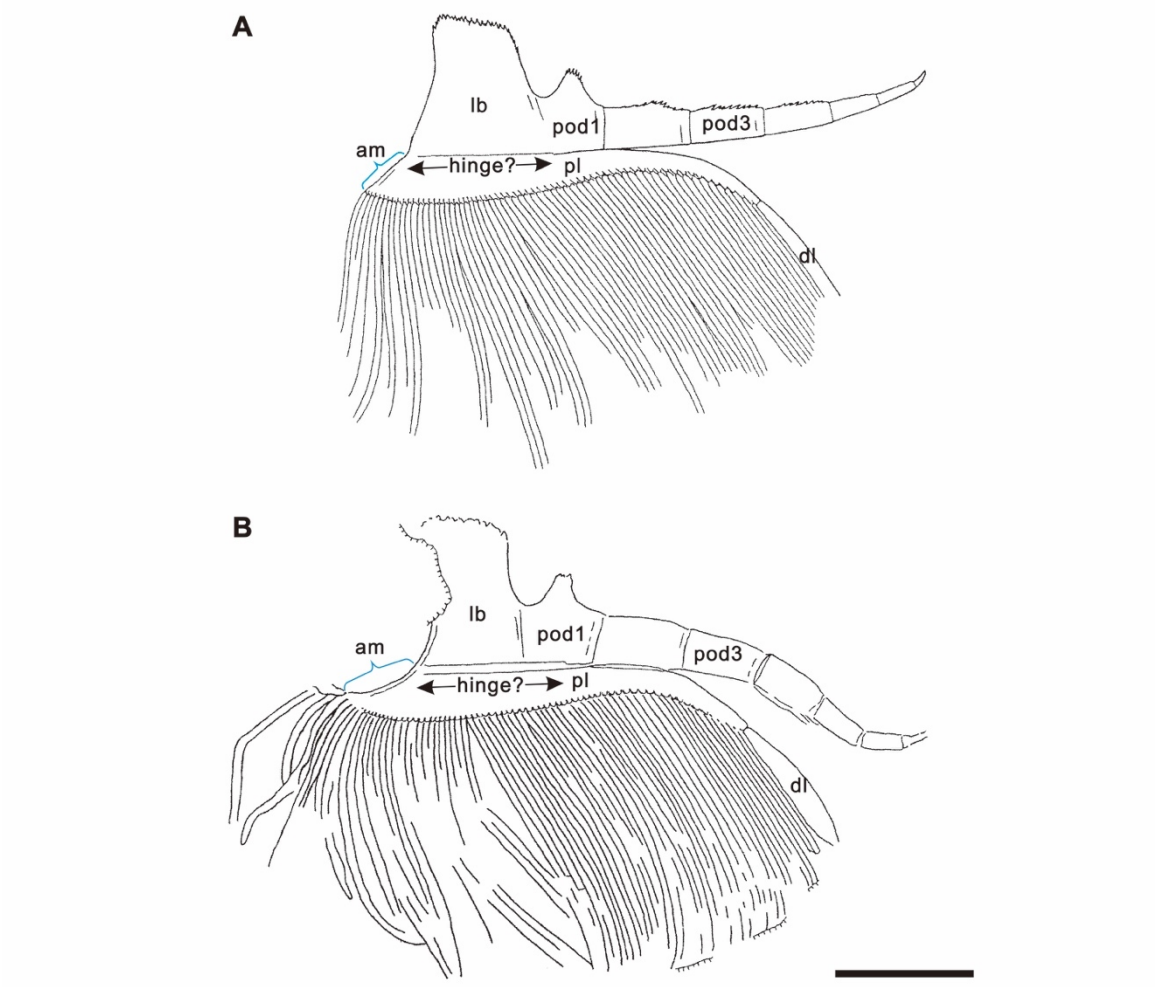

Figure 7 – Body-limb junction of the naraoiid *Misszhouia langicaudata*. (A–B) Isolated appendages with both upper branch and lower branch attached, modified from Chen et al. 1997 (Chen, *et al*. 1997). (A) No number available. (B) ELRC 1300a. Blue brackets mark the free margins of upper branches, which are articulated with extended arthrodial membrane. am, extended arthrodial membrane; dl, distal lobe of upper branch; lb, limb base (proximal segment of the lower branch); pl, proximal lobe of upper branch; po1-3, podomeres 1 to 3, respectively. Scale bars are 3 mm.

drawings (Chen, *et al*. 1997), a large, distinct area of the upper branch extends out of the limb base with an irregular curved margin (Fig. 7; marked by bracket), which provides additional evidence that the upper branch is attached to both the extended arthrodial membrane and the proximal limb base. The triangular to circular shape of the joint is preserved in a few specimens, in which wrinkles or annulations are present (Chen, *et al*. 1997). Additional evidence for the joint location is the gradual decrease in size of the setae towards the joint area, where they are absent. The common area between upper branch and lower branch consists of extended arthrodial membrane. The ventral part of the joint of the upper branch is thus apparently connected to the lower branch.

As *Misszhouia* and *Naraoia* are closely related with each other and distinguished mainly by the length ratio of the head and the trunk (Mayers *et al*. 2019; Bond and Edgecombe 2020), interpretations of *Misszhouia* may apply to *Naraoia* also. In an early reconstruction of *Naraoia* the upper branch was considered attached to the outer dorsal margin of limb base (Whittington 1977), but Zhang et al's fig. 30 (Zhang *et al*. 2007) suggests that the upper branch is attached entirely within the dorsal margin of the limb base. The evidence discussed here suggests this may not be the case. It has long been known that the upper branch is connected directly with the sclerotized limb base (Ramsköld and Edgecombe 1996), but naraoiid limbs show an apparently unarticulated area between the upper branch and the limb base, and that the proximal upper branch extends further inward than the limb base (Chen, *et al*. 1997; Hou and Bergström 1997). It means that the upper branch was not only connected with the limb base but was likely

also directly connected to the body-limb junction tissue via the extended arthrodial membrane.

Here we show that the extended arthrodial membrane pinpoints the location of the limb junction (Fig. 3A–I and S8A–C), which connects the limb to the body. This discounts the idea that the upper branch attached only to the limb base of the lower branch, because it was evidently attached both ventrally to the limb base of the lower branch and dorsally to the extended arthrodial membrane (Figs. 5C, 6C–D). The latter is a thin cuticle stiffened by chitin fibers (Hepburn and Chandler 1976) and used to connect rigid body segments, in this case the sclerotized upper limb, to the main body of the trilobite. The book gill of *Limulus* connects with the body in a similar way (Suzuki and Bergström 2008) and has been considered as the origin of the epipodite because the gill-bearing potion is located at the proximal limb base, rather than at the distal limb base where the exopod is typically attached (Suzuki and Bergström 2008). Regardless of the origin of the book gill in *Limulus* (Sharma 2017), this example is another case in which gill tissue is directly connected with the main body. The close connection between gill tissue and the main body may allow deoxygenated hemolymph to be easily transported to the gill tissues. This articulation might represent the ancestral junction type and this in turn would imply that in this trilobite gill tissues were not totally without direct connection to the main body. On the other hand, the articulation of the upper branch in *O. serratus* is also similar to that of the malacostracan arthrobranch gill, except that in malacostracans, the upper branch articulates only along the arthrodial membrane at the junction between the body and the thoracic limb (Boxshalll and Jaume 2009). The

appearance of gill tissues in this particular region in other arthropods shows that the gill structure can be present at the body-limb junction area.

Structural limitations of the upper branches

The upper branch of both trilobites was located between the ventral cuticle of the exoskeletal pleurae and the lower branch (Whittington 1975, 1980; Hessler 1985) (Fig. 4A–B) and, when viewed from the dorsal side of an animal facing anteriorly, its posterior branches appear to be consistently overlapped by anterior ones (Fig. 4D–E). The upper branches, characterized by this anterior imbrication style, suggest that the limbs may have been in their natural posture, positioned almost parallel to the plane of the dorsal exoskeleton, and also slightly tilted to permit the imbrication observed. This is because the upper branches are distinctly longer extrasagittaly than their associated dorsal segments. Movement of the upper branch was apparently limited to the space between the soft tissues adhering to the underside of the dorsal exoskeleton and the lower limb branch beneath it (Hessler 1985) (Fig. 4D–E), and this may have restricted the effectiveness of the limb for swimming. In *O. serratus*, the upper and lower branches are not preserved in an alternating, imbricated series, which might be expected at least occasionally if the upper branch had been able to rotate such that the lamellae were downwardly directed (Whittington 1980). The anterior imbrication of the upper branch would result in the majority of adaxial filaments being dorsal to those on more posterior limbs, suspended above the substrate, and thus unlikely to have been used in sediment processing. The posterior imbrication style of the lower limb branches, in which posterior structures cover

anterior ones in dorsal view, is much more common in the trunk region whereas anterior imbrication of the lower branches is more common in the cephalic region. Many early arthropods, such as *Misszhouia longicaudata* (Hou and Bergström 1997; Zhang, *et al*. 2007), *Naraoia compacta* (Whittington 1977), *Cindarella eucalla* (Ramsköld *et al*. 1997) and *Xandarella spectaculum* (Hou and Bergström 1997), display the same condition, with the upper branches showing anterior imbrication while the lower branches show both anterior and posterior imbrication. This difference may suggest that the cephalic lower branches and trunk lower branches displayed mechanical differences in that the cephalic lower branches tend to rotate forward, and the trunk lower branches backward, as is evident in some contemporary arthropod trace fossils (Seilacher 1990). The contrasting arrangement of the upper (only anterior imbrication) and lower (anterior and posterior imbrication) branches would have limited the range of movement possible for the upper branch. Such a limitation presumably protected the gill filaments and likely allowed better aeration but restricted the contribution of the upper branch toward locomotion.

Implications for the comparative biology of arthropod appendages

The underside of the trilobite pleural lobes has been proposed as the logical location for respiratory organs (Suzuki and Bergström 2008) because trilobite "exopodal" filaments have been thought to lack structures indicative of respiration (Suzuki and Bergström 2008; Haug and Haug 2016). Such reasoning also led to the upper branch being considered homologous with the exopod of modern arthropods (Walossek 1993; Walossek and Müller 1990). Here we have shown that both the physical structure of the

dumbbell-shaped filament, and its resemblance to known gill lamellae of living mandibulate arthropods (Fig. 4A), indicate that it performed gill function in trilobites. Fusion of the upper and lower branches is similar to that in the malacostracan arthrobranch gill and the book gill of *Limulus* (Figs. 4B, 5C) in that part of the upper branch is joined directly to the body wall, distinguishing it from the typical junction between the exopod and the limb base. The range of movement of the upper branch may have been relatively limited but sufficient for gill aeration (Fig. 4D–E). In particular, our interpretations support the idea that movement of the upper branch and lower branch during locomotion would have persistently forced water between the filaments of the upper branch in the animal (Whittington 1975). Thus the evidence presented indicates that the upper branch primarily served a respiratory function (Fig. 4A–E).

Based on its respiratory function and direct junction with the body along part of its length, we suggest that the trilobite upper limb branch may be homologous to the dorsal flap of gilled lobopodians, and that both may have shared respiratory function. Attachment of the upper branch or dorsal flap to the body wall characterized basal stem Euarthropoda, e.g. Radiodonta (Van Roy, *et al*. 2015; Daley, *et al*. 2009), and may have evolved independently in early Chelicerata (Briggs, *et al*. 2012), but is distinguished from the typical derived euarthropod exopod that is directly connected only to the protopodite (i.e. basis or coxa). Although the transition from independent attachment to complete fusion with the limb base has been theorized (Van Roy, *et al*. 2015; Daley, *et al*. 2009), evidence of an intermediary stage has not been forthcoming to date. Here the shared articulation of the upper branch with both the proximal limb base and body wall, as

shown here, may represent an intermediate condition prior to complete merger of two branches in more derived forms. The "biramous" or dichotomic limb in Trilobita thus may have resulted from the fusion of a walking leg with a respiratory appendage (Fig. 4B–E). This is consistent with the theory that the limbs of more basal stem Euarthropoda represent an evolutionary stage before the fusion of an exite and the endopod to form the Paleozoic "biramous" limb (Van Roy, *et al*. 2015; Daley, *et al*. 2009). Because of the dependence on specific and exceptional preservational modes, our observations on the limb-body junction are currently limited to a single trilobite species, *O. serratus* (the nature of pyrite replacement precludes the preservation of this feature in the *T. eatoni* material examined, but preliminary investigation of the naraoiid *Misszhouia* may suggest a similar style of attachment, see Fig. 10). New discoveries will be required to determine if the attachment of the upper limb to both the limb base and the body wall is indeed a trilobite synapomorphy and/or an intermediate state in an evolutionary trend toward complete fusion with the limb base.

The early Paleozoic evolutionary arms race (Trestman 2013; Hughes 2007; Edgecombe and Legg 2014; Vermeij 1987) was characterized by increasing exoskeletal regionalization and thicker, more robust armor with specialized joints. The latter would have limited the effectiveness of a distributed system of cuticular diffusion, which is restricted to small sized animals (Graham 1990). At larger sizes increased metabolic demand for oxygen exceeds that provided by cuticular diffusion alone (Mill 1972), and requires specialized respiratory organs as are apparent in the setal blades of Radiodonta (Van Roy, *et al*. 2015; Briggs 2015; Budd 1996; Daley, *et al*. 2009). Here we reveal

details of gill structure among early arthropods that were acquiring an increasingly reinforced exoskeleton.

Supplementary figures

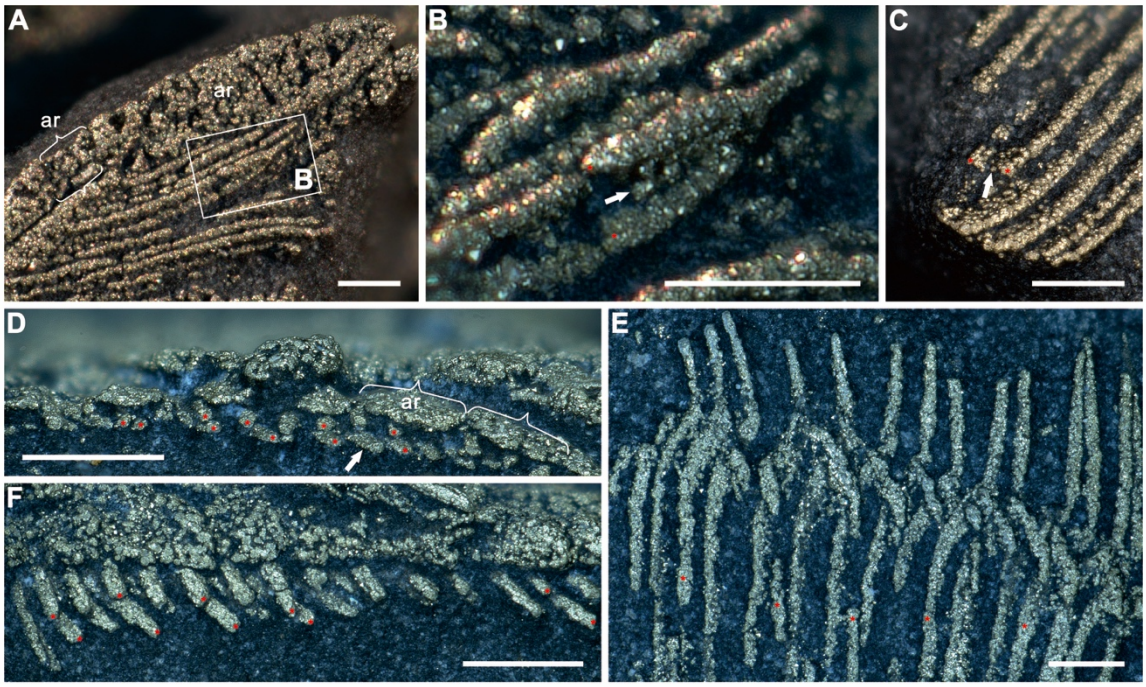

Figure S1 – Dumbbell-shaped filaments of *Triarthrus eatoni*. (A–G) All figures, except for B, are applied with stack function, GLAHM 163103. (A) Distal region of upper branch showing distal shaft article on the upper left corner; filaments parallelly attached along the posterior margin of the shaft and inclined to the bedding plane. (B) Enlargement of area with more oblique lighting than in figure A to show inflated marginal bulbs connecting by narrow central region (marked by white arrow) of filament. (C) Posterolateral view of filaments, of which one single filament shows a truncated cross-section with dumbbell-shaped outline. (D) Posterior view of truncated filaments to show inflated marginal bulbs, of which one marginal bulb (marked by a white arrow) thins from the marginal bulb (right side) to the narrow central region (left side). (E) Ventral view of distal region of filaments showing only the inflated marginal bulbs

overlapping with each other; distal spines of the filaments are clearly evident. (F) Posterior dorsal view of filaments showing paired inflated marginal bulbs. Asterisks locate the top and bottom inflated marginal bulbs of filaments. Brackets are used to mark articles of the shaft. ar, article of shaft. Scale bars, 200 μm (A, C–F), 100 μm (B).

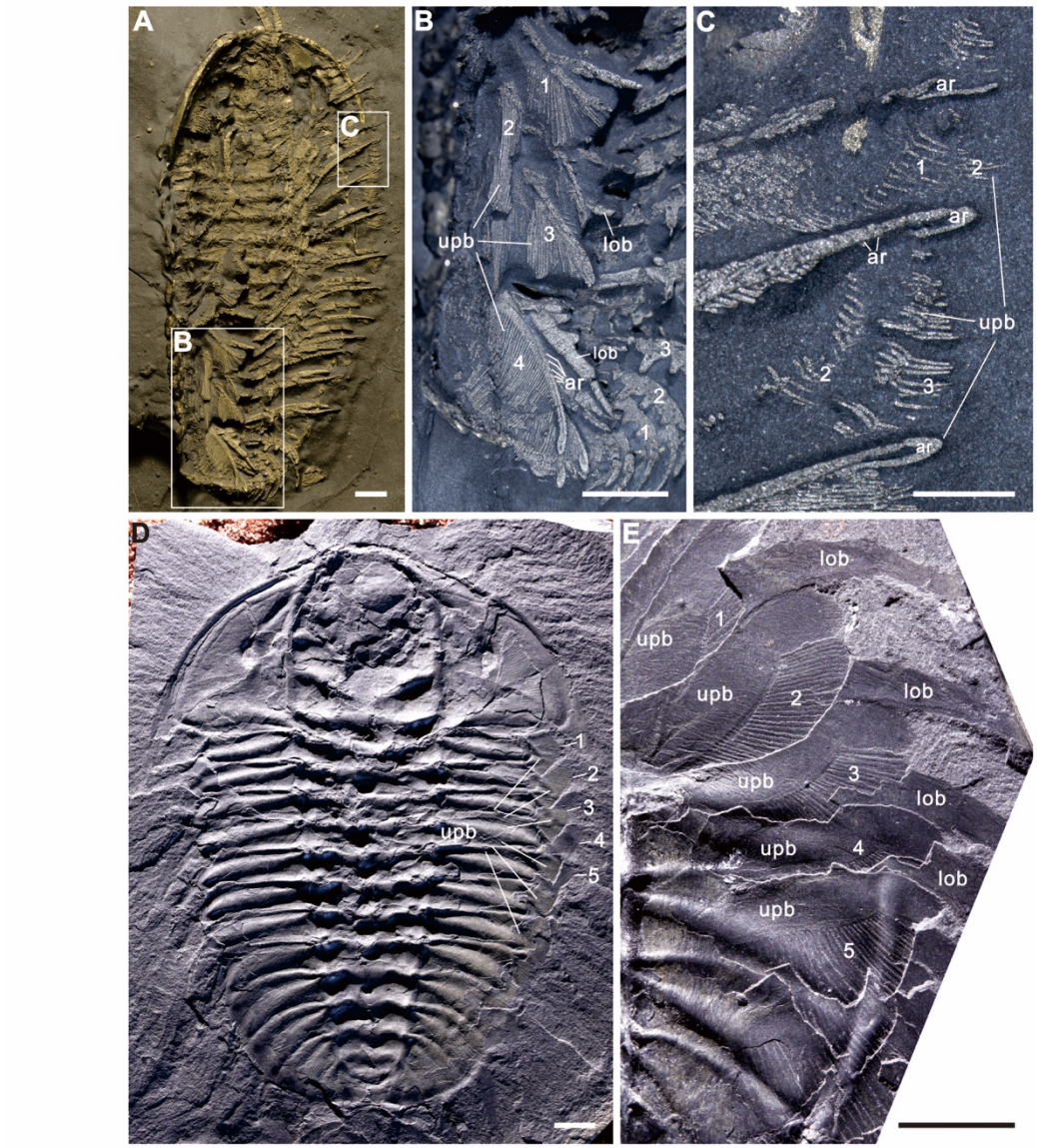

Figure S2 – Imbrication style of limb. (A–C) *Triarthus eatoni* showing the upper branch with anterior imbrication style and lower branch with posterior imbrication style, GLAHM 163103 (part; laterally compressed). (B) Light incident from upper-right direction; numbers on left side refer to upper branch and on lower right corner refer to lower branch. (C) Light incident from upper-left direction and stack function applied; ventral view of ventral surface of filaments showing the anterior imbrication style; the

filaments are preserved with distal part that bears a single spine. (D) Light incident from upper-left direction; ventral view of ventral surface of *Olenoides serratus* showing the upper branch with anterior imbrication style, USNM 273246 (counterpart); viewed from ventral surface, the small number is located at a layer beneath the layer marked with a large number. (E) Light incident from top of image; ventral view of ventral surface of *O. serratus* showing the upper branch with anterior imbrication style, USNM 65514 (counterpart). Anterior toward the top of all images. Small Arabic number is on a layer above the layer with the large number in the dorsal view of the animal. ar, article of shaft; lob and upb, lower and upper branches of the limb. Scale bars, 5 mm (A–B, D–E), 2 mm (C).

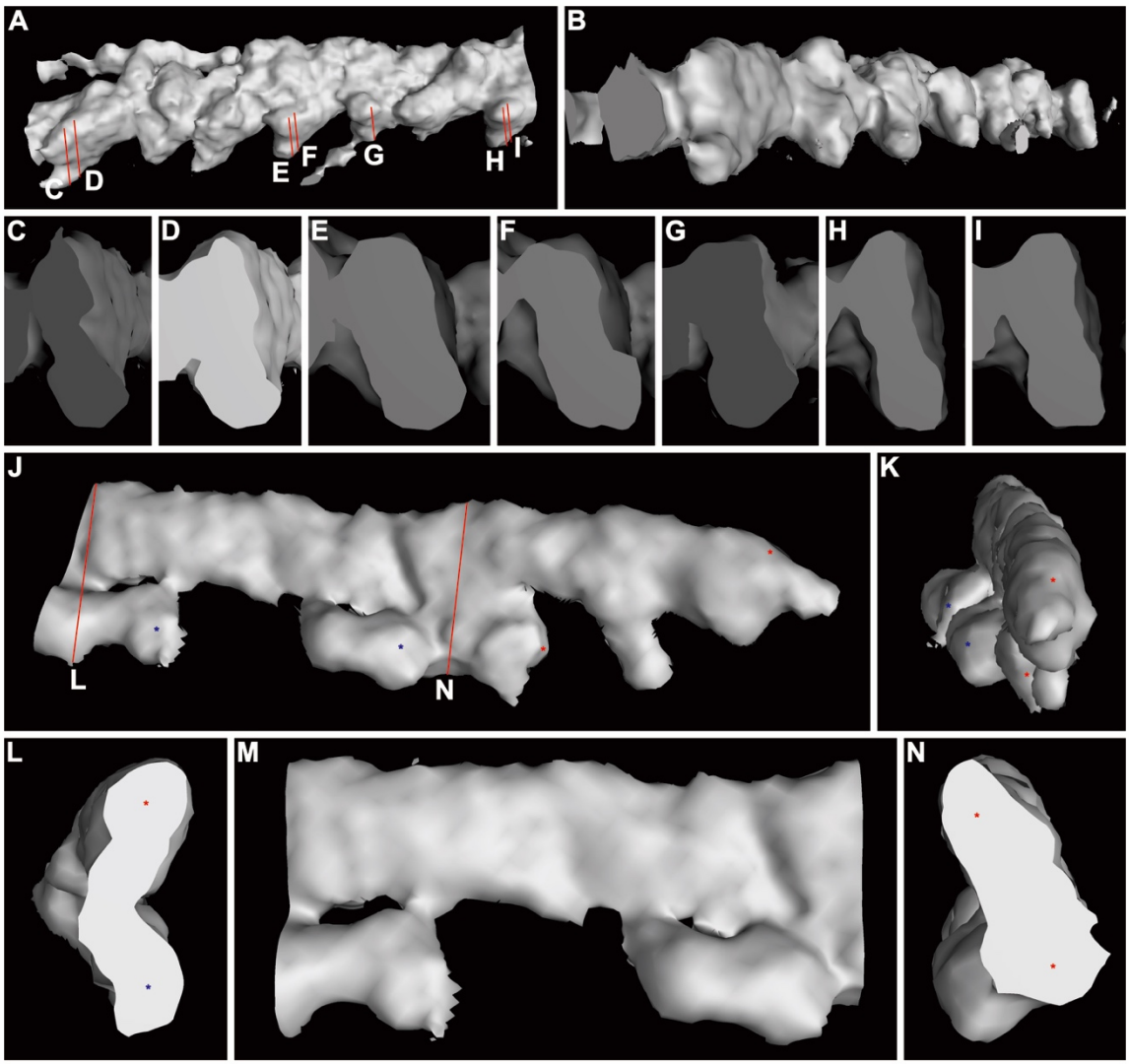

Figure S3 – Dumbbell-shaped filaments of *Triarthrus eatoni*. (A–N) CT-reconstruction of filaments showing dumbbell-shaped cross sections, AMNH 101394. (A) Dorsal lateral view showing the upper branch with filaments truncated by breakage. (B) Posterior view showing the outline of truncated filaments. (C–I) A series of cross sections of filaments (marked by red lines in figure 3A) showing the dumbbell-shaped outline, in which inflated marginal bulbs are wider than the narrow central region. (J–N) Filament cross-sections are distinguished based on taphonomic analysis. (J) Lateral view showing two

filaments merged together due to taphonomy. (K) Posterior view showing two filaments are distinguished based on the positions of marginal bulbs. (L) Cross section (left side of figure M) showing two filaments merged together; if viewed dorsally, these two filaments cannot be distinguished from each other. (M) Lateral view of same filament with two cross sections (figure L and figure N) on both sides. (N) Cross-section (right side of figure M) showing dumbbell-shaped filament. Asterisks indicate the paired inflated marginal bulbs of filaments. Same color of asterisks represents the same filament.

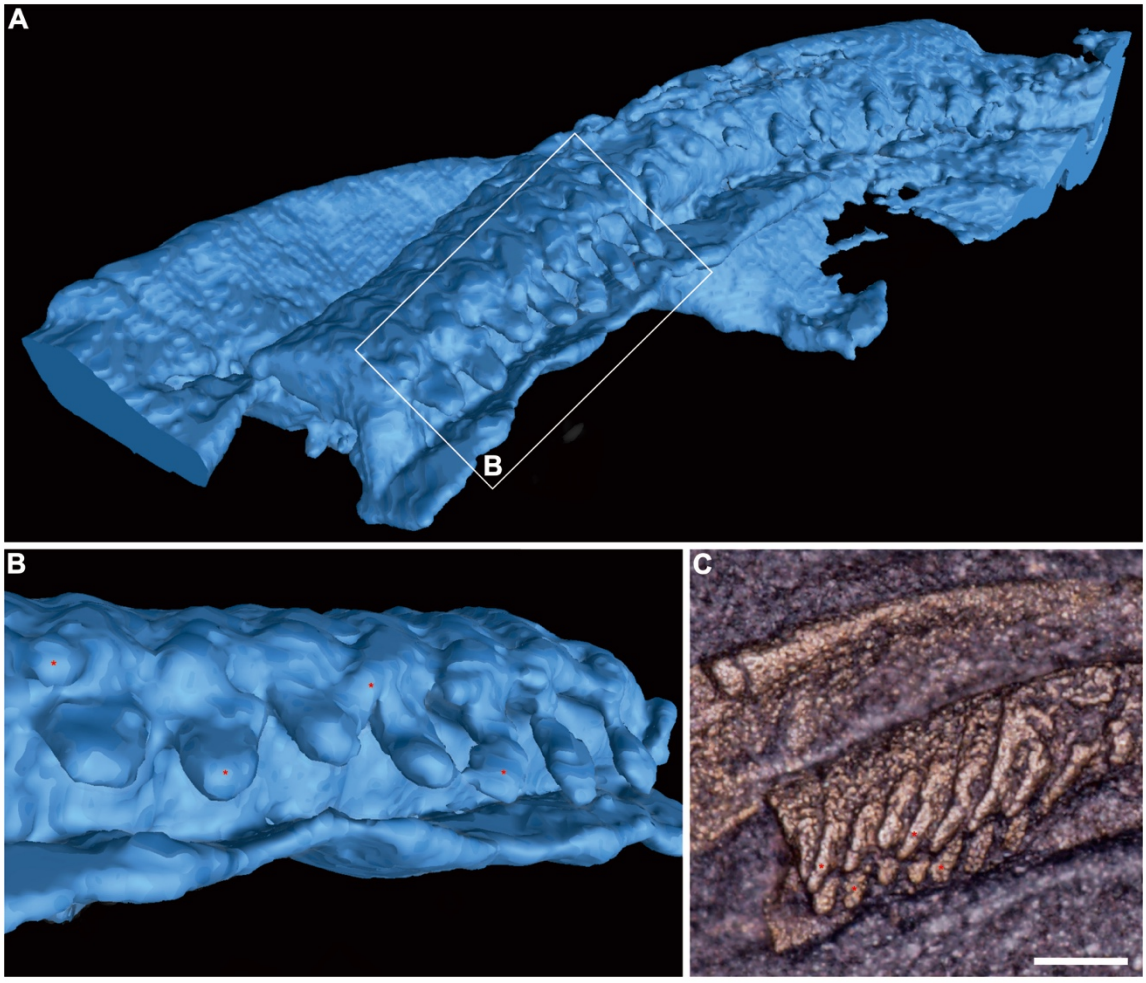

Figure S4 – Truncated filaments of *Triarthrus eatoni*. (A–C) Upper branch bearing a series of filaments with truncated proximal part, USNM 65527. (A) Dorsal lateral view of CT-reconstruction showing truncated filaments. (B) Posterior view of CT-reconstruction showing filaments with protrusion of inflated marginal bulbs. (C) Stack function applied; dorsal view of filaments showing filaments parallelly inclined to the bedding plane with distinct marginal bulbs which are separated from each other. Asterisks pinpoint the paired inflated marginal bulbs of the filaments. Both left and right pairs of asterisks represent two individual filaments. These two pairs of marginal bulbs show how the filaments are

inclined parallel to the bedding plane with the result that the marginal bulbs of each filament are mixed in dorsal view. The CT-reconstructions provide a direct way to distinguish the filaments and recognize the relationship between them. Scale bar, 200 μm (C).

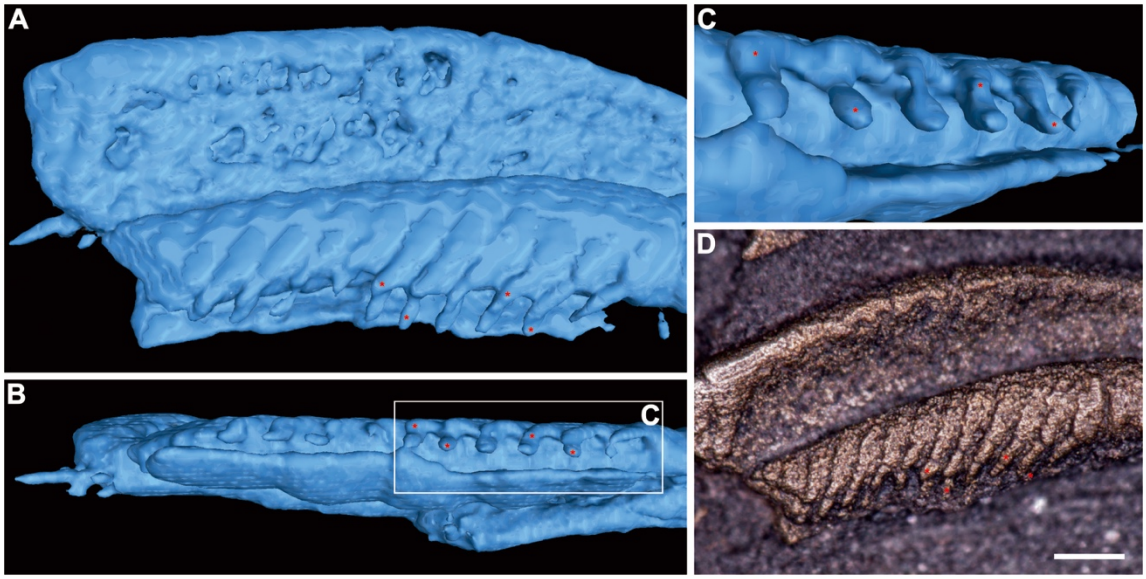

Figure S5 – Truncated filaments of *Triarthrus eatoni*. (A–C) Upper branch bearing series of filaments with truncated proximal parts, USNM 65527. (A) Dorsal view of CT-reconstruction showing filaments parallelly inclined to each other with inflated marginal bulbs. (B) Posterior view of CT-reconstruction showing inclined filaments merged with each other so that the marginal bulb of one filament is fused with the marginal bulb of the other. (C) Enlargement of white box in figure B to show the inclined fused filaments. (D) Stack function applied; dorsal view in digital image to show relative position of filaments in CT-reconstructions. Asterisks indicate the top and bottom inflated marginal bulbs of filaments. Both left and right pairs of asterisks represent two individual filaments. These two pairs of marginal bulbs show how the filaments are parallelly inclined to the bedding plane and result in the mixed marginal bulbs in dorsal view. The CT-reconstructions provide a direct way to distinguish filaments and recognize the relationship between them. Scale bar, 200 μm (D).

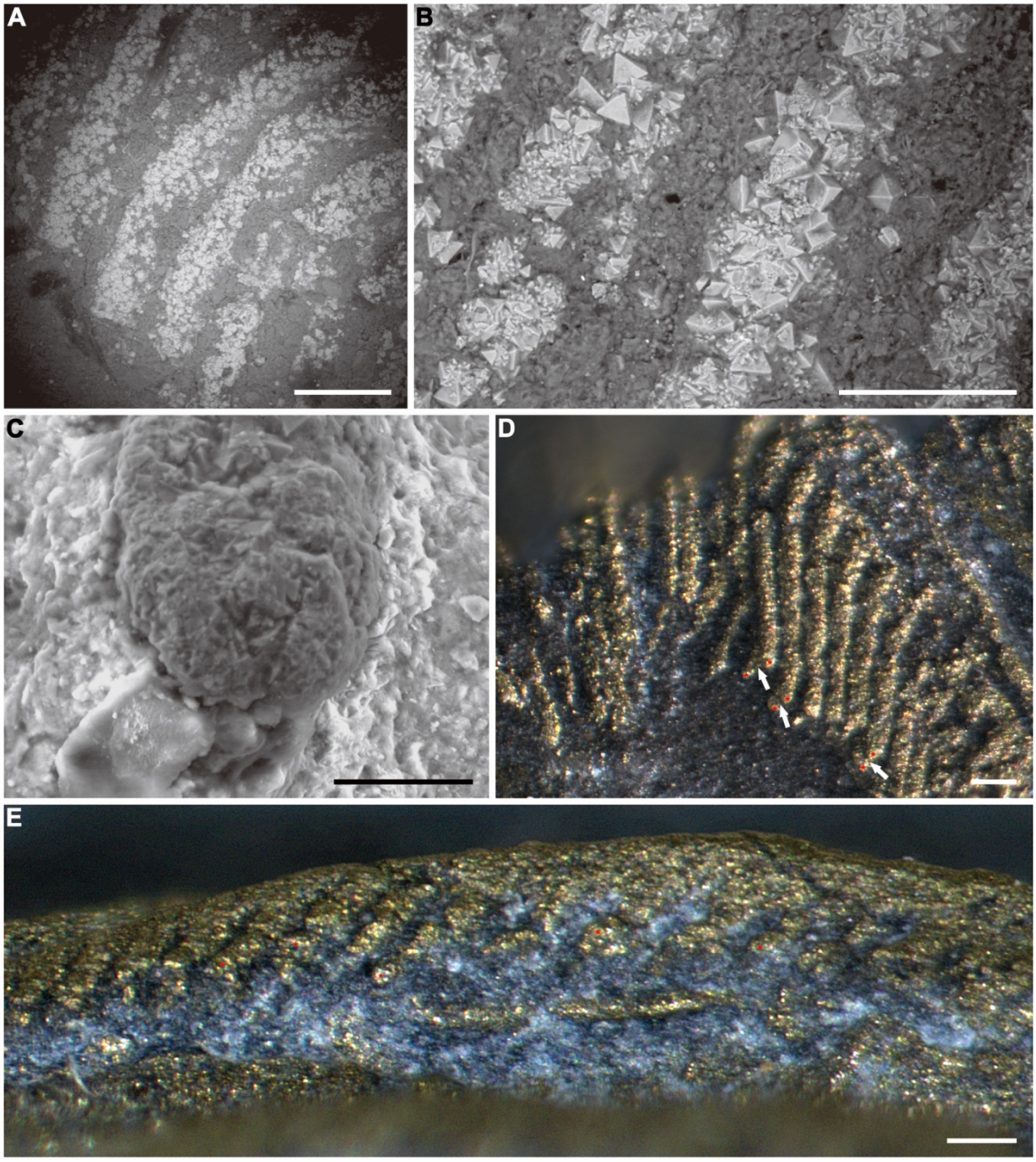

Figure S6 – Filaments of *Triarthrus eatoni*. (A–B) BSE image showing that filaments (bright color) are parallelly inclined to the bedding plane from dorsal view and separated from each other by surrounding matrix (dark color), YPM 226 (part). (C) GSE image showing a single filament (dark color) with only one inflated marginal bulb from dorsal

view, YPM 228. (D) Stacked image (posterior lateral view) of YPM 228 showing truncated filaments with paired inflated marginal bulbs and narrow central region. (E) Stacked image (posterior view) of YPM 204 showing only the top inflated marginal bulbs of filaments. Asterisks indicate the top and bottom inflated marginal bulbs of filaments. Small white arrows indicate the narrow central region of filament. Scale bars, 100 μm (A, D, E), 50 μm (B), 20 μm (C).

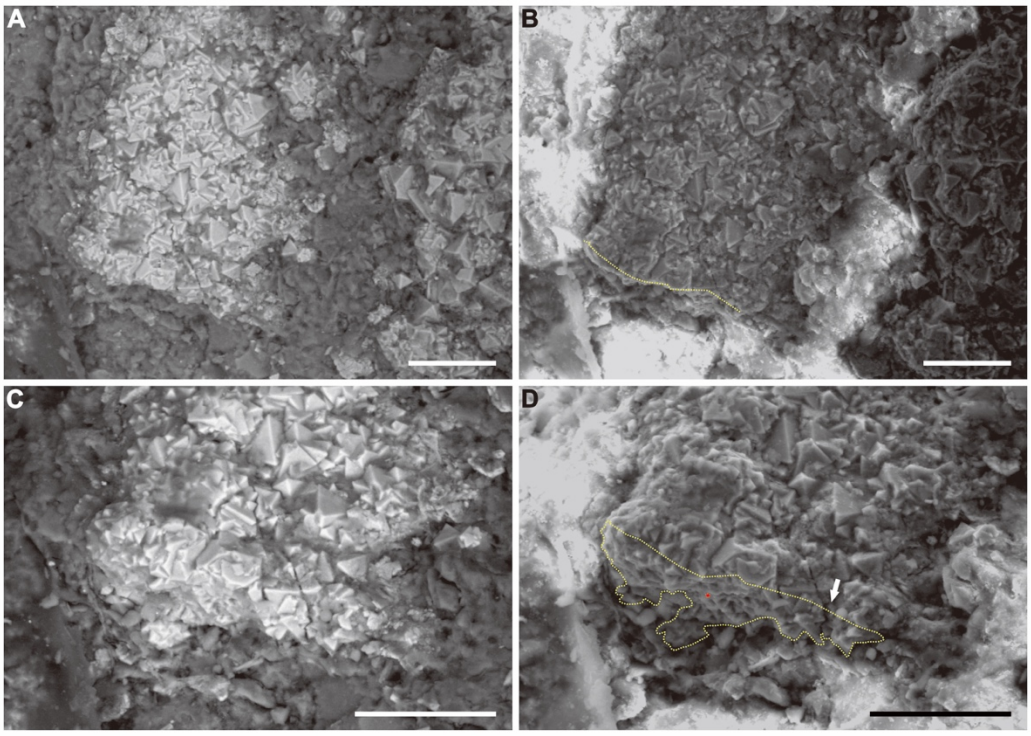

Figure S7 – Cross-section of filament of *Triarthrus eatoni*. (A–D) A single filament viewed from different angles and image techniques to show the morphology of its cross section, YPM 226. (A–B) Dorsal view of the filament showing only the top margin of its truncated cross section at bottom left side. (C–D) Posterior lateral view of filament, tilted about 40º to the top view, showing one inflated marginal bulb (marked with asterisk and on left side) thinning toward the narrow central region (on right side). BSE images (A, C) show the bright-colored filament from dark-colored surrounding matrix. GSE images (B, D) distinguish the dark-colored filament from bright-colored surrounding matrix. Yellow dashed lines are used to mark the cross-section of the filament. Red asterisk indicates the inflated marginal bulb of the filament. White arrow indicates the narrow central region. Scale bars are all 20 μm.

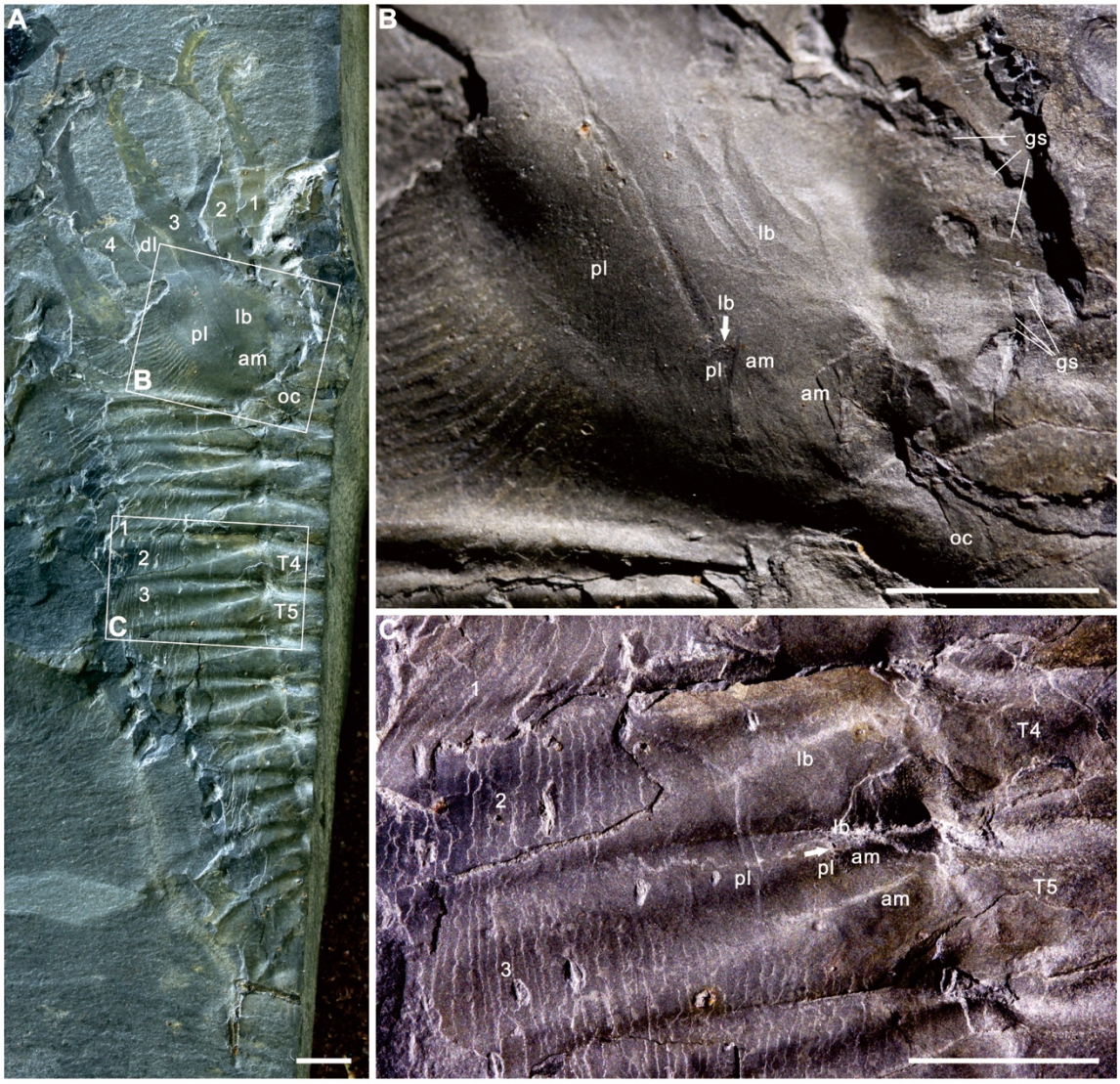

Figure S8 – Limbs of *Olenoides serratus*. (A–C) Anterior of specimen at top of image and dorsal view of the animal, USNM 65513 (part). (A) Light incident from upper left direction; lower branches rotated forward to display anterior imbrication style (Arabic numbers in the head region), and upper branch extending backward to display anterior imbrication style (Arabic numbers in the white box). (B) Light incident from upper right direction; close-up of the left cephalic "biramous" appendages in white box of figure A

showing the upper branch connected with the extended arthrodial membrane and separated from the lower branch by a boundary (marked by white arrow); the body-limb junction is close to the lateral occipital ring furrow. (C) Light incident from upper left direction; close-up of the left 5th thoracic appendages showing the upper branch connected with the extended arthrodial membrane and separated from the lower branch by a boundary (marked by white arrow). The body-limb junction is close to the lateral junction of the 4th and 5th axial rings, where the apodeme is located. Arabic numbers in this figure are all representing that the small number is in a layer above the layer with a large number. am, extended arthrodial membrane; gs, gnathobasic spine; lb, limb base; oc, occipital ring; pl, proximal lobe. Scale bars are 5 mm.

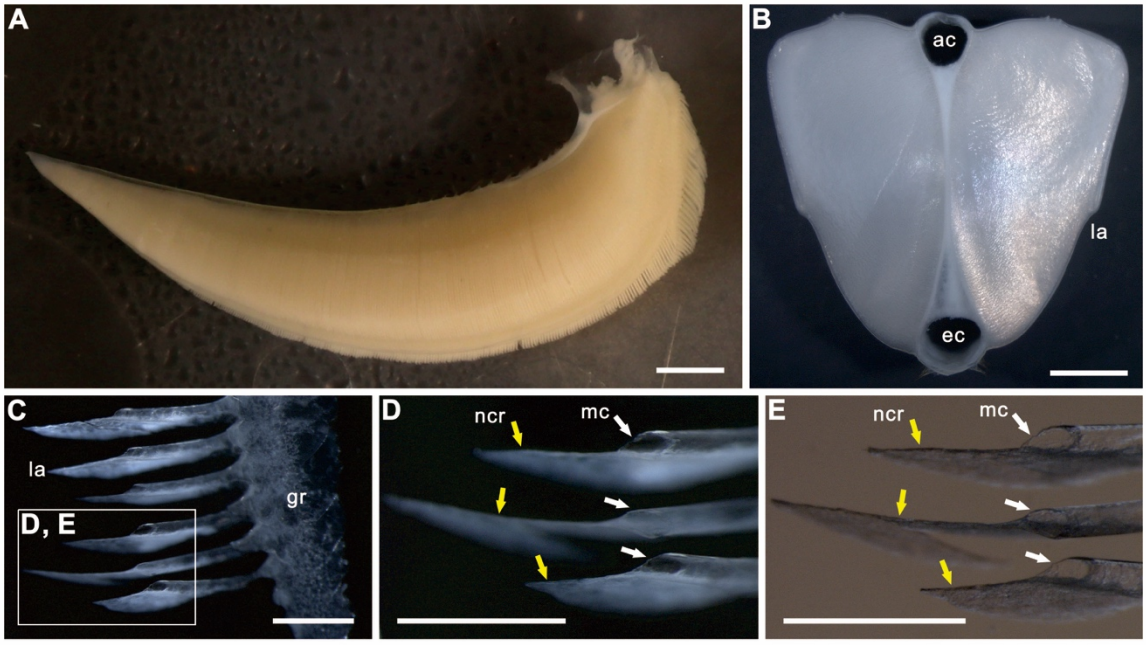

Figure S9 – Gills of the modern crab *Cancer (Metacarcinus) anthonyi*. (A) A complete gill branch showing series of gill filaments. (B) Cross cutting of a gill branch showing the morphology of filaments, afferent and efferent channels. (C) Gill lamellae showing cross sections of filaments with inflated marginal channels and narrow central region. (D–E) Enlargement of white box in figure C with different angles of illumination to show the gill lamellar structure with inflated marginal channels (marked by white arrows) and narrow central region (marked by yellow arrows). ac, afferent channel; ec, efferent channel; gr, gill raphe; la, lamella; mc, marginal channel; ncr, narrow central region. Scale bars, 5 mm (A–B), 1 mm (C–E).

CHAPTER 2. EFFICIENT COUNTERCURRENT GAS EXCHANGE ESTABLISHED AMONG EARLY METAZOANS

Abstract

The complex, large anatomies of early metazoans required that they respired oxygen, but the processes through which early animals obtained oxygen are barely known. Recently discovered, well-preserved gill structures in Paleozoic fossils provide opportunities to investigate this issue. Here we explore the respiratory mechanism of trilobite gills by considering how their morphology functioned to permit oxygen exchange. Inclination of the trilobite upper branch protected the respiratory filaments above their shaft and below the exoskeletal pleurae and associated soft tissues. Upward and forward rotation of the upper branch forced water between its filaments, forming a downward and backward flowing water current. Absorption of oxygen through the thin cuticle in the middle of each filament allowed absorbed oxygen to concentrate toward the top of each filament, resulting in a deoxygenated-to-oxygenated hemolymph gradient from the base of each filament to its top. The opposite directions of water current and hemolymph flow thus formed a countercurrent exchange system, comparable to systems observed in modern fish and crabs, that efficiently improved the oxygen uptake ability. The newly reconstructed gills of the deuterostome *Yunnanozoan* from the early Cambrian are comparable and also similar to modern fish gills, and accord with the countercurrent exchange mechanism inferred for trilobites. Thus evidence from both an early protostome and early deuterostome indicate that this highly efficient respiration mechanism was

already established in multiple metazoan lineages by the early Cambrian, suggesting that the countercurrent exchange mechanism was an early innovation in triploblastic diversification.

Introduction

The evolution of both oxygenation and life in the oceans have been closely interconnected throughout almost all of Earth's history (Lyons, *et al*. 2014) and the rise of early animals evidently correlates with a marked rise in the level of free oxygen (Knoll 2011; Sperling *et al*. 2013). Oxygen's reactivity facilitates highly complex series of reactions and, when effectively harnessed, ultimately permits the development of tissues, each specialized for particular functions. Effective transportation of oxygen throughout a body thus enables the development of large size and complex body structures and habits, such as mobility. As organismal volume and functional regionalization increased, the simple diffusion mechanism relied on in diploblastic and more basal metazoan groups gained assistance from, and eventually replacement by, dedicated solutions for transporting respiratory molecules deeper into the body and out again (Mill 1972). This is not only required an internal system for circulating oxygen and carbon dioxide, but also an effective interface for maximized exchange of both molecules between the external environment and the body's internal fluids.

A circulatory system that transported oxygen within metazoan bodies likely first appeared in the most basal of triploblasts, the protostome-deuterostome common ancestor (Monahan-Earley *et al*. 2013), and the extensional gill structures are convergently

evolved in different groups of the protostomes and deuterostomes. Paleozoic fossil Lagerstätten (Beecher 1895; Briggs, *et al*. 1994; Briggs *et al*. 1996; Müller and Walossek 1987; Shu, *et al*. 1999; Van Roy, *et al*. 2010; Yang, *et al*. 2013) have yielded large numbers of soft bodied fossils that have illuminated the early evolution of metazoans. The exquisitely preserved gill structures in some of these creatures provide the opportunity to decode the mechanisms that certain of these animals employed in oxygen uptake. Gill-bearing protostomes include arthropods and mollusks, of which the Paleozoic arthropods have preserved with a variety of gill structures, e.g. setal blades in the gilled lobopodians and the radiodonts (Budd 1996; Daley, *et al*. 2009; Van Roy, *et al*. 2015; Zhang and Briggs 2007; Briggs 2015), book lamellae in chelicerates (Briggs, *et al*. 2012; Aria and Caron 2019), and filaments in artiopods (Whittington 1975; Whittington and Almond 1987b; Williams, *et al*. 2011; Hou and Bergström 1997). Gill-bearing stem group deuterostomes also have a particularly good fossil record (Shu *et al*. 2003a; Ou *et al*. 2012) as do early chordates (Shu, *et al*. 1999; Shu *et al*. 2003b; Zhang and Hou 2004; Conway Morris and Caron 2014). These exquisitely preserved gill structures offer considerable insight into how oxygen uptake was mitigated.

Trilobites are Paleozoic arthropods that bear distinctly recognizable respiratory filaments on the upper branch (Whittington 1975; Bruton and Haas 2003; Hou *et al*. 2021). Through analyzing the structure of the trilobite gill branch, we can suggest how the hemolymph was charged with oxygen. Furthermore, the evidence from the early deuterostomes also shows an analagous charging system to that inferred in trilobites and observed in modern fishes. Evidence thus suggests that efficient oxygen charging was

established early in triploblast evolution, although apparently independently among different lineages of triploblasts.

Materials and methods

Materials described in this paper are housed in the Early Life Institute (ELI), Northwest University, China; The Hunterian Museum, University of Glasgow (GLAHM), UK; Yale Peabody Museum of Natural History (YPM), Yale University, USA. They are available for further research.

The pyritized specimens of *Triarthrus eatoni* are from the Beecher's Trilobite Bed of the Upper Ordovician Katian (or Caradocian) Frankfort Shale of upper New York State, USA and the Upper Ordovician Whetstone Gulf Formation ("Martin Quarry") (Briggs, *et al*. 1991; Farrell, *et al*. 2009). The Yunnanozoan *Haikouella jianshanensis* is from the Chengjiang Biota of the early Cambrian Heilinpu Formation in Haikou, near Kunming, China (Shu, *et al*. 2003a).

The specimens were photographed by the Canon EOS 50D, Leica MZ16 with DFC420 lens, Leica M205C with DFC 700T lens, and PHILIPS XL-30 Environmental Scanning Electron Microscope (ESEM). The Leica M205C is installed with stack or non-stack function. ESEM is used with both of backscattered-electron (BSE) and gaseous secondary electron (GSE) technique, which are described in the figures. As specimens are captured with different directions of light to show particular structures, the details are given in the image of the figures. Figures were prepared using CorelDRAW 2018.

Results and discussion

The circulatory system of arthropods can be simply divided into vascular and lacunar parts (Wirkner, *et al*. 2013), of which the latter includes accessory pulsative organs that supply hemolymph to different body parts and is the central focus of this paper. The recently determined gill structures in trilobites show a well-constructed afferent and efferent transporting system, comparable to the lacunar system of modern decapods (Hou, *et al*. 2021). The lacunar system in trilobites allowed deoxygenated hemolymph flowing through the afferent channel to be oxygenated, and then pass along the efferent channel back to the heart by an inferred pericardial sinus, a structure present in modern decapods (Wirkner, *et al*. 2013; McMahon 2001).

Stroke of the upper branch

The trilobite upper branch extended and flattened posterior-dorsally. The shaft formed the anterior of the upper branch and filaments attached to its posterior margin (Fig. 8A, B). The upper branch, characterized by anterior imbrication style (Hou, *et al*. 2021), indicates that the limbs, in their relaxed posture, were positioned almost parallel to the plane of the dorsal exoskeleton, and have been slightly tilted to permit imbrication (Fig. 8A, B). The trilobite gill shaft and filaments lay nearly parallel to the plane of the exoskeleton, a condition quite different from gills in some modern decapods that are protected within chambers. Here we consider the upper branch to contain the main ventilatory role for oxygen uptake, but it possible that this was augmented elsewhere in the body.

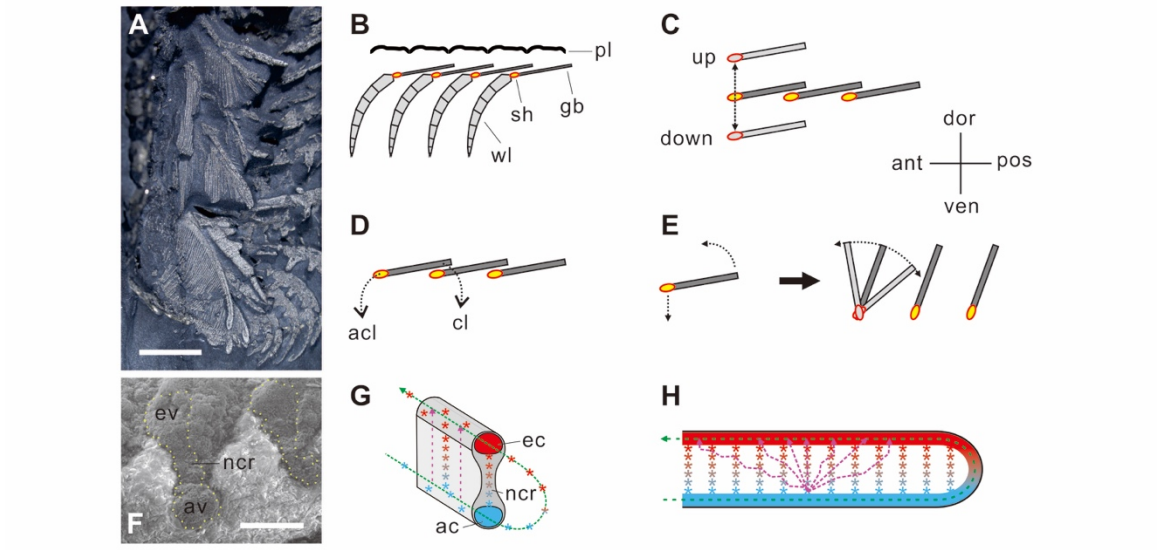

Figure 8 – Proposed rotation of upper branch and hemolymph flow path. (A) Imbricated gill branches of *Triarthrus eatoni*, GLAHM 163103.(B) Imbricated upper branch with shaft marked in yellow. (C) Upper branch lifts up and down with filaments mirroring this movement. (D) Anticlockwise (anteriorly upward) and clockwise (posteriorly downward) rotation of the upper branch, of which latter is not possible because it will be striped by the posterior gill branch. (E) Anticlockwise rotation of upper branch firstly lowers the shaft and then allows the filaments to rotated upwards and forwards. (F) Truncated cross section of the filament of *T. eatoni*, YPM 204. (G) Reconstruction of filament cross section showing hemolymph flow. (H) Reconstruction of longitudinal section of filament showing possible hemocyanin flow paths. Green dashed line with arrow represents the looped path that transports bulk flow of hemolymph from the afferent channel and out from the efferent channel. Purple dotted lines are the oxygen charging path of individual hemocyanin as they absorb oxygen. Stars represent individual hemocyanin, displaying lower concentration of oxygen with blue color and high concentration of oxygen with red

color. Acl, anticlockwise; ant, anterior; ac, afferent channel; cl, clockwise; dor, dorsal; ec, efferent channel; ncr, narrow central region; pos, posterior; ven, ventral. Scale bars, 5 mm (A), 50 μm (F).

In our model for gill ventilation the shaft is the mechanical center and rotational axis during ventilation. Two sceneries are suggested. Firstly, as the shaft moved up and down, the associated filaments followed in upward and downward motion (Fig. 8C), and the vertical movement of filaments created an opposing vertical water current. Secondly, during the stroke the shaft was initially rotated in an anticlockwise direction with the result that the associated filaments rotated upwards and forwards (Fig. 8D, E). In this movement, the shaft was likely first lowered ventrally and then the lobe and filaments rotated forwards and backwards (Fig. 8E). As opposed to the horizontal position (medial in Fig. 8C), the filaments were now inclined in dorsal direction (Fig. 8E) and located above the shaft but below the pleura. In this position, the filaments are protected by the pleurae, in a way that is functionally analogous to the sealing gill branches inside a lateral chamber in modern decapods. During the reverse stroke or the backward movement of the filaments, those of the anterior branches would always remain above those of the more posterior upper branches. The upper branch of the posterior limb would impede filaments anterior to them from rotation in a clockwise direction or movement posteriorly downward (Fig. 8D). In both movements detailed above, the filaments show some combination of up and down movement, and forward and backward movement.

Hemolymph flow

Enhanced efficiency in oxygen transfer that met increased metabolic and size-volume demands must have accompanied the increased animal size and functional diversity witnessed in the early Phanerozoic. The evolution of specialized gills helped increase total body surface area while minimizing the body volume (Mill 1972). The dumbbell shape of filaments provided robust structural support for the thin central laminae across which gaseous exchange took place, whose concave shape would have also served to increase the surface area of the gill (Hou, *et al*. 2021). Here we reconstruct the afferent channel to be at the bottom of the filament and the efferent vessel at its top (Fig. 8F). The distal loop that connected both channels would have enabled continuous flow of hemolymph from the lower vessel to the upper one (Fig. 8F), but the system presumably was such that restricted flow within the loop forced hemolymph to flow across the laminae whose narrow central area was adapted for the oxygen exchange (Fig. 8F) due to its thin cuticle. Pillar-like supporting structures inside arthropod gills build the hemocoels (blood space or hemolymph channels) (Goodman and Cavey 1990; Farrelly and Greenaway 1992; Farley 2010) that we infer to be likewise within trilobite filaments. The deoxygenated hemocyanin, a copper-based protein responsible for oxygen transport present in most arthropods (Van Holde et al. 2001), distributed from the afferent hemolymph flow, may thus have flowed through a variety of pathways through the narrow central region of the filament.

The complex and interconnected hemocoel in the narrow central region of filaments allowed hemocyanin moving upward to be fully charged with oxygen and

finally drain into the efferent channel (Fig. 8G, H). The morphology of the filaments is compatible with the inference that the gradient of oxygen concentration gradually changed between the afferent channel and the efferent channel (Fig. 8H). Because hemolymph reaching the efferent channel would have flowed to the heart, the path of any individual hemocyanin protein can be projected from any position to join the bulk flow of the efferent channel (Fig. 8H). The shortest path for oxygenation is that perpendicular to the filament but it is possible that individual proteins might have move in a non-direct path when being recharged (Fig. 8H). Whatever route individual hemocyanin took to the efferent channel, all of its paths would like to fit the gradient change of oxygen concentration from the bottom low to the top high value, otherwise the hemocyanin may stay in a position without charging with oxygen because of lacking gradient difference between itself and the surrounding water flow.

Interaction of the oxygen gradient and the water current

If the trilobite gills rotated as suggested above (Fig. 8C, E), currents created by their movements would have percolated through the space between filaments. In otherwise still water, the upstroke of the gill branch (efferent channel upper and afferent channel lower) would create a downward directed water current (Fig. 9A, C). This would mean that the first part of the gill to come in contact with fresh water would be the efferent channel that would be charged with oxygen, followed by the deoxygenated hemolymph in the central laminae and lastly by the afferent channel. (Fig. 9A, C). In contrast, the downstroke of the gill branch would create an upward directed water current, paralleling the direction of

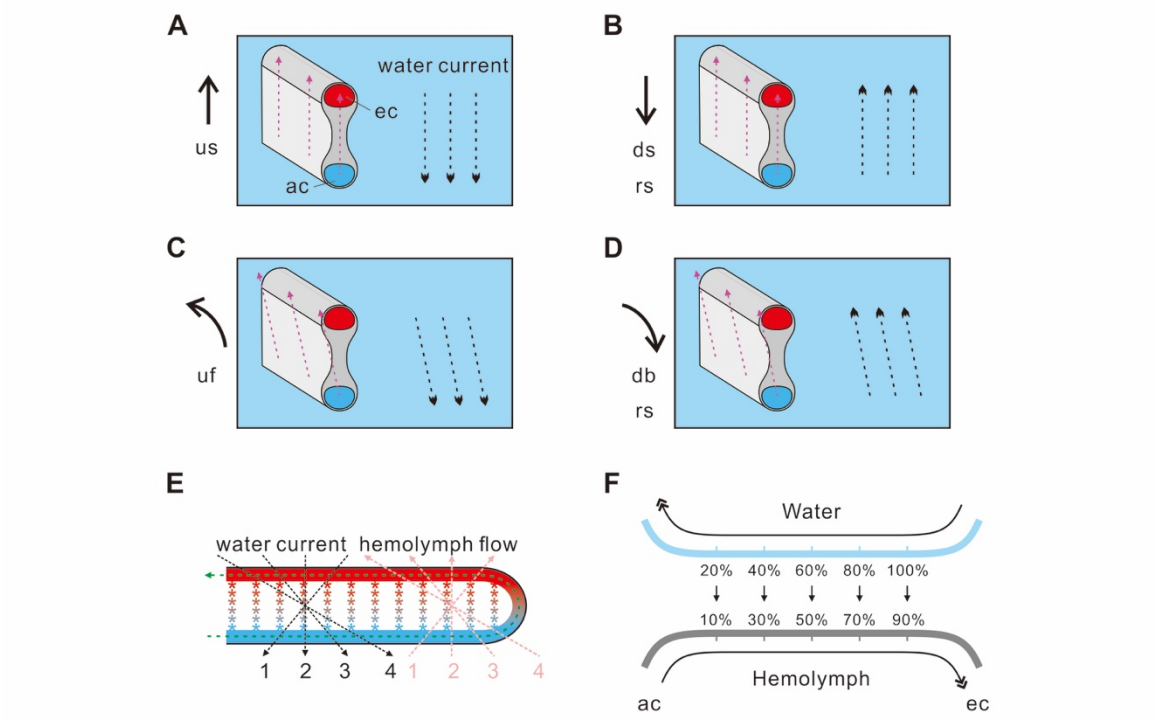

Figure 9 – Interaction of hemolymph flow and water current. (A) Upstroke of gill branch creates downward going water current, which forms a contrary direction with upward going hemolymph flow. (B) Reverse stroke of gill branch creates upward going water current, which is the same direction with upward going hemolymph flow. (C) Anticlockwise rotation of gill branch creates posteriorly downward going water current, which forms a contrary direction with upward going hemolymph flow. (D) Reverse stroke of gill branch creates upward going water current, which is the same direction with upward going hemolymph flow. (E) Any of water current going downward direction will always be paired with the countercurrent hemolymph flow in filaments. (F) A countercurrent exchange model shows how the contrary flow exchanges oxygen with gradient difference. The gradient of oxygen concentration does not represent the real oxygen capacity of hemolymph. Oxygen capacity of hemolymph is unknown but here is

suggested with 100% when it is fully charged with oxygen. Green dashed line with arrow represents the loop path that transports buck flow of hemolymph in from afferent channel and out from efferent channel. Pink dash lines with arrow represents the possible hemocyanin moving direction coming from any direction from bottom to top side. Purple dashed line with arrow is the oxygen charging path of individual hemocyanin that replaces lower concentration of oxygen with high concentration of oxygen. Stars represent individual hemocyanin, displaying lower concentration of oxygen with blue color and high concentration of oxygen with red color. Black dashed line with arrow represents the water current and its direction. The light blue background represents the water medium. Arabic numbers in figure E represent paired countercurrent flow. Ac, afferent channel; ec, efferent channel; db, down backward rotation; ds, downstroke; hem flow, hemolymph flow; uf, up forward rotation; us, upstroke; wat curr, water current; rs, reverse stroke.

upward flowing hemolymph (Fig. 9B, D). Within the gill, the gradient of oxygen concentration has been interpreted to have increased from the bottom to the top (Hou, *et al*. 2021), with hemolymph flowing upward in the narrow central region (Fig. 8F-H). During upward movement of the limb, the downward moving water current (Fig. 9A, C, E) would have flowed in an opposite direction to that of the upward going hemolymph flow (Fig. 9A, C, E), leading to what is termed “countercurrent flow”. Such a condition is the basis of the countercurrent exchange mechanism (Cowen 1973; Perry *et al*. 2019) (Fig. 9F) seen among modern fish. During downward movement of the limb the water

current would have flowed from bottom to top, the concurrent mechanism will be initiated (Fig. 9B, D). During the limb upstroke anticlockwise rotation of the gills also enabled the countercurrent exchange mechanism to operate (Fig. 9A, C, E, F). During a series of kinetic movements of the upper branch, the water can be totally disturbed and the current may be more complex than our models. For the advantage of the countercurrent being more efficient than concurrent exchange, the filaments move upwards and forwards will more likely be dominated for respiration because these movements can create the downward and backward going water current.

Withstanding oxygen stress

Small differences in oxygen uptake ability are of premium importance in a low oxygen setting. As the number of trilobite trunk segments was directly related to number of gill pairs and thus total respiratory surface area, the association of trilobites with multiple trunk segments and relatively deeper water, oxygen-poor settings has long been mooted, most notably in the recognition of the multisegmented and thin-shelled olenimorphic morphotype occurring in dark pyritic claystone (Fortey and Owens 1990; Fortey and Wilmot 1991). There is evidence that some olenimorphic species could flexibly adjust the production of trunk segments to meet ambient oxygen levels (Hughes 2005; Hughes *et al*. 2014). Periodic upwelling of anoxic sea water onto the shallow shelf in the Cambrian and earliest Ordovician caused a series of extinctions of shelfal communities that were replaced by olenimorphs adapted to oxygen deficiency (Palmer 1965, 1984; Wood and Erwin 2018). While it is clear that trilobite species varied significantly in their tolerance

of oxygen deficiency, bearing the countercurrent exchange mechanism evidently enables some trilobites to thrive in low-oxygen environments, e.g. those that are dysaerobic (Farrell *et al*. 2011; Fortey and Wilmot 1991), poikiloaerobic (Hughes, *et al*. 2014) or exaerobic (Gaines and Droser 2003) environments. The ability to occupy a broad range of habitats may have been a factor in high diversification rate of trilobites diversity and disparity in the Cambrian and Ordovician (Adrain, *et al*. 1998; Webster 2007).

Deuterostome

Gill structures in deuterostomes are well represented in early chordates, the fossil record of which can be traced back to the early Cambrian (Shu, *et al*. 1999; Shu, *et al*. 2003b). In the same strata, a large number of more phylogenetically enigmatic yunnanozoans (Donoghue and Purnell 2009), that most consider to root within the deuterostome lineage, are preserved with exquisite gill structures. Here we use the well preserved yunnanozoan *Haikouella jianshanensis* of the early Cambrian Chengjiang Biota (Fig. 10A, B) (Shu, *et al*. 2003a) to discuss its the oxygen uptake mechanism. *Haikouella*'s gills bear a central arch-like supporting structure, curved posteriorly and connected to the ventral blood vessels (Shu, *et al*. 2003a). Closely arranged paired filaments are attached on the lateral and possibly posterior surfaces of the supporting structure. The triangular filaments are flat and taper distally from its wide base. Paired filaments seem to be perpendicular to the supporting structure (Fig. 10B). The reconstructed cross section of the *Haikouella* shows the possible hemolymph circulation. The flat filaments leave the vessels near the lateral edges of the gill supporting structure. Afferent vessels are interpreted to be those on the

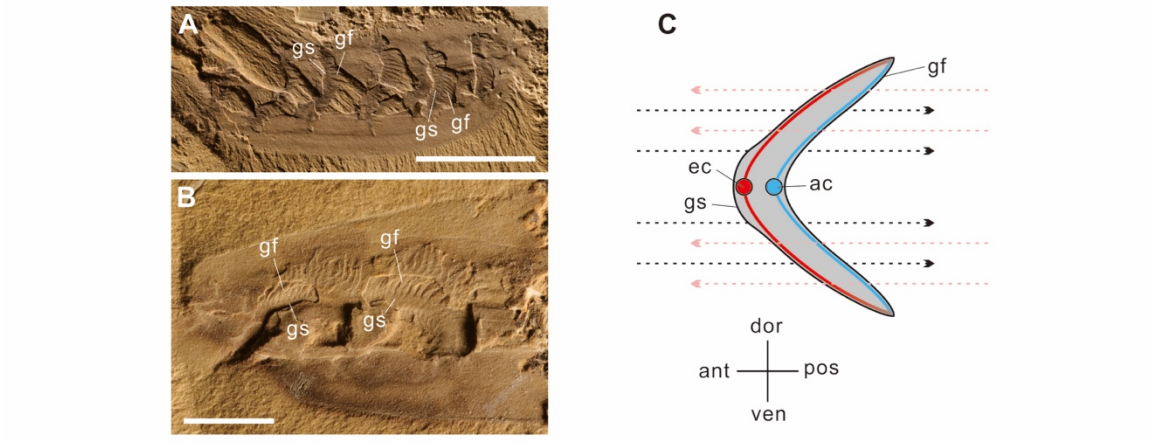

Figure 10 – Gas exchange in chordate *Haikouella jianshanensis*. (A) Well preserved gills of *H. jianshanesis* bearing a backward curved central supporting structure which is attached with many filaments that have wide base and pointy end. (B) Gills of *H. jianshanensis*. (C) Reconstruction of gill cross section of *H. jianshanesis* showing afferent and efferent vessels (based on Shu et al. 2003, fig. 2G). Black dashed lines with arrows represent the possible water current going posteriorly. Purple dotted arrow is the oxygen charging path of individual hemocyanin that replaces lower concentration of oxygen with high concentration of oxygen. Suggested water current passing the gill filaments from outer surface to inner surface, which forms countercurrent flow with hemolymph flow inside gill filaments. Ac, afferent channel; ec, efferent channel; gs, gill supporting structure; gf, gill filament. Scale bars, 5 mm (A), 2 mm (B).

inner side of the paired gill filaments and the efferent vessels inferred to be located at the outer side (Fig. 10C), which are closely comparable to the arrangement in modern fish gills (Randall 1970; Perry, *et al*. 2019). In the stem deuterostome vetulicolians unidirectional water currents have been suggested to egress in through the mouth and out via the gill slits (Ou, *et al*. 2012). We suggest *Haikouella* may have employed a similar unidirectional flow that came in through the mouth and out through the gill filaments, forming an unidirectional current flowing posteriorly through the pharynx. As in the trilobite *T eatoni,* in this reconstruction the incoming flow first contacts the oxygenated efferent vessel and then progresses to the deoxygenated afferent vessel, forming a distinct convection that initiates the countercurrent exchange mechanism (Fig. 10D). This inferred mechanism is extremely similar to the gas exchange mechanism in modern fish gills (Randall 1970; Perry, *et al*. 2019), and is consistent with known yunnanozoan morphology. This evidence indicates operation of the countercurrent exchange mechanism in the early Cambrian in deuterosomes at least.

Equivalent efficiency among all users employing the countercurrent exchange mechanism is not expected because many factors, such as pressure gradient, conductance, tissue perfusion, delivery of Hemocyl bound O_2 to the tissues and the oxygen loading capacity of the hemolymph or blood (McMahon 1981; Taylor 1990). The lower efficiency of countercurrent gas exchange demonstrated in modern crabs, contrary to the high efficiency in modern fishes, is mainly due to the properties of the diffusion barrier and not to less effective countercurrent (Perry, *et al*. 2019; Taylor and Butler 1978). The barrier deficiency may have been offset by increasing the number and size of gill branch

and/or respiratory filaments (Fortey 2004). However, the fewer and almost fixed number of gill structures in yunnanozoan may represent more thin membrane for efficient diffusion to satisfy its requirement when compared to that of trilobites.

The countercurrent exchange mechanism is present in almost all groups of fish (Perry, *et al*. 2019) but is reported rarely from other groups including a few cases in arthropods (Hughes *et al*. 1969; McMahon 1981; McMahon and Wilkens 1983; Woods *et al*. 2017). This may reflect the shared homologous origin of deuterostomes gills (Gillis *et al*. 2012) but the independent origins of arthropod respiratory systems (Sharma 2017). Here we report the earliest evidence of this mechanism during the initial diversification of triploblasts in the early Cambrian.

CHAPTER 3. MISMATCH OF EARLY EUARTHROPOD CEPHALIC STRUCTURES IS SOLVED WITH HIDDEN APPENDAGES

Abstract

Head segments, determined from the ventral appendages or sternites, play a critical role in revealing the relationships within major arthropods but the accurate determination of their number and relationship is challenging (Damen, *et al*. 1998; Telford and Thomas 1998; Budd 2002; Scholtz and Edgecombe 2006; Mayer, *et al*. 2013; Richter, *et al*. 2013). This is due to the decoupling of dorsal tergites and ventral limbs (Hughes 2003; Janssen *et al*. 2004; Wilson and Anderson 2004; Richter, *et al*. 2013; Dunlop and Lamsdell 2017; Fusco and Minelli 2013; Fu *et al*. 2018; Minelli 2003; Edgecombe and Ramsköld 1999). Traditionally, the coincidence of same number of dorsal transverse furrows, internal gut caeca and ventral appendages, leads to interpreting Trilobita to have four pairs of cephalic appendages and five dorsal segments (Scholtz and Edgecombe 2005; Park and Kihm 2017). This model has served the basis for understanding of euarthropod cephalic evolution (Scholtz and Edgecombe 2005; Scholtz 1998; Walossek and Müller 1998). Based improved analytical techniques applied to the best preserved soft-bodied specimens of the upper Ordovician olenid *Triarthrus eatoni* and middle Cambrian corynexochid *Olenoides serratus*, here we argue that an additional pair of cephalic "biramous" limbs occurred just behind the antennae, suggesting that Trilobita has five pairs of cephalic appendages and six dorsal segments. The mismatched dorsoventral segments resulted from fused muscle attachment sites that reduced the

expressions of dorsal furrows. The newly recognized limb pair may have improved the feeding ability as these limbs were located close to the mouth.

Introduction

Head segments, as determined from the number of cephalic appendage pairs, play a major role in higher-level classification of Panarthropoda (Damen, *et al*. 1998; Telford and Thomas 1998; Budd 2002; Scholtz and Edgecombe 2006; Mayer, *et al*. 2013; Richter, *et al*. 2013). Serial homology and segment identity in the head are obscured by fusion, loss and alteration of structures, and by morphogenetic movements and displacement during ontogeny (Scholtz 1998). The result is that segmental mismatch between ventral appendages and dorsal furrows/segments becomes a common phenomenon in arthropods (Hughes 2003; Janssen, *et al*. 2004; Wilson and Anderson 2004; Richter, *et al*. 2013; Dunlop and Lamsdell 2017; Fusco and Minelli 2013; Fu, *et al*. 2018; Minelli 2003; Edgecombe and Ramsköld 1999). Revealing the head segments and their relationship to the ventral structures is challenging (Damen, *et al*. 1998; Scholtz and Edgecombe 2006; Richter, *et al*. 2013).

Trilobites are critical for discussions on the evolution of Panarthropods due to their status as early euarthropods (Scholtz and Edgecombe 2005; Scholtz 1998; Walossek and Müller 1998). Estimates of the number of trilobite head segments, based on either observed limb pairs or furrows on the dorsal exoskeleton, have varied from five to eight segments (Palmer 1957; Bergström 1973b; Park and Kihm 2017). With respect to appendages, their rare preservation suggests a generally accepted model that three pairs

of obvious post-oral "biramous" cephalic appendages, consisting of an endopod, also known as walking leg, and a gill appendage, following a single pair of antennae (Scholtz and Edgecombe 2005; Park and Kihm 2017; Bruton and Haas 2003), with a fourth pair of post-oral "biramous" appendages arguably spanning the cephalon-thoracic boundary that are considered to be functionally part of the trunk (Edgecombe and Ramsköld 1999).

Here we document an additional frontal-most pair of cephalic "biramous" appendages in the best-preserved specimens of both *Olenoides serratus* and *Triarthrus eatoni,* revealing that five pairs of cephalic appendages (one pair of antennae followed by four pairs of "biramous" limbs) are correlated with four transverse furrows. The distinct mismatch between the ventral appendages and dorsal segments determined by furrows results from fused muscle attachment site underneath the cephalic shield.

Materials and methods

Material described in this paper is housed in the American Museum of Natural History (AMNH), New York, USA; Geological Survey of Canada (GSC), Ontario, Canada; Museum of Comparative Zoology of Harvard University (MCZ); National Museum of Natural History (NMNH) of Smithsonian Institution, Washington D.C., USA.

X-ray photos of *Olenoides serratus* are from the original collection of "Radiographs of Beecher Bed Trilobites by J. Cisne" organized by T. Whiteley.

The pyritized specimens of *Triarthrus eatoni* are from the Beecher's Trilobite Beds of the Katian (Late Ordovician) Frankfort Shale of upper New York State, USA and the Katian (Late Ordovician) Whetstone Gulf Formation ("Martin Quarry") (Briggs*, et al*.

1991; Farrell, *et al*. 2009). About 150 specimens of *T. eatoni* were examined and small, well-preserved ones were selected for the Environmental Scanning Electron Microscope (ESEM) and micro-CT scanning. Specimens of *Olenoides serratus* are from the Burgess Shale Biota of the middle Cambrian (Wuliuan Stage) Burgess Shale Formation (previously known as the Stephen Formation) of British Columbia, Canada (Briggs, *et al*. 1994). About 100 specimens of *O. serratus* were examined. Both species occupied relatively deep shelfal marine environments that may have experienced periodic oxygen availability stress.

Triarthrus eatoni specimens were scanned with a Phoenix | tome | x μCT scanner (General Electric Company, Fairfield, CT, USA) at the AMNH Microscopy and Imaging Facility. Post-processing and volume-rendering of the CT images was done using the Phoenix DATOS | x 2 reconstruction software (GE Sensing & Inspection Technologies, Hürth, Germany) and VGStudio MAX v. 3.2 (Volume Graphics, Heidelberg, Germany). Tiff image stacks are archived at www.morphosource.org, project P1197.

The specimens were photographed by the Olympus DSX100 Opto-Digital Microscopy, Canon EOS 50D and Leica MZ16 with DFC420 lens. The Olympus DSX100 Opto-Digital Microscopy and the Leica M205C are installed with stack or non-stack function. As specimens are captured with different directions of light to show particular structures, the details are given in the image of the figures. Figures were prepared using CorelDRAW 2018.

Description

Triarthrus eatoni

Micro-CT and X-ray analysis of eighty of well-preserved specimens of the soft-part bearing Upper Ordovician *Triarthrus eatoni* reveals a previously unrecognized pair of anterior cephalic "biramous" appendages in 7 of very best preserved specimens (Fig. 11–12 and figs. S10–14). Application of these techniques resolves distinct 1st and 2nd cephalic "biramous" appendages that have previously been taphonomically amalgamated into the "1st" cephalic "biramous" appendage pair during the preservation (Fig. 11–12 and figs. S10–S14). CT-scans of specimen AMNH 101409 (Fig. 12A, B) show that the proximal parts of the four pairs of the cephalic "biramous" appendages (Fig. 12A) at the area of the body-limb junction. An X-ray photo (Fig. 12C) rendered from the single slice of the CT-scan (Fig. 12D) shows a sharp boundary that resolves two limb bases as distinct entities and that prominent white spots resulted from the overlapping of two limb bases, which result the misinterpretation of two appendages as one appendage. Dark boundaries (Fig. 12C and figs. S14A–D, S15A–D) between the limb bases in X-ray photos of specimens AMNH 101409, MCZ 114108, MCZ 114109 resolve these as two appendages, previously unrecognized due to the poor preservation of the distal parts of the first appendage. Furthermore, in 13 specimens including some newly recovered, a stiff, convex, arcuate structure (Fig. 11A, C, D, and figs. S10A–E, S12A–C, S13A–E, S14A–E) is located behind the posterior margin of the hypostome, and represents the metastome previously reported by Beecher (Beecher 1895). Together, the metastome and the newly recognized 1st cephalic "biramous" appendage pair occupy a small gap between the

posterior margin of the hypostome and the 2nd pair of cephalic "biramous" appendages (Fig. 12A–E, 12A–D, and figs. S10A–E, S11A–C, S12A–C, S13A–E, S14A–E). Both X-rays and digital microscopy show that the hypostomal suture (anterior margin of the hypostome) was located posterior to the anterior glabellar margin and possibly beneath the first pair of glabellar furrows (Fig. 12C, and figs. S12A–C, S13A–D, S14A–D; see also Cisne (Cisne 1981), YPM 228, pl. 17). The hypostomal suture was previously suggested to lie within the narrow anterior cephalic doublure is because the weak impression is not recognized.

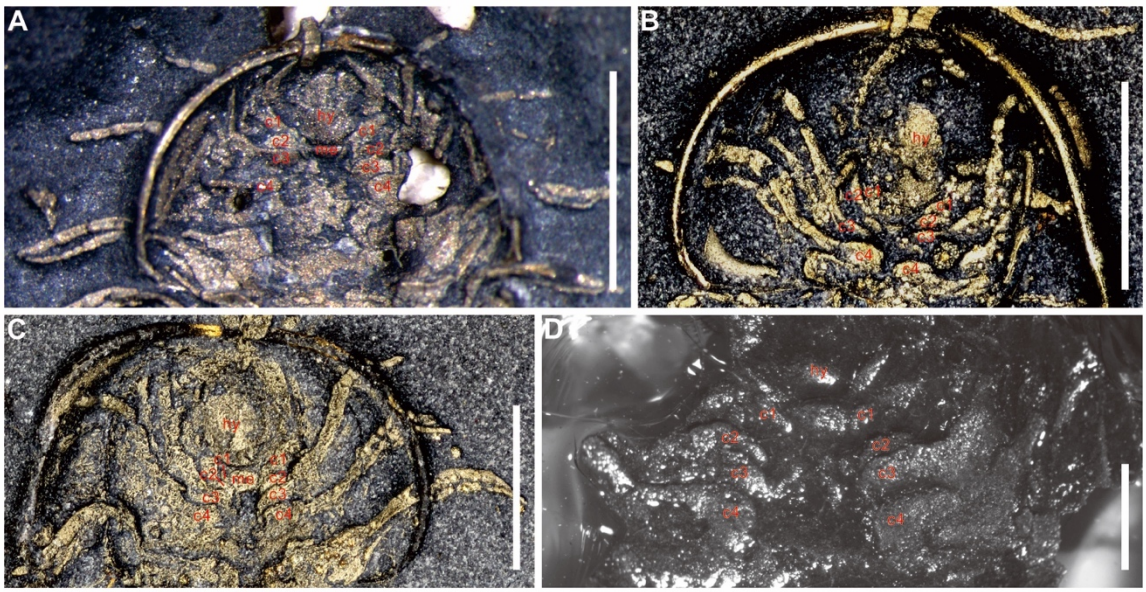

Figure 11 – *Triarthrus eatoni*. Four pairs of cephalic "biramous" appendages. (A) USNM 400935, innermost margin of c1 is located behind metastome. (B) AMNH 101398. (C) AMNH 101393, metastome is well preserved and located between paired c1. (D) MCZ 114109, innermost of c1 is located behind but surround metastome. Scale bars, 2 mm (A–C), 1 mm (D).

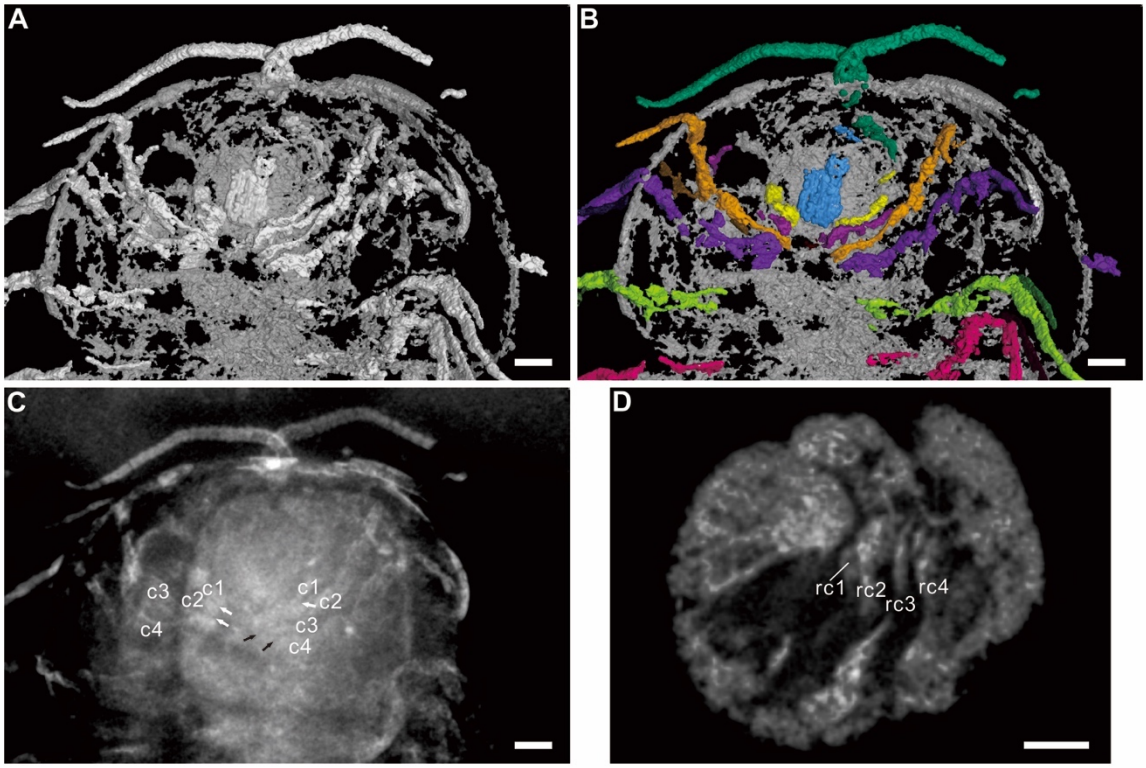

Figure 12 – *Triarthrus eatoni*. CT scans and X-rays showing cephalic appendages. (A–D) AMNH 101409. (A–B) cephalic appendages are shown by non-color and color rendering. (C) X-ray rendering as in figure a and b show four cephalic "biramous" appendages. Four cephalic appendages are marked. Two dark furrows (marked by two white arrows) distinguish the rc1 and rc2, but the rc3 and rc4 are hard to be distinguished. The lc1 and lc2 has a poor boundary at the most inner part until at the position marked with white arrow, but lc3 and lc4 are separated by dark furrows (marked by two dark arrows). (D) single slice of CT scan data showing four cephalic "biramous" limbs are clearly recognized. c1-4: cephalic "biramous" appendage 1 to 4 respectively; rc1-4: right cephalic "biramous" appendage 1 to 4 respectively. Scale bars, 0.6 mm (A–C), 0.35 mm (d).

Olenoides serratus

The middle Cambrian *Olenoides serratus* from the Burgess Shale fauna was described with three pairs of cephalic "biramous" appendages mainly based on three specimens, USNM 58588A, USNM 58588B and GSC 34693, which are considered to be preserved with the entire cephalic appendage series (Whittington 1975). The specimen USNM 65520 (Fig. 13C and fig S15) was originally described by Whittington (1975, p. 115) with four pairs of cephalic "biramous" appendages but not considered as convincing evidence as most of *O. serratus* specimens have three pairs of cephalic "biramous" appendages (Whittington 1975). However, in GSC 34693b the interpretation of one antenna and three "biramous" appendages belonging to the cephalon on left side based on the suggestion that they did not move significantly from their original position during preservation(Whittington 1975). In our interpretation, what was described as the "left antenna" in the counterpart GSC 34693b, is actually the 1st left cephalic "biramous" appendage (Fig. 13B and fig. S16A–D) evinced by the clear podomere boundaries of an endopod, and the thin spines located at the boundary of the endopodal segments (fig. S16E). These cannot be antennular articles because there are distinct steps in size along the sharply narrowing segmented shaft (figs. 16B, D), and this is characteristic of endopodal segment (fig. S16E), which contrasts with the gentle taper between antennal articles (fig. S16C).

In USNM 58588A the cephalic region exposures the flat and large proximal area of the exopods but generally reveals little trace of the endopods. The two anteriormost appendages (c1? and c2?) were overlooked based on their appearance anterior to what

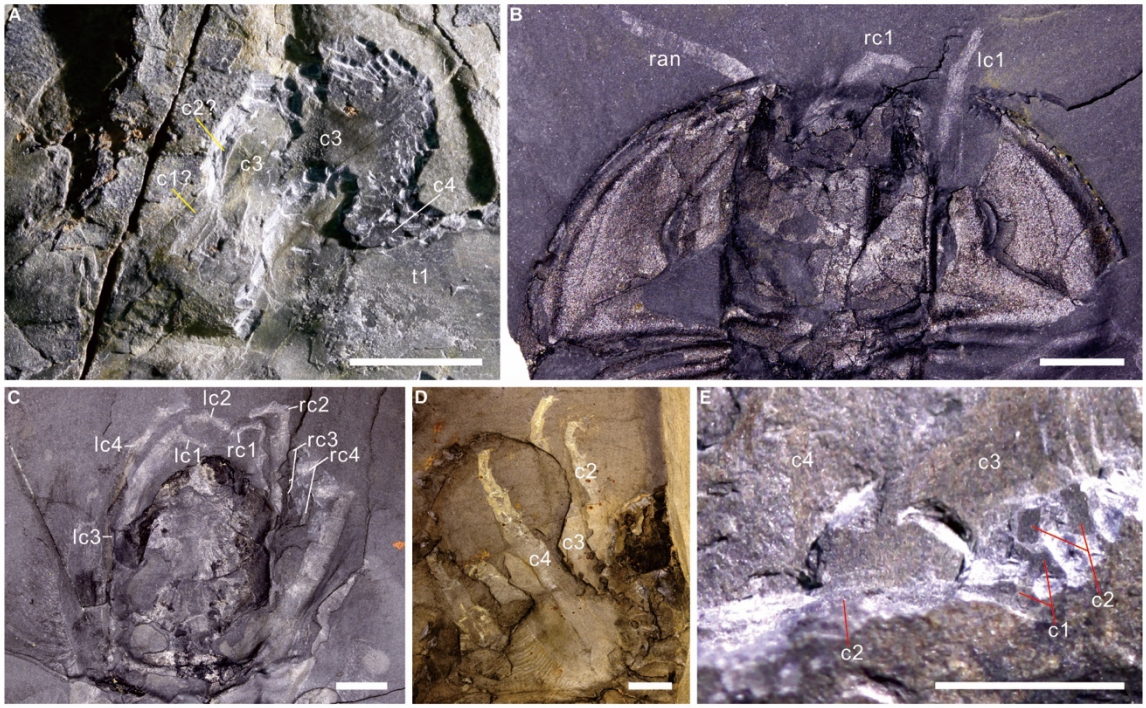

Figure 13 – *Olenoides serratus*. Four pairs of cephalic "biramous" appendages. (A) USNM 58588a, dorsal view. The c2? has only partial endites spines left above c3. The c1? is located above c2. (B) GSC 34693b, ventral view. Left c1 displays sharply narrowing segment, and antenna is gently curved anterolaterally. (C) USNM 65520, dorsal view. Four pairs of cephalic "biramous" appendages have distal regions well preserved. (D–E) USNM 65513, dorsal view. Two endite spines of c2 are left above c3 layer, and c1 has still two endite spines are left above c2 layer. c1-4: cephalic "biramous" appendage 1 to 4 respectively; ran: right antenna. Scale bars, 5 mm (A–C), 2 mm (D, E).

was traditionally interpreted as the "1st" cephalic "biramous" appendage (c3) (Fig. 13A and figs. S17A–E). c1? reveals part of limb base as it is located above c2?. c2? is the remains of a "biramous" appendage because of its characteristic endite spines extending from the limb base (fig. S17B). c2? is just above (anterior to) the third appendage pair (c3).

Lastly, the specimen USNM 65513 (Fig. 13D–E and figs. S18A–E) has c1 with a small trace of the limb base (and limb base spines) located above (anterior to) the endite spine of the c2 limb base, indicating four pairs of cephalic "biramous" appendages. c1 on this specimen has been damaged during preparation that removed the anteriormost appendage close to the dorsal tergite.

Discussion

Head segments of trilobites

The interpretation that trilobites had only three pairs of "biramous" appendages reflects the obscuring effect of rotation and forward imbrication of head appendages during preservation (Whittington 1975, 1980), which commonly hid the smaller first appendage pair beneath subsequent pairs (Fig. 11A–B, 2A–C, and figs. S10A–E, S11A–C, S12A–C). Compaction-related amalgamation of the hypostome, metastome, and the ventral surface of the body further obscures the mouth region, with the result that only the finest preserved specimens reveal the original structure of this region. Distal parts of the appendages tend to be displaced relative to the body (e.g. rotation, displacement, twist during compression; figs. S10A, S11A, S12A), obscuring those of the small first

appendage pair. However, the proximal parts of the appendages, especially the limb base, are near the ventral body wall, are larger and are more firmly anchored to ventral sternite and dorsal tergites. Here we show that the best-preserved specimens reveal a previously obscured first pair, confirmation of which required both the best specimens and improved observational equipment.

Similar preservational variation applies to the metastome, which Cisne (1981) reported but which Whittington and Almond (1987) discounted as a presentational artifact. The observation of this structure in excellently preserved specimens, including 6 newly recovered, confirms the occurrence of this structure in life. Here we also agree that specimens of *T. eatoni* previously considered to bear a conterminant hypostome (Whittington and Almond 1987b) are taphonomically altered, and that the hypostome was, likely, natant. This is because the hypostomal suture is weakly impressed far posterior to the anterior glabellar margin, likely underneath S4, rather than aligning with anterior glabellar margin as in previous reconstructions. The posteriorly located hypostome suture suggests that the anterior wings were attached underneath S4.

The newly discovered anteriomost dichotomic appendages in best preserved specimens indicate that trilobite heads bare one pair of uniramous antennae succeeded by four pairs of post-antennal "biramous" appendages rather than the three pairs commonly assumed. Four pairs of limb-bearing head (or five somites) are considered as the ground pattern of euarthropod head (Walossek and Müller 1998; Waloszek *et al*. 2005; Aria and Caron 2017a; Scholtz 1998), of which Trilobita is considered as one of the model representatives. Trilobites occupy a position as sister taxa to all other euarthropods (Aria

and Caron 2017a; Budd and Telford 2009) or as a sister group to either chelicerates (Wills *et al*. 1998; Legg, *et al*. 2013; Aria and Caron 2017b) or mandibulates (Scholtz *et al*. 2019; Stein, *et al*. 2013; Ortega-Hernández, *et al*. 2013). The six head segments ventrally with five limbs are coincident with the "ground pattern" of mandibulates (Damen, *et al*. 1998; Chipman 2015) and also within the range of chelicerates (Dunlop and Lamsdell 2017). The crownward position of trilobites in euarthropods is further strengthened.

Head segmental mismatch

A total of five cephalic appendage pairs (including antennae) have been mooted before for trilobites (Størmer 1951; Bergström and Brassel 1984), but have been rejected because definitive evidence of the anteriomost pair has been lacking (Scholtz and Edgecombe 2005; Edgecombe and Ramsköld 1999; Cisne 1974, 1975). The previous suggestion of four cephalic appendages (including antennae) coincides with the common occurrence of four cephalic transverse axial furrows/apodemes (the occipital furrow and three glabellar furrow pairs anterior to it) (figs. S19-S20) (Scholtz and Edgecombe 2005), and is also consistent with the observation in trilobites of up to four pairs of gut diverticula in the cephalon (Hopkins *et al*. 2017; Lerosey-Aubril *et al*. 2011), corresponding to four appendage-bearing cephalic segments. The five appendages recognized here indicate a distinct mismatch between four dorsal axial furrows (corresponding to five segments) and ventral appendages (Fig. 14).

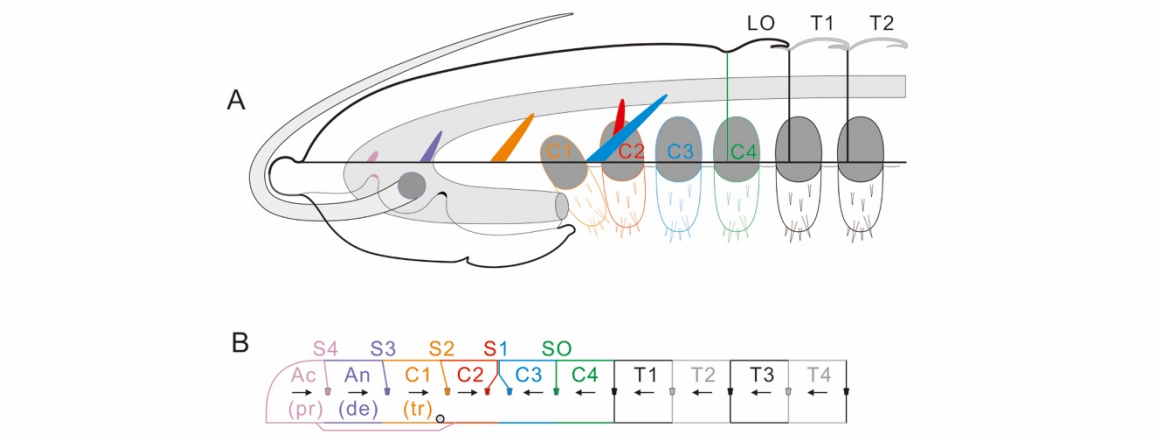

Figure 14 – Dorsoventral mismatch of trilobite head. (A) reconstruction showing cephalic segments divided by axial transverse furrows with different colors. Each transverse furrow has one corresponding muscle attachment site or apodeme for supporting its appendage. The mouth opening is located at the middle of second glabellar lobe. Each thoracic appendage inserts to the anterior apodeme of the host segment, which results an almost centrally located appendage. Bifurcation of S1 provides two muscle attachment sites, of which anterior one is supported for C2 and posterior one is supported for C3. (B) anterior attachment type begins from thoracic segments but ends at posterior branch of S1, and posterior attachment begins from hypostome and ends at anterior branch of S1.

Appendages, attached to corresponding apodemes (or appendifers) (Størmer 1939), are located centrally under each tergite junction (Edgecombe and Ramsköld 1999). Apodemes, an internal exoskeletal projection for muscle attachment, were located in the anterior of each tergite (Bruton and Haas 2003) and serve as markers for connecting appendages with exoskeletal segments. On the dorsal surface of the cephalon, transverse axial furrows (e.g. paired pits, paired glabellar furrows or transverse glabellar furrows) have commonly been to mark segment boundaries (Palmer 1957; Bergström 1973b), but if these mark apodemes, then they are not homologous with tergite boundaries in the trunk. Cephalic muscle attachment sites/apodemes are located underneath of those transverse furrows or anterior pits. However, transverse furrows are expressed differently, with up to a maximum of six visible furrows (e.g. in *Pseudoredlichia* (Zhang et al. 1980, pl. 28, fig. 9)). Four axial transverse furrows (SO, S1-S3), instead of five, are accepted as a general pattern in trilobites (Scholtz and Edgecombe 2005).

Many attempts have been made to correlate muscle attachment sites to the cephalic limbs (Harrington *et al*. 1959a; Campbell 1975; Geyer 1994). For simplicity, we accept that one apodeme per segment is linked to one appendage (Harrington, *et al*. 1959a; Hughes 2005) and use this as the basis for relating the two. This is supported by the observation that some apodemes extend postero-ventrally (Speyer 1988) possibly because it allows the ventral limb functioning for its host segment.

Anterior pits occur at different positions in trilobites. The anterior wings of hypostome extend upward and attach to the apodeme of anterior pits (or S4) (Whittington

and Evitt 1953; Whittington 1988b, a, 1990; Bruton and Haas 1997). S4 (anterior pits) is present in a few groups, e.g. olenellids and corynexochids but is usually reduced in most of trilobites. Trilobite ontogeny shows that eye ridge is bifurcated because the distinctly carved anterior pits appeared late during growth (Hou *et al*. 2017). It is reasonable that the hypostomal anterior wings are attached to the hidden attachment sites underneath the head shield in early growth period when anterior pits have not expressed yet. The situation of hidden attachment sites without expression of dorsal furrows (or pits) in the cephalon may explain the common phenomenon of reduced glabellar furrows in trilobites.

The foremost pair of muscle scars (anterior pits) is suggested for attaching the antennae (Whittington 1975; Whittington and Evitt 1953), however, such a suggestion conflicts with the evidence of hypostome morphology and its position underneath the cephalon (figs. S21and S22). Instead, antenna extended from the lateral notch of the hypostome (Whittington 1975; Whittington and Almond 1987b; Whittington and Evitt 1953; Whittington 1988b) (Figure S21). Compared to the position of lateral notch of hypostome, the antenna may not have been attached to the anterior boss (ventral impression of anterior pit) as previously suggested (Whittington and Evitt 1953; Whittington and Almond 1987b), but is likely attached to the apodeme of S3, one furrow posterior to the anterior pit, then curves down-laterally and forward coming out from the cephalic margin (fig. S22). By attaching to this furrow, the antenna is gently curving downward and extending forward, otherwise, it has to bend about 90 degrees (or more), firstly bending downward and then extending forward (Whittington 1988b). On the other

hand, S3 is the furrow most close to the point at which the antennae pass the hypostome and the anterior pits are too small to attach both antenna and the hypostomal anterior wing. Lateral and posterior margins of hypostome have a doublure (fig. S22) that extends adaxially to fuse with the ventral cuticle, which omits the possibility that any structure other than antenna can be inserted in hypostome. Hence only is the antenna surrounded by both anterior and posterior hypostomal wings.

In most hypostomes, the posterior margin is positioned somewhere between the middle of the first glabellar lobe and S2 (Note: some extend to S1, e.g. Sturmer and Bergstrom 1973 (Stürmer and Bergström 1973), p. 117). As most hypostomes rotate to become parallel to the dorsal exoskeleton in preservation, posterior margin of hypostome should be slightly anteriorly located in its original position than that in horizontal position, meaning the posterior tip of the hypostome that represents the mouth opening is the most backward position when compared with its original position. Based on suggested mouth position and the posterior margin of hypostome, the mouth opening likely lay slightly anterior to the preserved posterior of the hypostome (note: some but rare lay close to S1), which allows us to suggest that the mouth is possibly located at the middle of L2 for most trilobites. It is unlikely that the mouth opened any further posteriorly than glabellar furrow S2 (Eldredge 1971, p. 63). Because mouth lies at the back end of the hypostome (Fig. 14 and fig. S22), the posterior part of the hypostome will become the focus of any changes (Fortey and Owens 1999), which may extend the posterior margin of hypostome far more backward than less changed hypostome. The hypostome provides the reference landmark for recognizing the mouth opening, which is

the key structure further to reveal the attachments of first three cephalic dichotomic limbs. The antennae are the only structures surrounded by the hypostome mentioned above (in Antenna section). The mouth is considered as located at the posterior tip of the hypostome (Stürmer and Bergström 1973), above the posterior portion of the hypostome (Whittington and Almond 1987b) or the back of the hypostome (Fortey and Owens 1999), possibly being slightly anterior to the posterior margin of the hypostome. In the original position, the hypostome is slightly lift and tilted to the ventral region in some trilobites (Whittington 1988b, a, 1956).

Laterally located limbs allow the endite spines extending at posterior of mouth of feeding function (Müller and Walossek 1985). Endite spines of the limb bases, located at the posterior of the hypostome margin in *T. eatoni* (Figs. 11-12 and figs. S10-S14), indicate that C1 was located close to the mouth and could reach the posterior margin of hypostome (Fig. 14). As the mouth opening is usually parallel to S2 (see above Antenna section), the most likely attachment site for C1 is underneath S2. Compared with S2-S4, the relatively deeper S1 bifurcates at its inner portion in some trilobites (Hou *et al*. 2015; Yuan *et al*. 2002; Hopkins and Webster 2009; Zhang and Clarkson 2012; Chatterton and Ludvigsen 1998; Siveter 1977; Whittington 1941), of which the posterior branch is extended posteriorly adaxially (or bends 90 degrees to connect with SO) and anterior branch may extend adaxially parallel to SO. The fusion of muscle scars provides branched attachment sites, underneath S2, for two ventral appendages (Geyer 1994). Bifurcated furrows can provide attachment sites for two pairs of cephalic limbs (C2 and C3) respectively, because the L1, usually longer than L2 and OL, provides more space,

and the gradually decreased size of anterior cephalic limbs allows a small space for attachments for both C2 and C3.

In some trilobites muscle scars indicate a series of attachment sites along the glabella but are unexpressed on its dorsal surface. Appendages attached behind the hypostome can be recognized based on the hypostome's position. The mismatch between head segments and ventral limbs results from the fused muscle attachment sites that are hidden from the dorsal exoskeleton. The occipital furrow (SO) that is usually the strongest developed transverse axial furrow in the cephalon closely resembles the joints between of thoracic segments. By extrapolating the attachment of the thoracic limbs to the anteriorly located apodeme of their host segments, the similar condition of SO suggests that the same attachment site for the posteriormost cephalic limb, C4 (Fig. 14 and figs. S22).

Two types of attachment sites of cephalic appendages are suggested (Fig. 14). One (anterior attachment type) is similar to the trunk appendages that C3 and C4 are inserted to the anteriorly located ventral projections that each glabellar furrow represents, and the other one (posterior attachment type) is that C1, C2, and hypostome are inserted to the posteriorly located attachment sites. Appendages of the cephalon and anterior trunk are more adapted to feeding than the mid- to posterior trunk appendages (Stein and Selden 2012). The two opposite attachment types in the trilobite cephalic region bring cephalic appendages close to the mouth for feeding, of which position is referenced based on the posterior margin of the hypostome. Similarly, the posterior extension of glabellar

furrows (e.g. S1, S2 or even S3) may also indicate that cephalic appendages are brought close to the mouth, which has been posteriorly shifted during the Panarthropod evolution.

The anterior movement of trunk appendages undergo "cephalization" to support the head function (e.g. maxillipeds) (Scholtz and Edgecombe 2005) and the anterior shift of appendages in early growth stages moves cephalic limbs close to the mouth to assist in feeding (Walossek 1993). Posterior inclination of the glabellar furrows may relate to the anterolaterally shifted appendages that are functionally for capturing food or prey anteriorly. The crowed patch of cephalic dichotomic limbs results the fusion of muscle scars and/or dorsal furrows. The bifurcated S1 is typical of the most general mismatch pattern appeared among ventral appendages, dorsal furrows and dorsal segments, even if rare patterns are also present in some trilobites that have bifurcated S2, instead of S1, or a single longitudinal glabellar furrow. The fusion of muscle attachment sites that provide evidence for the hidden or invisible attachment sites in arthropods is responsible for the mismatch of ventral appendages and dorsal furrows in the cephalon.

Supplementary information

Taphonomy of trilobite appendages

Anterior appendages show distinct distortions because limb base rotates forward and distal podomeres rotate either forward or backward, resulting a complex compression. Posterior appendages close to pygidium are in normal state because the entire limb, including limb base and distal podomeres, rotates backward. During the transportation or compression, the appendages tend to move forward or backward. In the cephalon-thoracic boundary, the appendages are likely to move forward, because they are much close to the cephalon rather than the thorax, and the distinct convex glabella leaves more space for the appendages to shift anteriorly. The limb base of cephalic appendages is rotated forward and then imbricated together. The limb base of anterior appendages is covering the limb base of posteriorly following appendage, characterized of anterior imbrication style (Hou et al. xx), which results that anterior cephalic appendages are in a hidden state.

Figure legends and abbreviations

Green, antenna;

Blue, hypostome;

Yellow, first cephalic “biramous” appendages;

Pink, second cephalic “biramous” appendages;

Brown, third cephalic “biramous” appendages;

Purple, fourth cephalic “biramous” appendages;

Olive green, first thoracic “biramous” appendages;

Grey, structure unknown.

Dashed line representing supposed outline of some structure.

an, antenna; en, endopod; hy, hypostome; c1-c4, 1st to 4th pair of cephalic biramous appendages respectively; lc1-lc4, 1st to 4th pair of left cephalic biramous appendages respectively; me, metastome; ran, right antenna; rc1-rc4, 1st to 4th pair of right cephalic biramous appendages respectively; t1, 1st thoracic “biramous” limb.

Comments on *Triarthrus eatoni*

USNM 400935 (Fig. S10A-E) is firstly described by Whittington and Almond (1987, figs. 9, 11) (Whittington and Almond 1987b), who recognized three pairs of biramous appendages in cephalon. The “3rd” pair of cephalic appendages described in Whittington and Almond (1987) (Whittington and Almond 1987b) is here re-explained as the 1st pair of thoracic appendages (Fig. S10A-C) because of forwardly shifted ventral sternites during compression and anteriorly rotated frontal appendages. The “2nd” pair of cephalic appendages described in Whittington and Almond (1987) is now explained as the 4th pair of cephalic appendages (Fig. S10A-E). The “1st” pair of cephalic appendages described in Whittington and Almond (1987) (Whittington and Almond 1987b) is now corrected as remains of 1st, 2nd, and 3rd pair of appendages, which are marked by yellow, pink, and brown color, respectively. The left “e1?” described in Whittington and Almond (1987, figs. 9, 11) (Whittington and Almond 1987b) is the remains of the 1st cephalic appendages. The location marked with the first “c” on the left side of the specimen

described in Whittington and Almond (1987, figs. 9, 11) (Whittington and Almond 1987b) is the remains of the 2nd cephalic appendages. The "e2?" possibly belongs to the remains of the 2nd cephalic appendages of current description. The left "w1" described in Whittington and Almond (1987, figs. 9, 11) (Whittington and Almond 1987b) is the 3rd cephalic biramous appendages. A convex metastome is located just behind the hypostome, marked with red color.

MCZ 114108 (fig. S14A-E) is described by Cisne (1981, pl. 22, fig. 3; Text-fig. 26) (The figure shown by Cisne is left-right reversed as dorsal view; our figure is the standard ventral view), who recognized two pairs of biramous appendages in cephalon. The "2nd" pair of cephalic appendages described in Cisne (1981) is here re-explained as the 3rd pair of biramous cephalic appendages. The "1st" pair of cephalic appendages described in Cisne (1981) is now explained as the 3rd pair of cephalic appendages (fig. S14A-E). 1st and 2nd pairs of cephalic biramous appendages are crashed together and partly displayed. Outlines of antennae and hypostome are also supposed. A bright structure known as metastome is also recognized.

Comments on *Olenoides serratus*

Whittington (1975)(Whittington 1975) recognized one specimen USNM 65520 with four pairs of cephalic "biramous" appendages but he thought that only three key specimens, USNM 58588a, USNM 58588b, and GSC 34693, have all their appendages completely preserved. Here we show that there are one more pair of cephalic biramous appendages

recognized in two of three key specimens trusted by Whittington (1975) (Whittington 1975), except for USNM 58588b not showing new evidence.

GSC 34693b, the counterpart of the specimen GSC 34693, shows four pairs of cephalic biramous appendages. USNM 58588a is described with four pairs of biramous appendages but the cephalic region is still covered by the matrix, the possible traces of four pairs of cephalic appendages are marked. Additionally, two more specimens, USNM 65513 and 65520, show four pairs of cephalic biramous appendages, which enforce the evidence of trilobite head with one pair of antennae and four pairs of biramous appendages.

GSC 34693a (Whittington, 1975, fig. 21; pl. 19, fig. 1-3) is described with an incompletely preserved "left antenna". Sinking the counterpart of this specimen, GSC 34693b (fig. S15A-D), in water, shows robust endopodal segments (P5 and P6) which are sharply narrowing distally from proximal segments. This contrasts with the gently narrowing articles of the antenna. The "left antenna" described by Whittington (1975) is the left 1st pair of cephalic biramous appendages. Four pairs of cephalic biramous appendages are observed in this specimen.

USNM 58588a (fig. S16A-E) (Whittington, 1975, fig. 6; pl. 2, fig. 1-3; pl. 3, fig. 1) (Whittington 1975) is originally described as only three pairs of the cephalic biramous appendages. Here we found two more possible cephalic biramous appendages that have not been recognized by Whittington. 1st pair of cephalic biramous appendages is distinctly above the layer of 2nd pair of appendages that is above the 3rd pair of appendages. The traditional "1st" pair of appendages is here regarded as the 3rd pair of

cephalic appendages, the "2nd" is here as "4th" and "3rd" is here as "1st" pair of thoracic appendages. Because this specimen is still covered with matrix in the head region, these two pair of cephalic appendages could be recognized based on their location relative to other appendages. However the "1st" pair of cephalic appendages is most close to the dorsal exoskeleton, it is hard to distinguish it from the exoskeleton with confidence.

USNM 65513 (fig. S17A-E) (Whittington, 1975, fig. 10; pl. 7, figs. 1, 3, 4) (Whittington 1975) is originally described as only three pairs of cephalic biramous appendages. Herein we found one more pair of appendages is located just anterior to the traditional "1st" pair. Four pairs of cephalic biramous appendages are observed in this specimen.

USNM 65520 (fig. S18) (Whittington, 1975, fig. 16; pl. 13, fig. 1-3) (Whittington 1975) is originally described as four pairs of cephalic biramous appendages but Whittington did not accept this observation because it is not the three key specimens he suggested. Here, the new observation confirms this specimen has four pairs of cephalic "biramous" appendages.

Comments on relationship of dorsoventral structures

In the modified work of mismatching muscle attachments with ventral structures in *Ectilaenus (katzeri) katzeri* (fig. S22A-C), the dash lines connect the same positions of cephalic limbs to indicate the wrong correlation of muscle attachment sites and possible positions of ventral limbs. In this case, the muscle attachment site of C1 is wrongly

correlated to the position of the rostral plate, muscle attachment site of C2 is wrongly correlated to the distinctly recognized lateral notch of the hypostome.

The foremost scar of four paired muscle scars in cephalon has been suggested to support the 1st "biramous" limbs in *Ectillaenus (katzeri) katzeri* (Harrington et al. 1959 treatise in Moore, fig. 70, p. O97). In the specimen preserved with hypostome, this scar is located in front of the anterior ends of the anterior branches of facies sutures and is aligning almost parallel with the anterior wings of the hypostome (Bruthansova 2003, fig. 2e)(Bruthansová 2003) (fig. S22B-C). For C1 has the function for manipulating foods to the mouth, the foremost position of C1, in this case, can not perform such a function as it is located in front of the antenna that is marked by the lateral notch of the hypostome.

Transverse furrows are not related to limbs in one by one relationship. In trilobites with five axial transverse furrows (Yuan, *et al*. 2002; Sundberg and Mccollum 1997), the antenna and C1 will extend far beyond the mouth opening or posterior margin of the hypostome if one furrow corresponds to one appendage. Hence, the anterior pits (or S4) are the attachment sites most likely for anterior wings of the hypostome and S3 is for antennae.

Supplementary figures

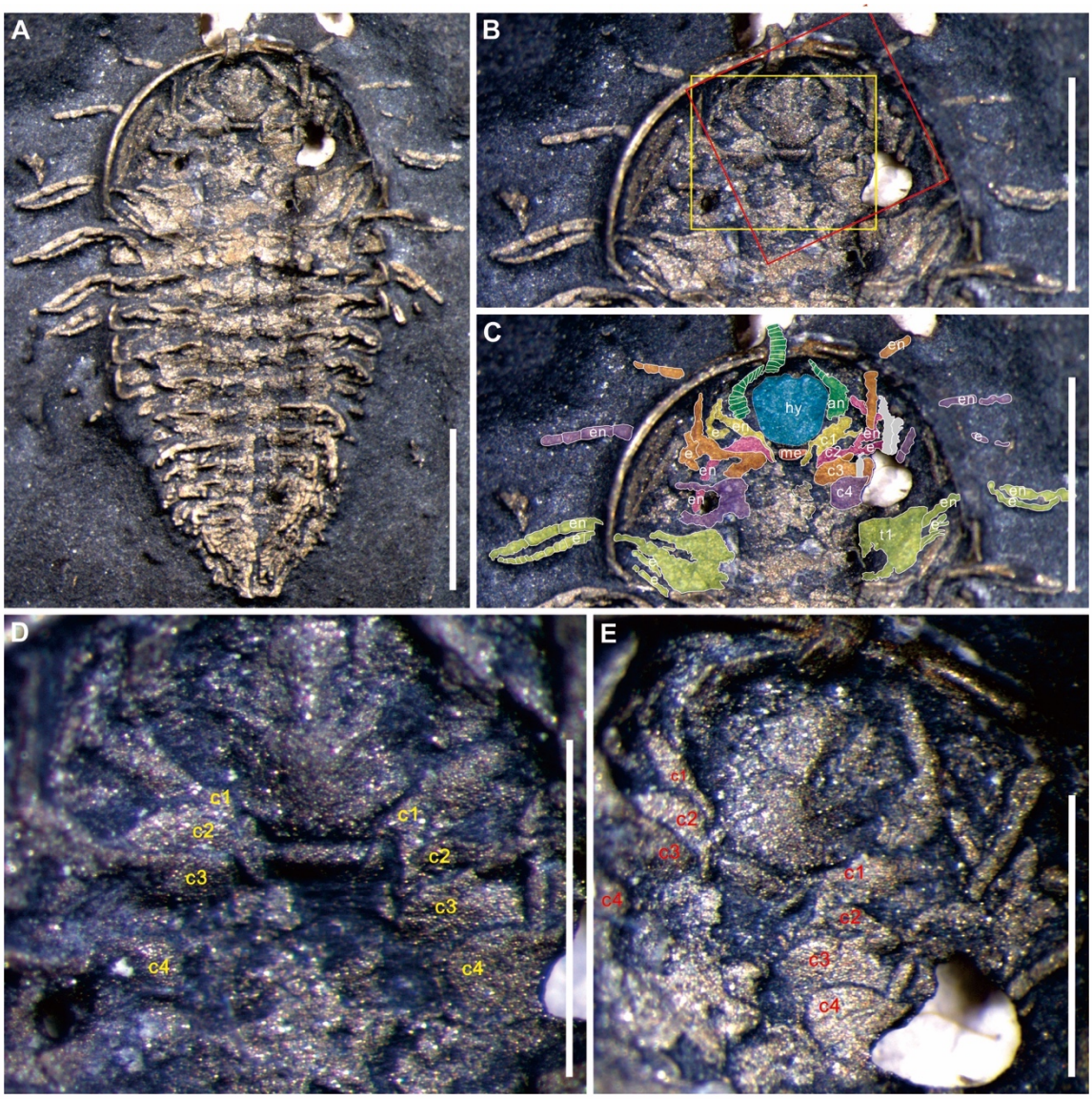

Figure S10 – *Triarthrus eatoni*. (A) ventral view of the specimen USNM 400935. (B) close-up of the cephalic appendages. (C) hypostome, metastome, and ventral appendages are colored. (D) close-up of the yellow box in figure b to show cephalic appendage bases. (E) close-up of the red box in figure b to show the cephalic appendage bases in different light direction. Scale bars, 2 mm (A, B, C), 1 mm (D, E).

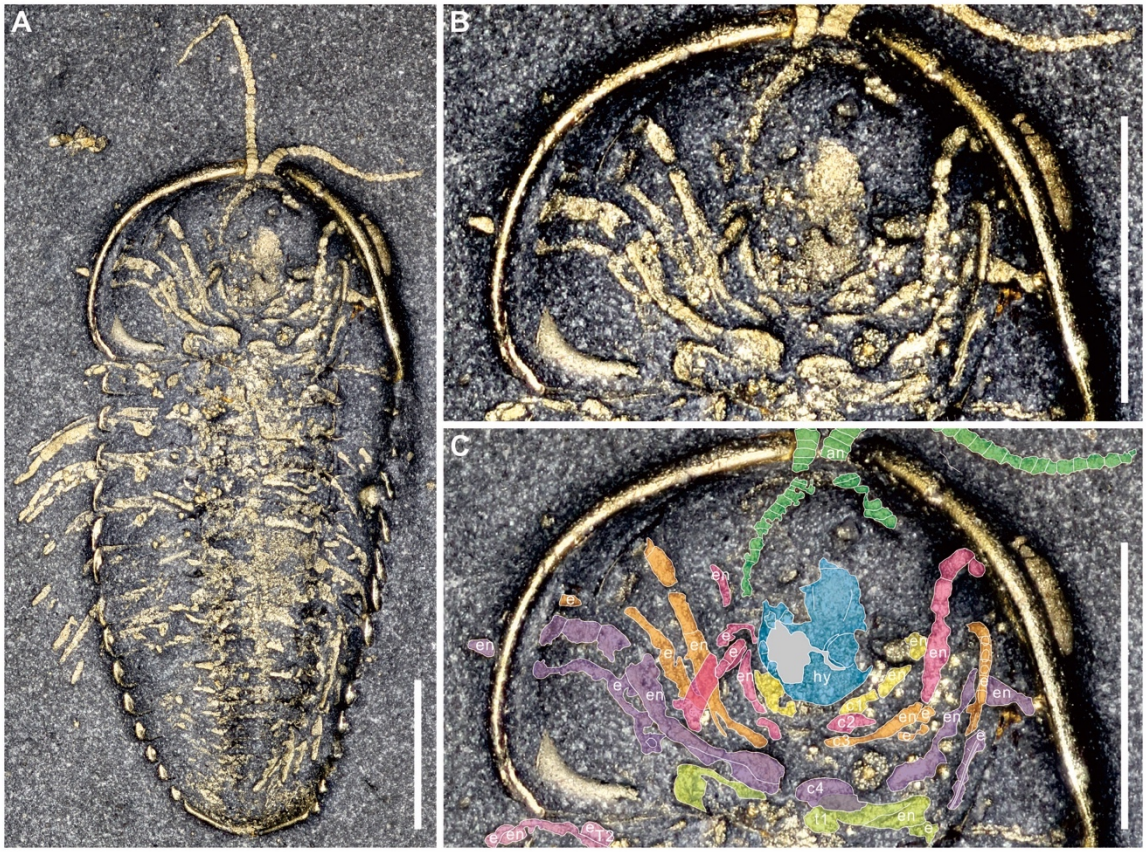

Figure S11 – *Triarthrus eatoni*. (A) ventral view of the specimen AMNH 101398. (B) close-up of the cephalic appendages. (C) hypostome and ventral appendages are colored to show the cephalic biramous appendages. Scale bars are 2mm.

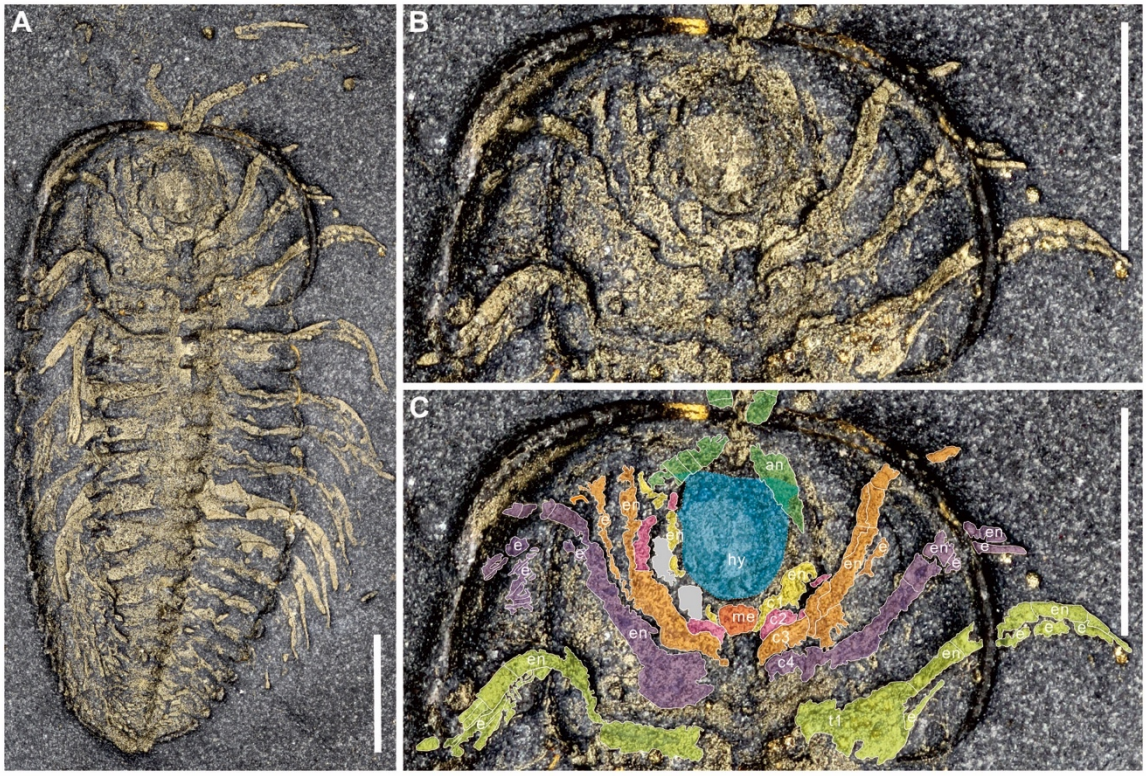

Figure S12 – *Triarthrus eatoni*. (A) ventral view of the specimen AMNH 101393. (B) close-up of the cephalic appendages. (C) hypostome, metastome, and ventral appendages are colored to show the cephalic biramous appendages. Scale bars are 2 mm.

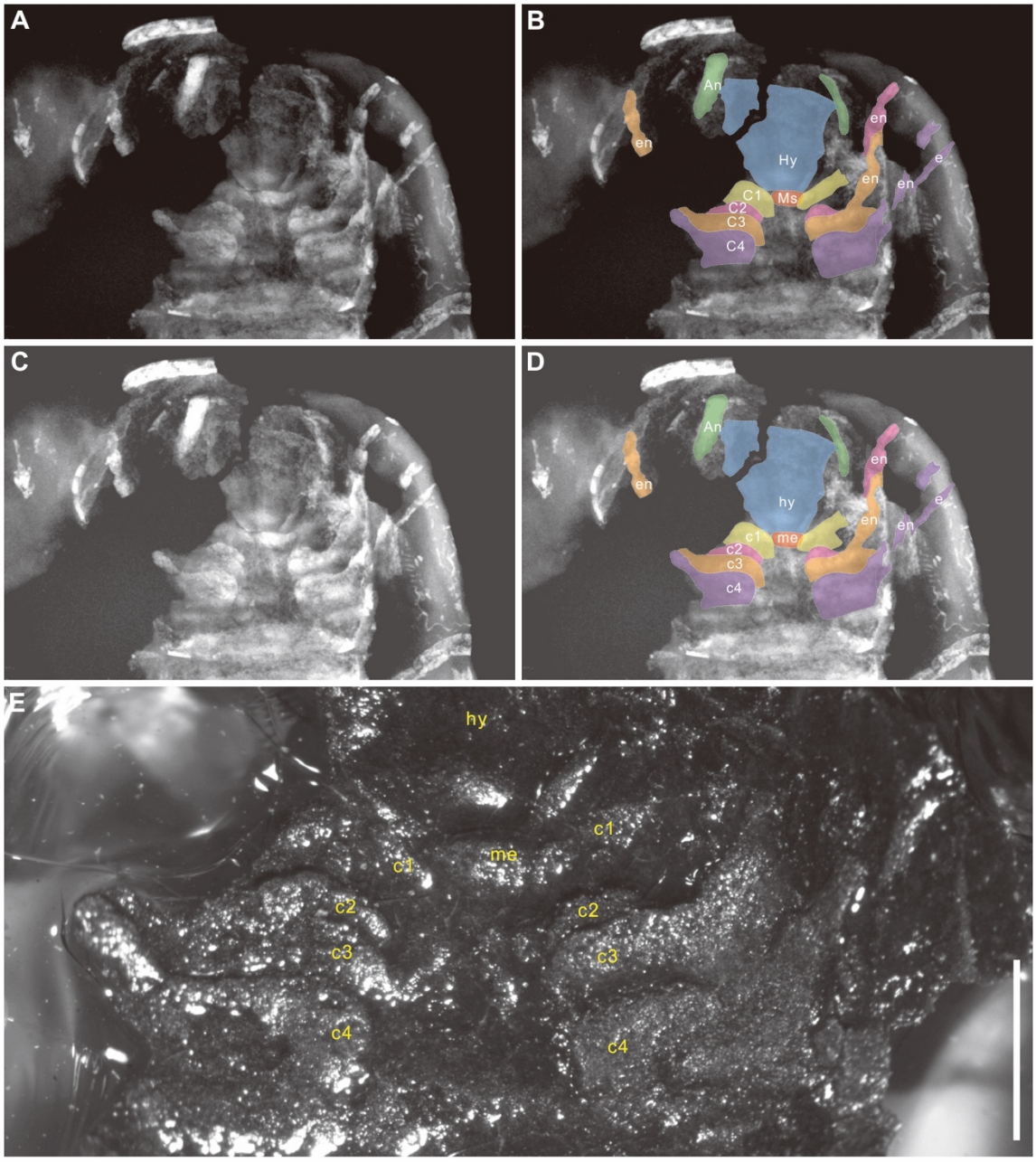

Figure S13 – *Triarthrus eatoni*. X-ray photo. (A) cephalic region of the specimen MCZ 114109 (former MCZ 7190/25). (B) colored cephalic appendages, hypostome, and metastome for comparing with figure a. (C) high contrast on the cephalic region to show cephalic structures. (D) colored cephalic appendages, hypostome, and metastome for

comparing with figure c. The brightest areas along the sagittal line (in fig. a) represent the limb bases well displayed because of their high mineralization, which is rotated forward and imbricated. (E) cephalic appendages, hypostome, and metastome are photographed under normal light condition. The X-ray photos are from the collection of "Radiographs of Beecher Bed trilobite by J. Cisne", organized by T. Whiteley. Scale bar is 1 mm for (E).

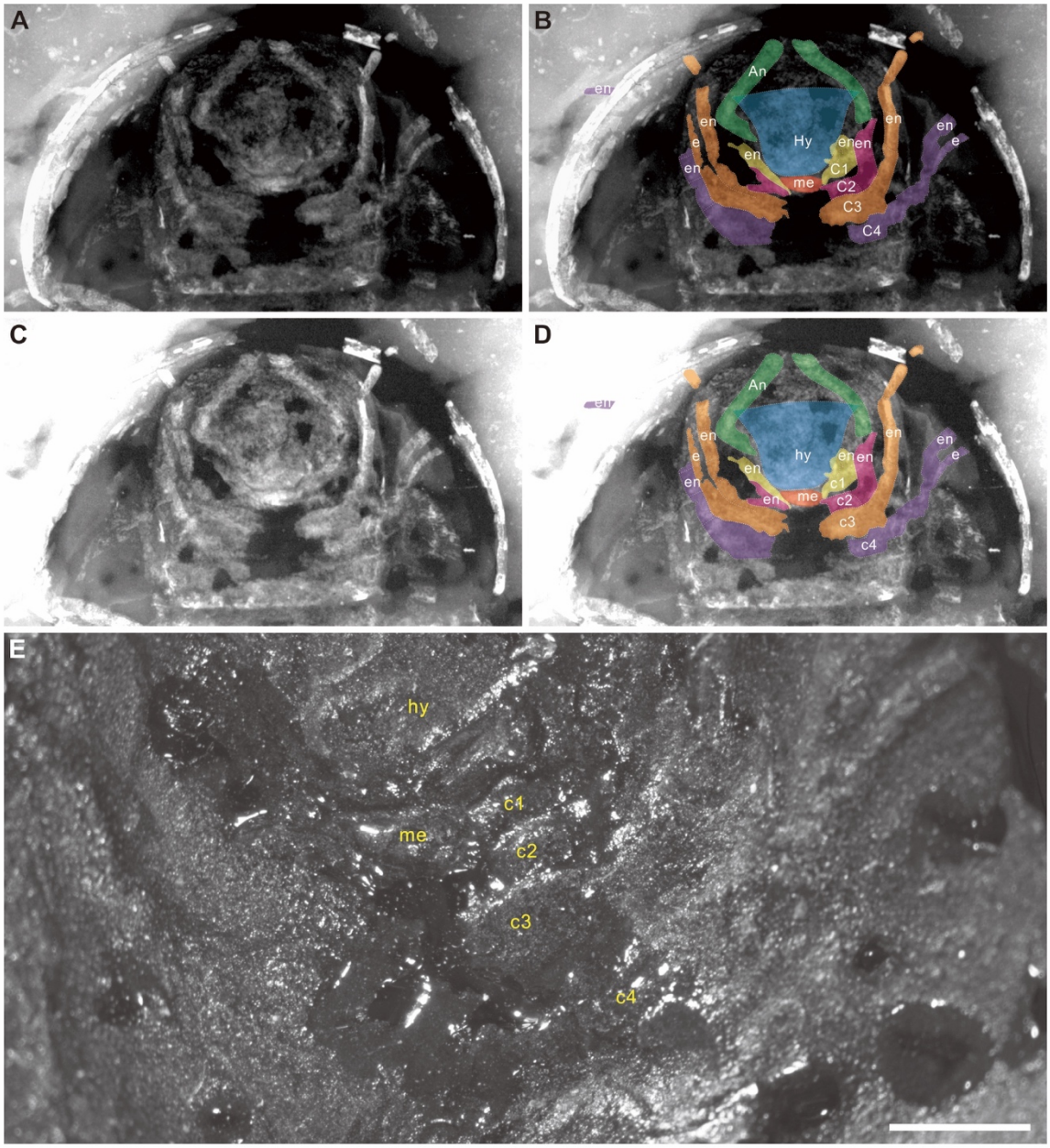

Figure S14 – *Triarthrus eatoni*. (A) cephalic region of the specimen MCZ 114108 (former MCZ 7190/22). (B) colored cephalic appendages, hypostome, and metastome for comparison with figure a. (C) high contrast on the cephalic region to show cephalic structures. (D) colored cephalic appendages, hypostome and metastome for comparison with figure c. (E) cephalic appendages, hypostome and metastome are photographed

under normal light condition. The X-ray photos are from the collection of “Radiographs of Beecher Bed trilobite by J. Cisne”, organized by T. Whiteley. Scale bar is 1 mm for (E).

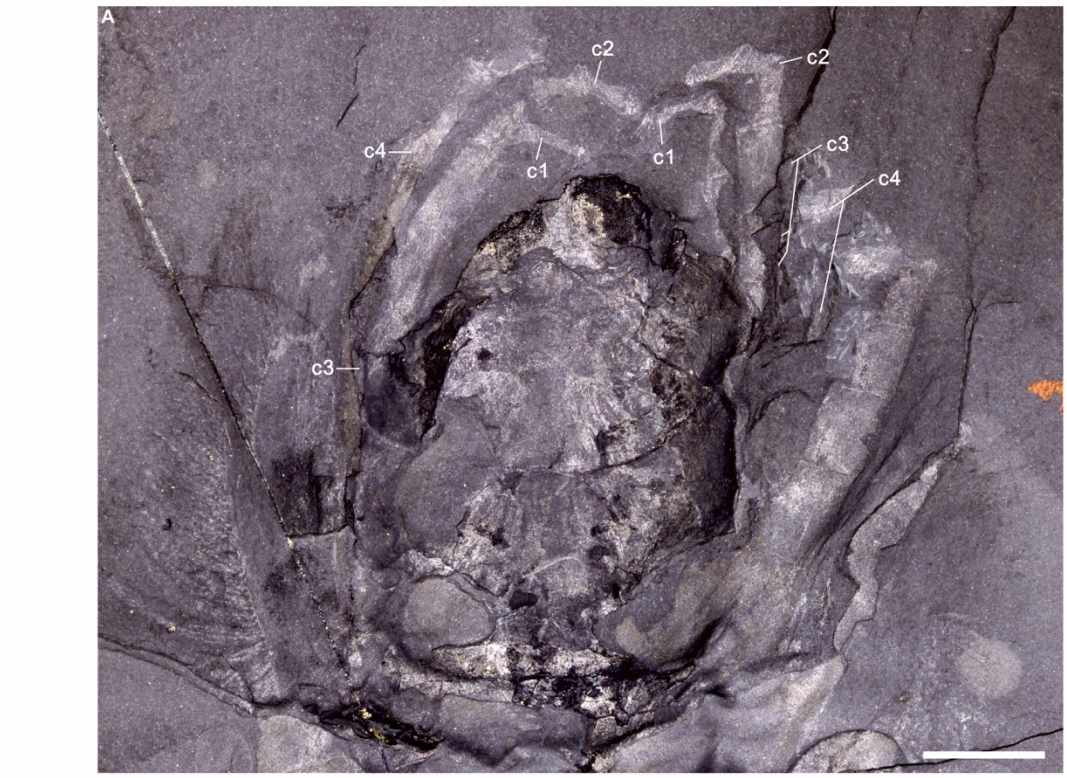

Figure S15 – *Olenoides serratus*. Four cephalic biramous appendages are recognized. Dorsal view of the specimen USNM 65520 shows four pairs of cephalic biramous appendages. Scale bar is 5 mm.

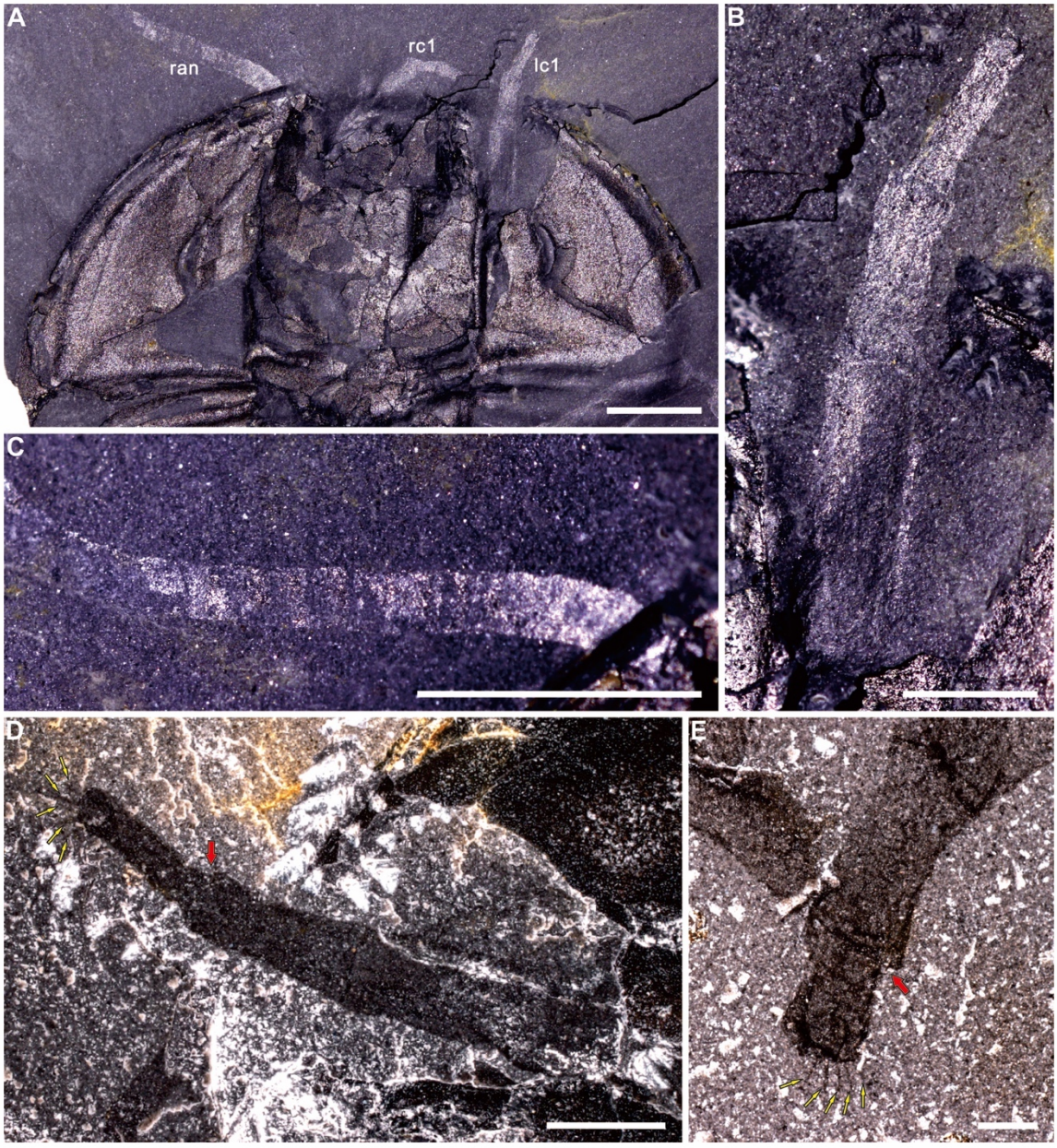

Figure S16 – *Olenoides serratus*. "Left antenna" is the 1st pair of cephalic biramous appendages. (A-D) ventral view of GSC 34693b, the counterpart of GSC34693. (A) ventral view of the head of the specimen GSC 34693b showing the right antenna, right first appendage, and left first appendage. (B) close-up of the left first cephalic appendage which is originally described as "left antenna". The appendage width is sharply

narrowing distally rather than gently reducing the width, and the appendage segments are also visible. (C) close-up of the right antenna to show articles with diameter gently narrowing distally. (D) close-up of the left first cephalic appendage with extinction lights showing boundaries of endopodal segments and about five spines around the boundary. (E) close-up of specimen GSC 34695 showing five spines around the boundary of endopod podomeres. Scale bars, 5 mm (A), 2 mm (B-D), 0.5 mm (E).

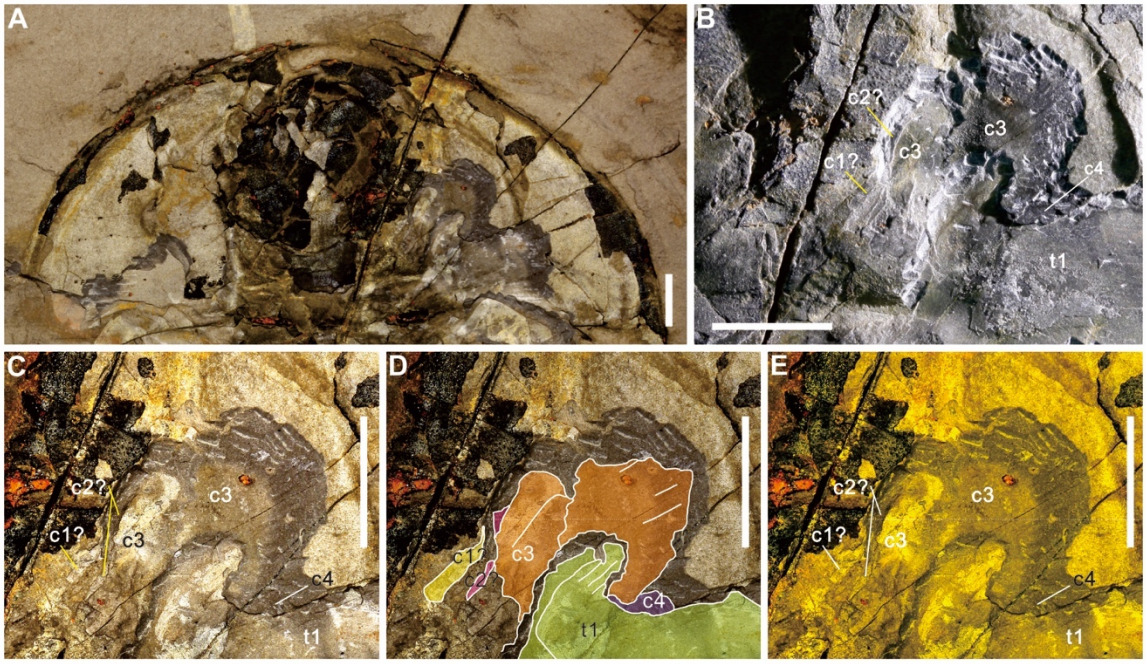

Figure S17 – *Olenoides serratus*. Four biramous cephalic appendages are recognized. (A) dorsal view of the specimen USNM 58588a to show the newly recognized possible 1st and 2nd pairs of cephalic biramous appendages. (B) close-up of the cephalic appendages. (C-E) same close-up of the cephalic regions to show the newly recognized possible 1st and 2nd pairs of cephalic appendages. A thin white dash line is a reference line for tracing the right 2nd pair of cephalic biramous appendages. Scale bars are 5 mm (A), 2 mm (B–D), 0.5 mm (E).

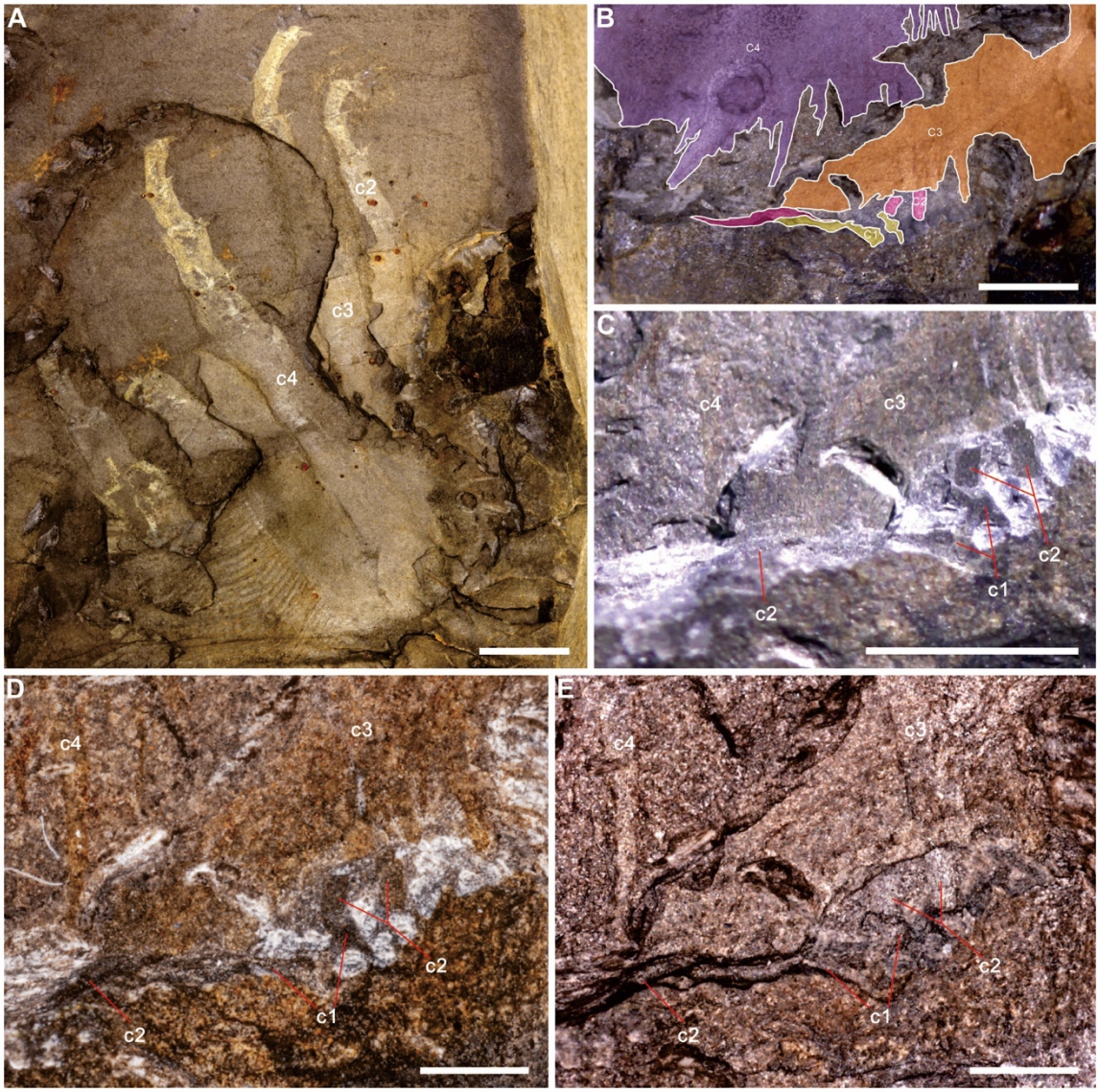

Figure S18 – *Olenoides serratus*. Four biramous cephalic appendages recognized. (A) dorsal view of the specimen USNM 65513. (B) close-up of the hidden cephalic appendages. The 1st pair of cephalic biramous appendages is in a layer above the 2nd pair of biramous appendages which is originally described as the "1st" pair of appendages. (C) close-up of the same area in Figure b but with more contrast to show the appendage structures. (D) close-up of the similar area with extinction lights. (E) close-up of the same

area as Figure d with maximum transmission lights. Scale bars, 2 mm (A-C), 1 mm (D, E).

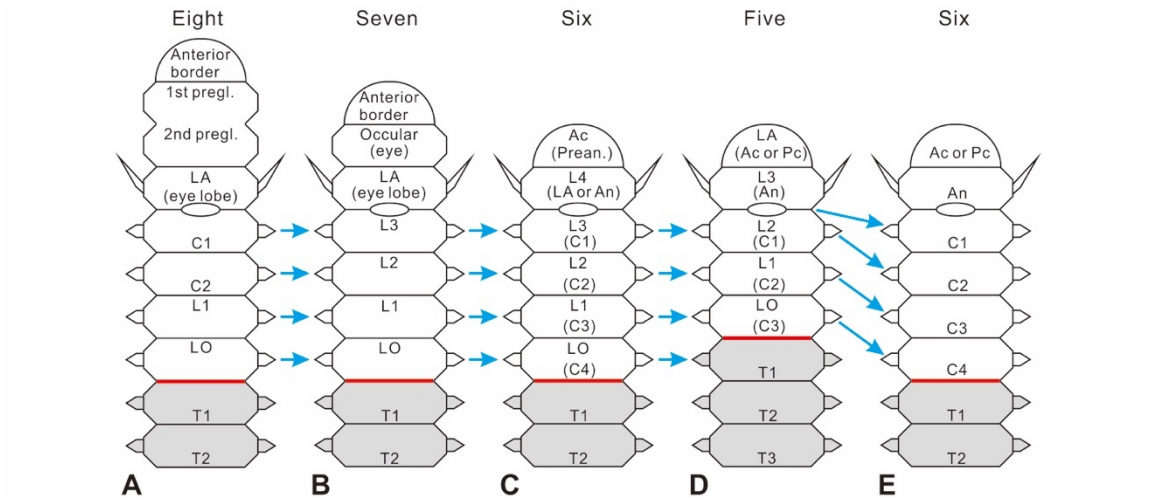

Figure S19 – Head segmentation models of Trilobita. (A) eight segments (Palmer 1957). (B) seven segments (Walcott 1910). (C) six segments (Beecher 1895, 1896; Størmer 1939; Stürmer and Bergström 1973; Walcott 1918; Bergström 1973a). (D) five segments (Brusca and Brusca 1990; Cisne 1974, 1975, 1981; Scholtz 1998; Walossek and Müller 1998; Whittington and Almond 1987a; Park and Kihm 2017). (E) six segments (current paper).

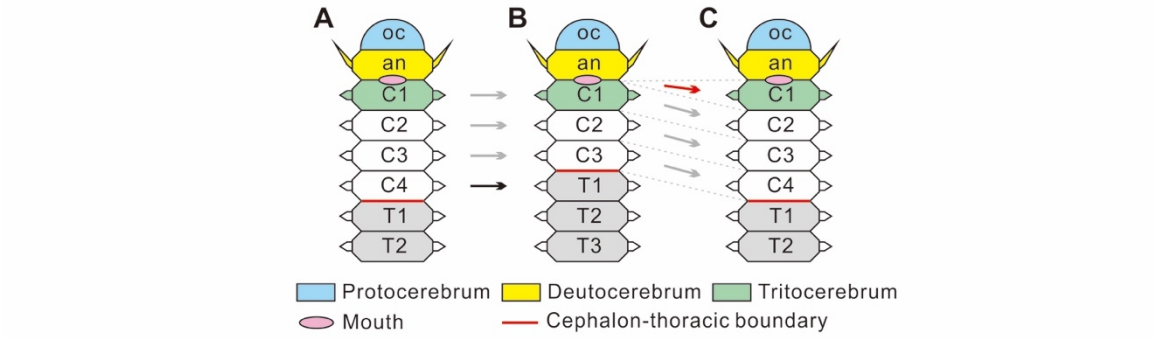

Figure S20 – Current model of head segmentation in Trilobita. (A) earliest model of trilobites with four pairs of cephalic biramous appendages which correspond to six head segments (Beecher 1895, 1896; Størmer 1939; Stürmer and Bergström 1973; Walcott 1918; Bergström 1973a). (B) widely accepted trilobite model with three pairs of cephalic biramous appendages which correspond to five head segments (Brusca and Brusca 1990; Cisne 1974, 1975, 1981; Scholtz 1998; Walossek and Müller 1998; Whittington and Almond 1987a; Park and Kihm 2017); the fourth pair of cephalic biramous appendages in Figure a is belonging to the first thoracic segment because of the anterior shift of the thoracic appendages. (C) the revised model of trilobites with four pairs of cephalic biramous appendages based on a newly observed appendage in this study, which corresponds to six head segments. Black arrow represents that the previously described "4th" cephalic appendages are belonging to the first thoracic segment. Red arrow represents that the newly discovered appendages are located between the hypostome and traditional "1st" cephalic biramous appendages. Gray arrows represent that the traditional "1st", "2nd", and "3rd" cephalic biramous appendages are changed through history to become 2nd, 3rd, and 4th cephalic biramous appendages respectively.

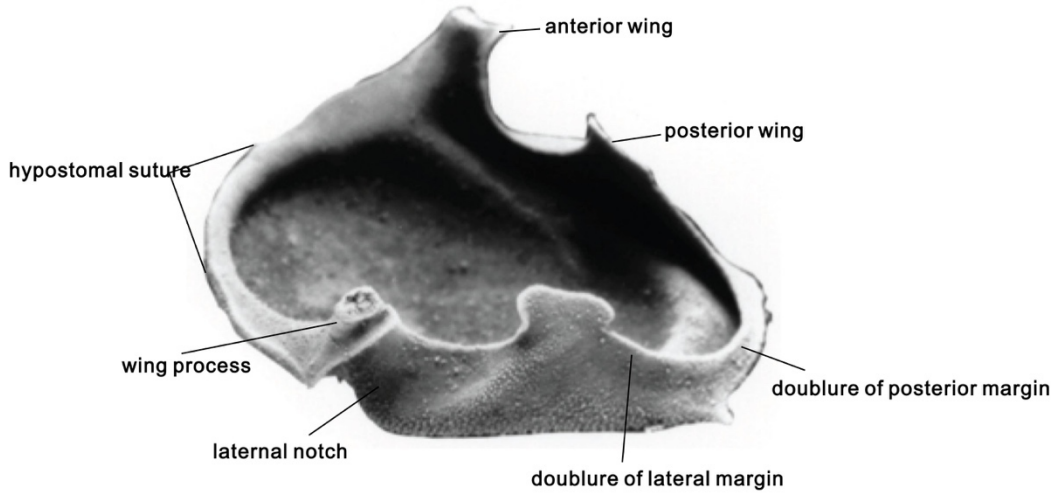

Figure S21 – Hypostome. Hypostome of trilobite *Ceraurinella typa* (modified from Whittington and Evitt 1953, pl. 10, fig. 12)(Whittington and Evitt 1953).

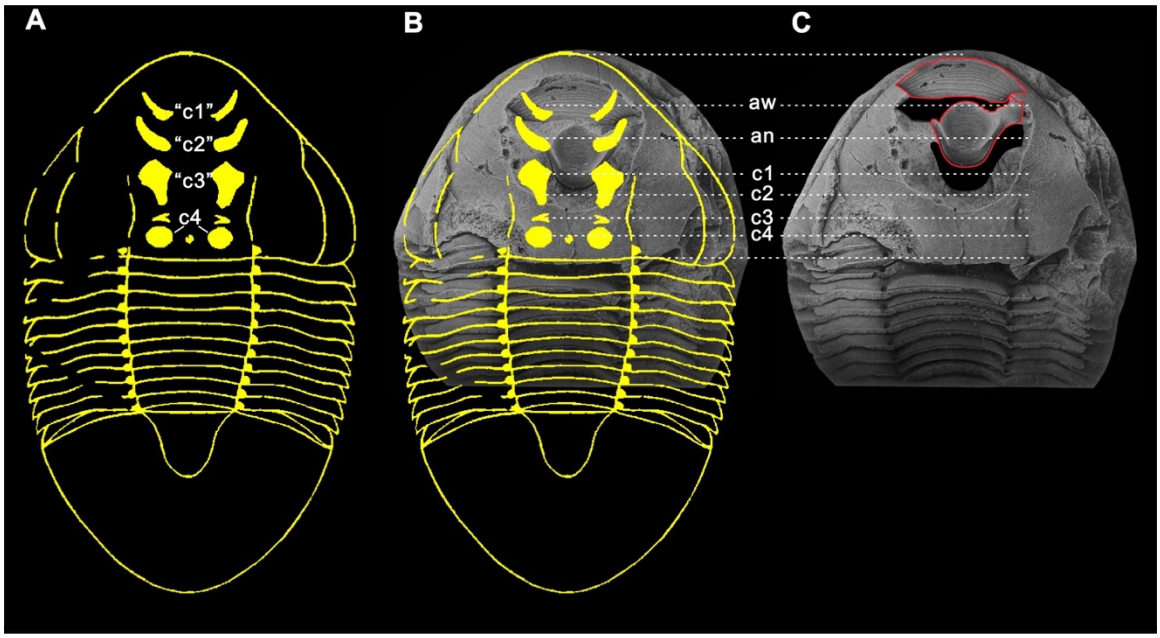

Figure S22 – Mismatching muscle attachments with limbs. (A-C) *Ectilaenus (katzeri) katzeri*. (A) reconstruction shows four pairs of muscle attachment sites on the cephalon are correlated to the four pairs of cephalic "biramous" limbs (modified from Harrington et al. 1959, p. O95, fig. 70B)(Harrington *et al*. 1959b). (B) overlapping reconstruction and specimen preserved with hypostome and rostrum in situ (Bruthansová 2003, fig. 2e)(Bruthansová 2003). (C) hypostome and rostrum marked with the red outline to be artificially moved anteriorly to align with the cephalic margin.

CONCLUSION

This study is mainly around the trilobite limbs to discuss whether trilobites bear a respiratory gill or not and how efficient the oxygen uptake is and how cephalic limbs influence our understanding of the development of arthropod heads.

For answering the first question, three pieces of evidence are liked together to support the respiratory function. One is the cross-section of filament that is most comparable to the gill system of modern crustaceans. The circulation of afferent and efferent channels made the deoxygenated-to-oxygenated hemolymphs to be transported. The other evidence is the articulation between the limb and the body. The upper branch is connected ventrally to the limb base of the lower branch and dorsally to the body wall by the extended arthrodial membrane. This articulation type is similar to the book gills of *Limulus* connected with the body wall. The last is revealed from the anterior imbrication of upper branches. Such an imbrication has limited the upper branch to be located between the ventral dorsal exoskeleton and lower branch, restricting the efficient swimming ability and protecting the fragile gill filaments.

Secondly, the mechanical rotation of upper branch is restricted to the up and forward direction, and their reserve strokes, and the filaments point upward direction. The general up forward rotation creates down backward goring water current. The hemolymphs in the filaments are charged with oxygens in a path generally flowing upward. The convention of down backward going water current and upward flowing hemolymph initiated the efficient countercurrent exchange mechanism. Such a design is also suggested to be present in the early Cambrian deuterostome Yunnaozoan. An

efficient gas exchange mechanism is, at least, already established in the early Cambrian protostomes and deuterostomes.

Lastly, one more pair of limbs, with little trace left on the cephalic region, is located in front of the traditionally recognized "1st" pair of cephalic biramous limbs. This pair of limbs revised the trilobite head with five pairs of cephalic limbs, one pair of antennae followed by four pairs of "biramous" limbs. This challenges the well match between cephalic limbs and their dorsal furrows. Compared to the location of hypostome, the cephalic limbs are all related with their corresponding muscle attachment sites. The merged muscle attachment sites of 2nd and 3rd pairs of cephalic limbs, because of the bifurcation of glabellar furrow, are responsible for the distinct mismatch. This may represent the general mismatch pattern among arthropods as the anteriorly moving trunk appendages to the head region are helping the feeding function.

REFERENCES

ADRAIN, J. M., FORTEY, R. A. and WESTROP, S. R. 1998. Post-Cambrian Trilobite Diversity and Evolutionary Faunas. *Science*, **280**, 1922–1925.

ARIA, C. and CARON, J.-B. 2017a. Burgess Shale fossils illustrate the origin of the mandibulate body plan. *Nature*, **545**, 89–92.

--- 2017b. Mandibulate convergence in an armoured Cambrian stem chelicerate. *BMC Evolutionary Biology*, **17**, 261.

--- 2019. A middle Cambrian arthropod with chelicerae and proto-book gills. *Nature*, **573**, 586–589.

ASTALL, C. A., ANDERSON, S. J., TAYLOR, A. C. and ATKINSON, R. J. A. 1997. Comparative studies of the branchial morphology, gill area and gill ultrastructure of some thalassinidean mud-shrimps (Crustacea: Decapoda: Thalassinidea). *Journal of Zoology*, **241**, 665–688.

BEECHER, C. E. 1893. On the thoracic legs of *Triarthrus*. *American Journal of Science*, **46**, 467–470.

--- 1895. Further observations on the ventral structure of *Triarthrus*. *American Geologist*, **15**, 91–100.

--- 1896. The morphology of Triarthrus. *American Journal of Science*, **1**, 251–256.

BERGSTRÖM, J. 1969. Remarks on the appendages of trilobites. *Lethaia*, **2**, 395–414.

--- 1973a. Fossils and Strata. *Organization, life, and systematics of trilobites*. Universitetsforlaget, Oslo, 69 pp.

--- 1973b. Fossils and Strata. *Organization, life, and systematics of trilobites*. Universitetsforlaget, Oslo.

BERGSTRÖM, J. and BRASSEL, G. 1984. Legs in the trilobite *Rhenops* from the Lower Devonian Hunsrück Slate. *Lethaia*, **17**, 67–72.

BOND, A. D. and EDGECOMBE, G. D. 2020. Phylogenetic response of naraoiid arthropods to early–middle Cambrian environmental change. *Palaeontology*.

BOXSHALL, G. A. 2004. The evolution of arthropod limbs. *Biological Reviews*, **79**, 253–300.

BOXSHALLL, G. A. and JAUME, D. 2009. Exopodites, epipodites and gills in crustaceans. *Arthropod Systematics & Phylogeny*, **67**, 229–254.

BRIGGS, D. E. G. 2015. Extraordinary fossils reveal the nature of Cambrian life: a commentary on Whittington (1975)'The enigmatic animal *Opabinia regalis*, Middle Cambrian, Burgess Shale, British Columbia'. *Philosophical Transactions of the Royal Society B: Biological Sciences*, **370**, 20140313.

BRIGGS, D. E. G., BOTTRELL, S. H. and RAISWELL, R. 1991. Pyritization of soft-bodied fossils: Beecher's Trilobite Bed, Upper Ordovician, New York State. *Geology*, **19**, 1221–1224.

BRIGGS, D. E. G., ERWIN, D. H. and COLLIER, F. J. 1994. *The fossils of the Burgess Shale*. Smithsonian Institution Press, Washington and London.

BRIGGS, D. E. G. and FORTEY, R. A. 1989. The early radiation and relationships of the major arthropod groups. *Science*, **246**, 241–243.

BRIGGS, D. E. G., SIVETER, D. J. and SIVETER, D. J. 1996. Soft-bodied fossils from a Silurian volcaniclastic deposit. *Nature*, **382**, 248–250.

BRIGGS, D. E. G., SIVETER, D. J., SIVETER, D. J., SUTTON, M. D., GARWOOD, R. J. and LEGG, D. 2012. Silurian horseshoe crab illuminates the evolution of arthropod limbs. *Proceedings of the National Academy of Sciences of the United States of America*, **109**, 15702–15705.

BRUSCA, R. C. and BRUSCA, G. J. 1990. Sinauer Associates, Sunderland, Mass. *Invertebrates*. 922 pp.

BRUTHANSOVÁ, J. 2003. The trilobite Family Illaenidae Hawle et Corda. 1847 from the Ordovician of the Prague Basin (Czech Republic). *TRANSACTIONS-ROYAL SOCIETY OF EDINBURGH*, **93**, 167–190.

BRUTON, D. L. and HAAS, W. 1997. Functional morphology of Phacopinae (Trilobita) and the mechanics ofenrolment. *Palaeontographica Abteilung A*, **245**, 1-43.

--- 2003. Making *Phacops* come alive. *Special Papers in Palaeontology*, **70**, 331–348.

BUDD, G. E. 1996. The morphology of *Opabinia regalis* and the reconstruction of the arthropod stem-group. *Lethaia*, **29**, 1–14.

--- 2002. A palaeontological solution to the arthropod head problem. *Nature*, **417**, 271–275.

BUDD, G. E. and DALEY, A. C. 2012. The lobes and lobopods of *Opabinia regalis* from the middle Cambrian Burgess Shale. *Lethaia*, **45**, 83–95.

BUDD, G. E. and TELFORD, M. J. 2009. The origin and evolution of arthropods. *Nature*, **457**, 812–817.

CAMPBELL, K. S. W. 1975. The functional anatomy of phacopid trilobites: musculature and eyes. 168–188. *Journal and Proceedings, Royal Society of New South Wales*.

CHATTERTON, B. D. E. and LUDVIGSEN, R. 1998. Upper Steptoean (Upper Cambrian) trilobites from the McKay Group of southeastern British Columbia, Canada. *Memoir (The Paleontological Society)*, **49**, 1–43.

CHEN, J. Y., EDGECOMBE, G. D. and RAMSKÖLD, L. 1997. Morphological and ecological disparity in naraoiids (Arthropoda) from the Early Cambrian Chengjiang Fauna, China. *Records of the Australian Museum*, **49**, 1–24.

CHIPMAN, A. D. 2015. An embryological perspective on the early arthropod fossil record. *BMC Evolutionary Biology*, **15**, 285.

CISNE, J. L. 1974. Trilobites and the origin of arthropods. *Science*, **186**, 13–18.

--- 1975. Anatomy of *Triarthrus* and the relationships of the Trilobita. *Fossils and Strata*, **4**, 45–63.

--- 1981. Palaeontolographica America. *Triarthrus eatoni (Trilobita): anatomy of its exoskeletal, skeletomuscular, and digestive systems*. Paleontological Research Institution, Ithaca, New York, U.S.A., 142 pp.

CONWAY MORRIS, S. and CARON, J. B. 2014. A primitive fish from the Cambrian of North America. *Nature*, **512**, 419–422.

COWEN, R. 1973. Respiration in metazoan evolution. *Evolution*, 696–701.

DALEY, A. C., BUDD, G. E., CARON, J.-B., EDGECOMBE, G. D. and COLLINS, D. 2009. The Burgess Shale anomalocaridid *Hurdia* and its significance for early euarthropod evolution. *Science*, **323**, 1597–1600.

DAMEN, W. G. M., HAUSDORF, M., SEYFARTH, E. A. and TAUTZ, D. 1998. A conserved mode of head segmentation in arthropods revealed by the expression pattern of Hox genes in a spider. *Proceedings of the National Academy of Sciences of the United States of America*, **95**, 10665–10670.

DONOGHUE, P. C. J. and PURNELL, M. A. 2009. Distinguishing heat from light in debate over controversial fossils. *BioEssays*, **31**, 178–189.

DROSER, M. L., TARHAN, L. G. and GEHLING, J. G. 2017. The rise of animals in a changing environment: global ecological innovation in the late Ediacaran. *Annual review of earth and planetary sciences*, **45**, 593–617.

DUNLOP, J. A. and LAMSDELL, J. C. 2017. Segmentation and tagmosis in Chelicerata. *Arthropod structure & development*, **46**, 395–418.

EDGECOMBE, G. D. and LEGG, D. A. 2014. Origins and early evolution of arthropods. *Palaeontology*, **57**, 457–468.

EDGECOMBE, G. D. and RAMSKÖLD, L. 1999. Relationships of Cambrian Arachnata and the systematic position of Trilobita. *Journal of Paleontology*, **73**, 263–287.

FARLEY, R. D. 2010. Book gill development in embryos and first and second instars of the horseshoe crab *Limulus polyphemus* L.(Chelicerata, Xiphosura). *Arthropod Structure & Development*, **39**, 369–381.

FARRELL, U. C., BRIGGS, D. E. G. and GAINES, R. R. 2011. Paleoecology of the olenid trilobite *Triarthrus*: new evidence from Beecher's Trilobite Bed and other sites of pyritization. *Palaios*, **26**, 730-742.

FARRELL, U. C., MARTIN, M. J., HAGADORN, J. W., WHITELEY, T. and BRIGGS, D. E. G. 2009. Beyond Beecher's Trilobite Bed: Widespread pyritization of soft tissues in the Late Ordovician Taconic foreland basin. *Geology*, **37**, 907–910.

FARRELLY, C. A. and GREENAWAY, P. 1992. Morphology and ultrastructure of the gills of terrestrial crabs (Crustacea, Gecarcinidae and Grapsidae): adaptations for air-breathing. *Zoomorphology*, **112**, 39–49.

FOOTE, M. 1993a. Contributions of individual taxa to overall morphological disparity. *Paleobiology*, **19**, 403–419.

--- 1993b. Discordance and concordance between morphological and taxonomic diversity. *Paleobiology*, **19**, 185–204.

FORTEY, R. A. 2001. Trilobite systematics: the last 75 years. *Journal of Paleontology*, **75**, 1141–1151.

--- 2004. Lifestyles of the trilobites. *American Scientist*, **92**, 446–453.

FORTEY, R. A. and OWENS, R. M. 1990. Trilobites. *Evolutionary trends*, 121–142.

--- 1999. Feeding habits in trilobites. *Palaeontology*, **42**, 429-465.

FORTEY, R. A. and WILMOT, N. V. 1991. Trilobite cuticle thickness in relation to palaeoenvironment. *Paläontologische Zeitschrift*, **65**, 141–151.

FU, D., ORTEGA-HERNÁNDEZ, J., DALEY, A. C., ZHANG, X. and SHU, D. 2018. Anamorphic development and extended parental care in a 520 million-year-old stem-group euarthropod from China. *BMC evolutionary biology*, **18**, 147.

FUSCO, G. and MINELLI, A. 2013. Arthropod segmentation and tagmosis. 197–221. *In* MINELLI, A., BOXSHALL, G. and FUSCO, G. (eds). *Arthropod biology and evolution*. Springer, 9 pp. Custom 7.

GAINES, R. R. 2014. Burgess Shale-type preservation and its distribution in space and time. *The Paleontological Society Papers*, **20**, 123–146.

GAINES, R. R., BRIGGS, D. E. G. and ZHAO, Y. L. 2008. Cambrian Burgess Shale–type deposits share a common mode of fossilization. *Geology*, **36**, 755.

GAINES, R. R. and DROSER, M. L. 2003. Paleoecology of the familiar trilobite *Elrathia kingii*: An early exaerobic zone inhabitant. *Geology*, **31**, 941–944.

GEYER, G. 1994. Cambrian corynexochid trilobites from Morocco. *Journal of Paleontology*, **68**, 1306–1320.

GILLIS, J. A., FRITZENWANKER, J. H. and LOWE, C. J. 2012. A stem-deuterostome origin of the vertebrate pharyngeal transcriptional network. *Proceedings of the Royal Society B: Biological Sciences*, **279**, 237-246.

GOODMAN, S. H. and CAVEY, M. J. 1990. Organization of a phyllobranchiate gill from the green shore crab *Carcinus maenas* (Crustacea, Decapoda). *Cell and Tissue Research*, **260**, 495–505.

GRAHAM, J. B. 1990. Ecological, evolutionary, and physical factors influencing aquatic animal respiration. *American Zoologist*, **30**, 137–146.

HALL, J. 1838. Descriptions of two species of Trilobites, belonging to the genus *Paradoxides*. *American Journal of Science and Arts*, **33**, 137–142.

HARRINGTON, H. J., HENNINGSMOEN, G., HOWELL, B. F., JAANUS-SON, V., LOCHMAN-BALK, C., MOORE, R. C., POULSEN, C., RASETTI, F., RICHTER, E., RSCHMIDT, H., SDZUY, K., STRUVE, W., STØRMER, L., STUBBLEFIELD, C. J., TRIPP, R., WELLER, J. M. and WHITTINGTON, H. B. 1959a. *Treatise on Invertebrate Paleontology. Part O, Arthropoda 1, Arthropoda-General features, Protarthropoda, Euarthropoda-General features, Trilobitomorpha*. Geological Society of America and University of Kansas Press, New York and Lawrence, Kansas, 560 pp.

HARRINGTON, H. J., MOORE, R. C. and STUBBLEFIEDL, C. J. 1959b. Morphological terms applied to Trilobita. 117–126. *In* MOORE, R. C. (ed.) *Treatise on Invertebrate Paleontology (O) Arthropoda 1*. Geological Society of America and University of Kansas Press, New York and Lawrence, Kansas, pp. Custom 7.

HAUG, C. and HAUG, J. T. 2016. New insights into the appendage morphology of the Cambrian trilobite-like arthropod *Naraoia compacta*. *Bulletin of Geosciences*, **91**, 221–227.

HEPBURN, H. R. and CHANDLER, H. D. 1976. Material properties of arthropod cuticles: the arthrodial membranes. *Journal of Comparative Physiology B: Biochemical, Systemic, and Environmental Physiology*, **109**, 177–198.

HESSLER, R. R. 1985. Swimming in crustacea. *Earth and Environmental Science Transactions of The Royal Society of Edinburgh*, **76**, 115–122.

HOPKINS, M. J., CHEN, F., HU, S. and ZHANG, Z. 2017. The oldest known digestive system consisting of both paired digestive glands and a crop from exceptionally preserved trilobites of the Guanshan Biota (Early Cambrian, China). *PloS one*, **12**, e0184982.

HOPKINS, M. J. and WEBSTER, M. 2009. Ontogeny and geographic variation of a new species of the corynexochine trilobite *Zacanthopsis* (Dyeran, Cambrian). *Journal of Paleontology*, **83**, 524–547.

HOU, J. B., HUGHES, N. C. and HOPKINS, M. J. 2021. The trilobite upper limb branch is a well-developed gill. *Science Advances*, **7**, eabe7377.

HOU, J. B., HUGHES, N. C., LAN, T., YANG, J. and ZHANG, X. G. 2015. Early postembryonic to mature ontogeny of the oryctocephalid trilobite *Duodingia duodingensis* from the lower Cambrian (Series 2) of southern China. *Papers in Palaeontology*, **1**, 497–513.

HOU, J. B., HUGHES, N. C., YANG, J., LAN, T., ZHANG, X. G. and DOMINGUEZ, C. 2017. Ontogeny of the articulated yiliangellinine trilobite *Zhangshania typica* from the lower Cambrian (Series 2, Stage 3) of southern China. *Journal of Paleontology*, **91**, 86–99.

HOU, X. G. and BERGSTRÖM, J. 1997. Fossils and Strata. *Arthropods of the Lower Cambrian Chengjiang fauna, southwest China*. Scandinavian University Press, Oslo, Norway, 116 pp.

HUGHES, G. M., KNIGHTS, B. and SCAMMELL, C. A. 1969. The distribution of PO2 and hydrostatic pressure changes within the branchial chambers in relation to gill ventilation of the shore crab *Carcinus maenas* L. *Journal of Experimental Biology*, **51**, 203–220.

HUGHES, N. C. 2003. Trilobite tagmosis and body patterning from morphological and developmental perspectives. *Integrative and Comparative Biology*, **43**, 185–206.

--- 2005. Trilobite construction: Building a bridge across the micro- and macroevolutionary divide. 139–158. *In* BRIGGS, D. E. G. (ed.) *From evolving form and function: fossils and development*. Peabody Museum of NAtural History, Yale University New Haven, Connecticut, pp. Custom 7.

--- 2007. The Evolution of Trilobite Body Patterning. *Annual Review of Earth and Planetary Sciences*, **35**, 401–434.

HUGHES, N. C., KŘÍŽ, J., MACQUAKER, J. H. S. and HUFF, W. D. 2014. The depositional environment and taphonomy of the Homerian "*Aulacopleura* shales" fossil assemblage near Loděnice, Czech Republic (Prague Basin, Perunican microcontinent). *Bulletin of Geosciences*, **89**, 219–238.

JANSSEN, R., PRPIC, N. M. and DAMEN, W. G. M. 2004. Gene expression suggests decoupled dorsal and ventral segmentation in the millipede *Glomeris marginata* (Myriapoda: Diplopoda). *Developmental Biology*, **268**, 89–104.

KNOLL, A. H. 2011. The multiple origins of complex multicellularity. *Annual Review of Earth and Planetary Sciences*, **39**, 217–239.

LE CONTE, J. 1900. *Outlines of the comparative physiology and morphology of animals*. D. Appleton and Company, New York.

LEGG, D. A., SUTTON, M. D. and EDGECOMBE, G. D. 2013. Arthropod fossil data increase congruence of morphological and molecular phylogenies. *Nature Communications*, **4**, 2485.

LEROSEY-AUBRIL, R., HEGNA, T. A. and OLIVE, S. 2011. Inferring internal anatomy from the trilobite exoskeleton: the relationship between frontal auxiliary impressions and the digestive system. *Lethaia*, **44**, 166–184.

LIU, Y., HOU, X. G. and BERGSTRÖM, J. 2007. Chengjiang arthropod *Leanchoilia illecebrosa* (Hou, 1987) reconsidered. *GFF*, **129**, 263–272.

LUQUET, C. M., ROSA, G. A., FERRARI, C. C., GENOVESE, G. and PELLERANO, G. N. 2000. Gill morphology of the intertidal estuarine crab *Chasmagnathus granulatus* Dana, 1851 (Decapoda, Grapsidae) in relation to habitat and respiratory habits. *Crustaceana*, **73**, 53–68.

LYONS, T. W., REINHARD, C. T. and PLANAVSKY, N. J. 2014. The rise of oxygen in Earth's early ocean and atmosphere. *Nature*, **506**, 307–315.

MAINA, J. N. 1990. The morphology of the gills of the freshwater African crab *Potamon niloticus* (Crustacea: Brachyura: Potamonidae): a scanning and transmission electron microscopic study. *Journal of Zoology*, **221**, 499–515.

MANTON, S. M. 1978. Habits, functional morphology and the evolution of pycnogonids. *Zoological Journal of the Linnean Society*, **63**, 1–22.

MAYER, G., MARTIN, C., RUDIGER, J., KAUSCHKE, S., STEVENSON, P. A., POPRAWA, I., HOHBERG, K., SCHILL, R. O., PFLUGER, H. J. and SCHLEGEL, M. 2013. Selective neuronal staining in tardigrades and onychophorans provides insights into the evolution of segmental ganglia in panarthropods. *BMC Evolutionary Biology*, **13**, 230.

MAYERS, B., ARIA, C. and CARON, J. B. 2019. Three new naraoiid species from the Burgess Shale, with a morphometric and phylogenetic reinvestigation of Naraoiidae. *Palaeontology*, **62**, 19–50.

MCMAHON, B. R. 1981. Oxygen uptake and acid-base balance during activity in decapod crustaceans. 299–335. *In* HERREID II, C. F. and FOURTNER, C. R. (eds). *Locomotion and energetics in arthropods*. Plenum Press, New York, pp. Custom 7.

--- 2001. Control of cardiovascular function and its evolution in Crustacea. *Journal of Experimental Biology*, **204**, 923–932.

MCMAHON, B. R. and WILKENS, J. L. 1983. Ventilation, perfusion and oxygen uptake. 289–372. *In* BLISS, D. E. (ed.) Internal anatomy and physiological regulation, *The biology of Crustacea*. Academic Press, New York, pp. Custom 7.

MILL, P. J. 1972. *Respiration in the Invertebrates*. The Macmillan Press Limited, London, 212 pp.

MINELLI, A. 2003. *The development of animal form: ontogeny, morphology, and evolution*. Cambridge University Press, Cambridge.

MONAHAN-EARLEY, R., DVORAK, A. M. and AIRD, W. C. 2013. Evolutionary origins of the blood vascular system and endothelium. *Journal of Thrombosis and Haemostasis*, **11**, 46–66.

MÜLLER, K. J. and WALOSSEK, D. 1985. Fossils and Strata. *Skaracarida, a new order of Crustacea from the Upper Cambrian of Västergötland, Sweden*. Universitetsforlaget, Oslo, 1–65 pp.

--- 1987. Fossils and Strata. *Morphology, ontogeny, and life habit of Agnostus pisiformis from the Upper Cam brian of Sweden. Fossils and Strata*. Universitetsforlaget, Oslo , Norway, 124 pp.

ORTEGA-HERNÁNDEZ, J., LEGG, D. A. and BRADDY, S. J. 2013. The phylogeny of aglaspidid arthropods and the internal relationships within Artiopoda. *Cladistics*, **29**, 15–45.

OU, Q., CONWAY MORRIS, S., HAN, J., ZHANG, Z., LIU, J., CHEN, A., ZHANG, X. and SHU, D. 2012. Evidence for gill slits and a pharynx in Cambrian vetulicolians: implications for the early evolution of deuterostomes. *BMC Biology*, **10**, 81.

PALMER, A. R. 1957. Ontogenetic development of two olenellid trilobites. *Journal of Paleontology*, **31**, 105–128.

--- 1965. Biomere: A new kind of biostratigraphic unit. *Journal of Paleontology*, **39**, 149–153.

--- 1984. The biomere problem: evolution of an idea. *Journal of Paleontology*, **58**, 599–611.

PARK, T. Y. S. and KIHM, J. H. 2017. Head segmentation of trilobites. *Lethaia Focus*, **50**, 1–6.

PERRY, S. F., LAMBERTZ, M. and SCHMITZ, A. 2019. *Respiratory Biology of Animals: evolutionary and functional morphology*. Oxford University Press, New York, United States of America, 256 pp.

RAMSKÖLD, L., CHEN, J. Y., EDGECOMBE, G. D. and ZHOU, G. Q. 1997. Cindarella and the arachnate clade Xandarellida. *Transactions of the Royal Society of Edinburgh: Earth Sciences*, **88**, 19–38.

RAMSKÖLD, L. and EDGECOMBE, G. D. 1996. Trilobite appendage structure - *Eoredlichia* reconsidered. *Atcheringa*, **20**, 269-276.

RANDALL, D. J. 1970. Gas Exchange in Fish. 253–292. *Fish physiology*. Academic Press, London, pp. Custom 7.

RICHTER, S., STEIN, M., FRASE, T. and SZUCSICH, N. U. 2013. The arthropod head. 223–240. *In* MINELLI, A., BOXSHALL, G. and FUSCO, G. (eds). *Arthropod Biology and Evolution- Molecules, Development, Morphology*. Springer, Berlin Heidelberg, pp. Custom 7.

ROMINGER, C. 1887. Description of primordial fossils from Mount Stephens, NW Territory of Canada. *Proceedings of the Academy of Natural Sciences of Philadelphia*, **39**, 12–19.

SCHOLTZ, G. 1998. Cleavage, germ band formation and head segmentation: the ground pattern of the Euarthropoda. 317–332. *In* FORTEY, R. A. and THOMAS, R. H. (eds). *Arthropod Relationships*. Springer Science+Busness Media Dordrecht, Chapman & Hall, London, pp. Custom 7.

SCHOLTZ, G. and EDGECOMBE, G. D. 2005. Heads, Hox and the phylogenetic position of trilobites. 139–165. *In* KOENEMANN, S. and JENNER, R. A. (eds). *Crustacea and arthropod relationships*. CRC Press, pp. Custom 7.

--- 2006. The evolution of arthropod heads: reconciling morphological, developmental and palaeontological evidence. *Development Genes and Evolution*, **216**, 395–415.

SCHOLTZ, G., STAUDE, A. and DUNLOP, J. A. 2019. Trilobite compound eyes with crystalline cones and rhabdoms show mandibulate affinities. *Nature Communications*, **10**, 2503.

SEILACHER, A. 1985. Trilobite palaeobiology and substrate relationships. *Transactions of the Royal Society of Edinburgh*, **76**, 231–237.

--- 1990. Paleozoic trace fossils. 649–670. *In* SAID, R. (ed.) *The Geology of Egypt*. Routledge, London, 32 pp. Custom 7.

SHARMA, P. P. 2017. Chelicerates and the conquest of land: a view of arachnid origins through an evo-devo spyglass. *Integrative and Comparative Biology*, **57**, 510–522.

SHU, D., MORRIS, S. C., ZHANG, Z. F., LIU, J. N., HAN, J., CHEN, L., ZHANG, X. L., YASUI, K. and LI, Y. 2003a. A new species of yunnanozoan with implications for deuterostome evolution. *Science*, **299**, 1380–1384.

SHU, D. G., CONWAY MORRIS, S., HAN, J., ZHANG, Z. F., YASUI, K., JANVIERK, P., CHEN, L., ZHANG, X. L., LIU, J. N., LI, Y. and LIU, H. Q. 2003b. Head and backbone of the Early Cambrian vertebrate *Haikouichthys*. *Nature*, **421**, 526–529.

SHU, D. G., GEYER, G., CHEN, L. and ZHANG, X. L. 1995. Redlichiacean trilobites with preserved soft-parts from the Lower Cambrian Chengjiang Fauna, South China. *Beringeria Special issue*, **2**, 203–241.

SHU, D. G., LUO, H. L., CONWAY MORRIS, S., ZHANG, X. L., HU, S. X., CHEN, L., HAN, J., ZHU, M., LI, Y. and CHEN, L. Z. 1999. Lower Cambrian vertebrates from south China. *Nature*, **402**, 42–46.

SIVETER, D. J. 1977. The Middle Ordovician of the Oslo Region, Norway, 27. Trilobites of the family Calymenidae. *Norsk Geologisk Tidsskrift*, **56**, 335–396.

SIVETER, D. J., SUTTON, M. D., BRIGGS, D. E. G. and SIVETER, D. J. 2003. An ostracode crustacean with soft parts from the Lower Silurian. *Science*, **302**, 1749–1751.

SPERLING, E. A., FRIEDER, C. A., RAMAN, A. V., GIRGUIS, P. R., LEVIN, L. A. and KNOLL, A. H. 2013. Oxygen, ecology, and the Cambrian radiation of animals. *Proceedings of the National Academy of Sciences of the United States of America*, **110**, 13446–13451.

SPERLING, E. A., KNOLL, A. H. and GIRGUIS, P. R. 2015. The ecological physiology of Earth's second oxygen revolution. *Annual Review of Ecology, Evolution, and Systematics*, **46**, 215–235.

SPEYER, S. E. 1988. Biostratinomy and functional morphology of enrollment in two Middle Devonian trilobites. *Lethaia*, **21**, 121–138.

STEIN, M., BUDD, G. E., PEEL, J. S. and HARPER, D. A. 2013. *Arthroaspis* n. gen., a common element of the Sirius Passet Lagerstätte (Cambrian, North Greenland), sheds light on trilobite ancestry. *BMC Evolutionary Biology*, **13**, 99.

STEIN, M. and SELDEN, P. A. 2012. A restudy of the Burgess Shale (Cambrian) arthropod *Emeraldella brocki* and reassessment of its affinities. *Journal of Systematic Palaeontology*, **10**, 361–383.

STØRMER, L. 1939. Studies on trilobite morphology: the thoracic appendages and their phylogenetic significance. *Norsk Geologisk Tidsskrift*, **19**, 10–273.

--- 1951. Studies on trilobite morphology, Part Ill, The ventral cephalic structures with remarks on the zoological position of the trilobites. *Norsk Geologisk Tidsskrift*, **29**, 108–158.

STÜRMER, W. and BERGSTRÖM, J. 1973. New discoveries on trilobites by X-rays. *Paläontologische Zeitschrift*, **47**, 104–141.

SUNDBERG, F. A. and MCCOLLUM, L. B. 1997. Oryctocephalids (Corynexochida: Trilobita) of the lower-middle Cambrian boundary interval from California and Nevada. *Journal of Paleontology*, **71**, 1065–1090.

SUZUKI, Y. and BERGSTRÖM, J. 2008. Respiration in trilobites: a reevaluation. *GFF*, **130**, 211–229.

TAYLOR, E. W. and BUTLER, P. J. 1978. Aquatic and aerial respiration in the shore crab, *Carcinus maenas* (L.), acclimated to 15 °C. *Journal of Comparative Physiology*, **127**, 315–323.

TAYLOR, H. H. 1990. Pressure-flow characteristics of crab gills: implications for regulation of hemolymph pressure. *Physiological Zoology*, **63**, 72–89.

TELFORD, M. J. and THOMAS, R. H. 1998. Expression of homeobox genes shows chelicerate arthropods retain their deutocerebral segment. *Proceedings of the National Academy of Sciences of the United States of America*, **95**, 10671–10675.

TRESTMAN, M. 2013. The Cambrian explosion and the origins of embodied cognition. *Biological Theory*, **8**, 80–92.

VAN ROY, P., DALEY, A. C. and BRIGGS, D. E. G. 2015. Anomalocaridid trunk limb homology revealed by a giant filter-feeder with paired flaps. *Nature*, **522**, 77–80.

VAN ROY, P., ORR, P. J., BOTTING, J. P., MUIR, L. A., VINTHER, J., LEFEBVRE, B., EL HARIRI, K. and BRIGGS, D. E. 2010. Ordovician faunas of Burgess Shale type. *Nature*, **465**, 215–8.

VANNIER, J., ARIA, C., TAYLOR, R. S. and CARON, J.-B. 2018. *Waptia fieldensis* Walcott, a mandibulate arthropod from the middle Cambrian Burgess Shale. *Royal Society Open Science*, **5**, 172206.

VERMEIJ, G. J. 1987. *Evolution and escalation: an ecological history of life*. Princeton University Press, Princeton, New Jersey, 527 pp.

WALCOTT, C. D. 1881. The trilobite: new and old evidence relating to its organization. *Bulletin of the Museum of Comparative Zoology at Harvard University*, **8**, 191–224.

--- 1910. Cambrian Geolog and Paleontology, No. 6. *Olenellus* and other genera of the Mesonacidae. *Smithsonian Miscellaneous Collections*, **53**, 231–422.

--- 1918. Cambrian Geolog and Paleontology IV, No. 4. Appendages of trilobites. *Smithsonian Miscellaneous Collections*, **67**, 115–216.

WALOSSEK, D. 1993. Fossils and Strata. *The Upper Cambrian Rehbachiella and the phylogeny of Branchiopoda and Crustacea*. Scandinavian University Press, Oslo , Norway, 202 pp.

WALOSSEK, D. and MÜLLER, K. J. 1990. Upper Cambrian stem-lineage crustaceans and their bearing upon the monophyletic origin of Crustacea and the position of *Agnostus*. *Lethaia*, **23**, 409–427.

--- 1998. Cambrian 'Orsten'-type arthropods and the phylogeny of Crustacea. 139–153. *In* FORTEY, R. A. and THOMAS, R. H. (eds). *Arthropod Relationships*. Springer, pp. Custom 7.

WALOSZEK, D., CHEN, J. Y., MAAS, A. and WANG, X. Q. 2005. Early Cambrian arthropods—new insights into arthropod head and structural evolution. *Arthropod Structure & Development*, **34**, 189–205.

WEBSTER, M. 2007. A Cambrian peak in morphological variation within trilobite species. *Science*, **317**, 499–502.

WHITTINGTON, H. B. 1941. Silicified Trenton trilobites. *Journal of Paleontology*, **15**, 492–522.

--- 1956. Silicified Middle Ordovician trilobites: the Odontopleuridae. *Bulletin of the Museum of Comparative Zoology*, **114**, 155–288.

--- 1975. Trilobites with appendages from the Middle Cambrian , Burgess Shale, British Columbia. *Fossils and Strata*, 97–136.

--- 1977. The Middle Cambrian Trilobite *Naraoia*, Burgess Shale, British Columbia. *Philosophical Transactions of the Royal Society of London, Series B: Biological Sciences*, **280**, 409–443.

--- 1980. Exoskeleton, moult stage, appendage morphology, and habits of the Middle Cambrian trilobite *Olenoides serratus*. *Palaeontology*, **23**, 171–204.

--- 1988a. Hypostomes and ventral cephalic sutures in Cambrian trilobites. *Palaeontology*, **31**, 577–609.

--- 1988b. Hypostomes of post-Cambrian trilobites. *New Mexico Bureau of Mines and Mineral Resources, Memoir*, **44**, 321–339.

--- 1990. Articulation and exuviation in Cambrian trilobites. *Philosophical Transactions of the Royal Society of London. Series B: Biological Sciences*, **329**, 27–46.

WHITTINGTON, H. B. and ALMOND, J. E. 1987a. Appenadages and Habits of the Upper Ordovician Trilboite *Triarthrus eatoni*. *Philosophical Transactions of the Royal Society of London. Series B, Biological Sciences*, **317**, 1–46.

--- 1987b. Appendages and Habits of the Upper Ordovician Trilboite *Triarthrus eatoni*. *Philosophical Transactions of the Royal Society of London, Series B: Biological Sciences*, **317**, 1–46.

WHITTINGTON, H. B. and EVITT, W. R. 1953. Silicified middle Ordovician trilobites. *Geological Society of America Memoirs*, **59**, 1–169.

WILLIAMS, M., VANNIER, J., CORBARI, L. and MASSABUAU, J. C. 2011. Oxygen as a driver of early arthropod micro-benthos evolution. *PloS one*, **6**, e28183.

WILLS, M. A., BRIGGS, D. E. G., FORTEY, R. A., WILKINSON, M. and SNEATH, P. H. A. 1998. An arthropod phylogeny based on fossil and recent taxa. 33–105. *In* EDGECOMBE, G. D. (ed.) *Arthropod fossils and phylogeny*. Columbia University Press, New York, 2 pp. Custom 7.

WILSON, H. M. and ANDERSON, L. I. 2004. Morphology and taxonomy of paleozoic millipedes (Diplopoda: Chilognatha: Archipolypoda) from Scotland. *Journal of Paleontology*, **78**, 169–184.

WIRKNER, C. S., TÖGEL, M. and PASS, G. 2013. The arthropod circulatory system. 343–391. *In* MINELLI, A., BOXSHALL, G. and FUSCO, G. (eds). *Arthropod Biology and Evolution: Molecules, Development, Morphology*. Springer, pp. Custom 7.

WOLFF, C. and SCHOLTZ, G. 2008. The clonal composition of biramous and uniramous arthropod limbs. *Proceedings of the Royal Society B: Biological Sciences*, **275**, 1023–1028.

WOOD, R. A. and ERWIN, D. H. 2018. Innovation not recovery: dynamic redox promotes metazoan radiations. *Biological Reviews*, **93**, 863–873.

WOODS, H. A., LANE, S. J., SHISHIDO, C., TOBALSKE, B. W., ARANGO, C. P. and MORAN, A. L. 2017. Respiratory gut peristalsis by sea spiders. *Current Biology*, **27**, R638–R639.

XIAO, S. H., ZHANG, Y. and KNOLL, A. H. 1998. Three-dimensional preservation of algae and animal embryos in a Neoproterozoic phosphorite. *Nature*, **391**, 553-558.

YANG, J., ORTEGA-HERNÁNDEZ, J., BUTTERFIELD, N. J. and ZHANG, X. G. 2013. Specialized appendages in fuxianhuiids and the head organization of early euarthropods. *Nature*, **494**, 468–471.

YUAN, J. L., ZHAO, Y. L., LI, Y. and HUANG, Y. Z. 2002. *Trilobite fauna of the Kaili Formation (uppermost lower Cambrian-lower middle Cambrian) from*

southeastern Guizhou, South China. Shanghai Science and Technology Press, Shanghai, 423 pp.

ZHANG, X. G. and CLARKSON, E. N. K. 2012. Palaeontographica, Abteilung A: Palaeozology-Stratigraphy. *Phosphatized eodiscoid trilobites from the Cambrian of China*. Schweizerbart Science Publishers, 121 pp.

ZHANG, X. G. and HOU, X. G. 2004. Evidence for a single median fin-fold and tail in the Lower Cambrian vertebrate, *Haikouichthys ercaicunensis*. *Journal of Evolutionary Biology*, **17**, 1162–1166.

ZHANG, X. L. and BRIGGS, D. E. G. 2007. The nature and significance of the appendages of *Opabinia* from the Middle Cambrian Burgess Shale. *Lethaia*, **40**, 161–173.

ZHANG, X. L., SHU, D. G. and ERWIN, D. H. 2007. Cambrian naraoiids (arthropoda): Morphology, ontogeny, systematics, and evolutionary relationships. *Journal of Paleontology*, **81**, 1–52.